Optimizing Polycationic Transfection for Improved Gene Delivery in Mammalian Cells

Von der Fakultät für Ingenieurwissenschaften

der Universität Bayreuth

zur Erlangung der Würde

Doktor-Ingenieur (Dr.-Ing.)

genehmigte Dissertation

von

Daniel Keim, M.Sc.

aus

Fritzlar

Erstgutachterin: Frau Prof. Dr. Ruth Freitag

Zweitgutachterin: Frau Jr. Prof. Dr. Meike Leiske

Tag der mündlichen Prüfung: 25.10.2024

Lehrstuhl Bioprozesstechnik

Universität Bayreuth

2024

Table of contents

Danksagung

An dieser Stelle möchte ich mich bei all jenen bedanken, die mich während der Promotion unterstützt und begleitet haben.

Zunächst gebührt mein Dank Prof. Dr. Ruth Freitag, für die fachliche Betreuung, wertvollen Hinweise und das konstruktive Feedback während der gesamten Zeit meiner Forschungsarbeit.

Ebenso danke ich Dr. Valérie Jérôme, für ihre wertvollen Anregungen und kritischen Fragen, die maßgeblich zur Qualität dieser Arbeit beigetragen haben. Ihre Geduld und Expertise waren für mich eine unverzichtbare Stütze.

Ich möchte mich auch bei meinen Kolleginnen und Kollegen, Elisabeth Ranze, Leif Meyer, Dr. Simon Riedl, Thomas Steiner, Pooja Parmar, Gabriel Salas, Dr. Santislava Milnar, Johanna Fritsche, Dr. Moritz Helm und Dr. Matthias Völkl bedanken, für die anregenden Diskussionen, für ihre Hilfe und für die gute Zusammenarbeit. Ich bedanke mich bei Andrea Schott und Jana Ullmann für ihre Arbeit im Labor sowie bei Edith Hübner und Kristina Thompson für die zügige Bearbeitung aller größeren oder kleineren Probleme und für die zuverlässige Zusammenarbeit.

Auch meinen Studienkollegen der ersten Stunde, Dr. Yannick Jännsch, Dr. Thomas Tran und Felix Wenzel, möchte ich danken, die wöchentlichen „Dudes-Dienstage" waren ein Highlight und haben die Woche immer schöner gemacht.

Ich möchte weiterhin auch den Doktoranden anderer Lehrstühle, Dr. Nora Meides, Johanna Schmidtmann, Laura Wegner, Dimitri Seidenath und Dr. Teresa Menzel, für die täglichen Termine um 11:15 Uhr danken, bei denen es nie an Unterhaltung gefehlt hat.

Meinen Eltern und Familienmitgliedern danke ich von Herzen für ihre unermüdliche Unterstützung, ihr Verständnis und ihren Glauben an mich.

Ebenso gilt mein Dank den Studierenden die ich während meiner Zeit als Doktorand betreuen durfte und die einen Teil der Vorarbeiten und Ergebnisse dieser Arbeit mit erarbeitet haben. Besonders möchte ich dabei Xuan Song (ARPE-19 Transfektion), Elisabeth Ranze (mRNA Synthese, B-Zell Transfektion) und Margulan Otanuly (pDNA Experimente) danken.

List of abbreviations

°	degree
AFM	atomic force microscopy
AMD	age-related macular degeneration
ANOVA	Analysis of Variance
AO	Acridine orange
ATCC	American Type Culture Collection
ATRP	atom transfer radical polymerization
A.U.	arbitrary unit
C	Celcius
CD	Cluster of differentiation
CG	Cells in the gate
CHO	Chinese hamster ovary
CRISPR	clustered regularly interspaced short palindromic repeats
CV	cell viability
Da	Dalton
DLS	dynamic light scattering
DMEM	Dulbecco´s Modified Eagle Media
DMSO	Dimethylsulfoxide
DNA	deoxyribonucleic acid
DPBS	Dulbecco's phosphate-buffered saline
E. coli	Escherichia coli
EDTA	Ethylenediaminetetraacetic acid
EtBr	Ethidium bromide
EGFP	Enhanced Green fluorescent protein
et al.	et alia
FACS	Fluorescence-activated cell sorting
FC	Flow cytometry
FCS	Fetal calf serum
FITC	Fluoresceinisothiocyanat
FSC	Forward scatter
g	gram
g	gravity

h	hours
HBG	Hepes buffered glucose
HBSS	Hanks Balanced Salt Solution
HEK	Human embryo kidney
IL	Interleukin
L	Liter
LD_{50}	Median lethal Dosis, at which point 50% of the population dies
m	meter
M	Molar
MFI	median fluorescence intensity
min	minute
M_n	number average molar mass
mRNA	messenger Ribonucleic acid
MTT	3-(4,5-Dimethylthiazol-2-yl)-2,5-diphenyltetrazoliumbromid
M_w	weight average molar mass
N/P (ratio)	nitrogen to phosphate ratio
PBS	phosphate-buffered saline
PDMAEMA	Poly-2-(Dimethylamino)ethyl methacrylate
pDNA	plasmid deoxyribonucleic acid
PDI	polydispersity index
PEG	polyethylene glycol
PEI	poly(ethyleneimine)
PI	Propidium iodide
RAFT	reversible-addition-fragmentation chain-transfer polymerization
R_h	hydrodynamic radius
RNA	ribonucleic acid
rpm	rounds per minute
RT	room temperature
SAXS	small-angle X-ray scattering
SCID	severe combined immunodeficiency
sec	second
siRNA	small interfering Ribonucleic acid
SSC	side scatter
TE	transfection efficiency

V	Volt
v/v	volume/volume
VEGF	vascular endothelial growth factor
w/v	weight/volume

Kurzfasssung

In dieser Arbeit wurde eine detaillierte Untersuchung der nicht-viralen, polykationischen Transfektion von ARPE-19-Zellen und primären humanen B-Zellen durchgeführt. Dabei kamen zwei unterschiedliche Polykationen zum Einsatz: das kommerziell erhältliche lineare l-PEI und ein am Lehrstuhl synthetisierter Nanostern.

Ein erster Untersuchungsschwerpunkt stellte die Fähigkeit der verwendeten Polykationen dar, negativ geladene Polynukleotide wie pDNA oder mRNA in einem Polyplex zu binden. Die Quantifizierung des erforderlichen Mengenverhältnisses von genetischem Material zu Polykation (N/P Verhältnis), um eine vollständige Komplexierung zu gewährleisten, erfolgte mittels verschiedener Standardmethoden. Des Weiteren wurde für die Optimierung der Transfektionseffizienz eine Vielzahl von experimentellen Parametern, wie Transfektionsvolumen, Kontaktzeit zwischen Polyplexen und Zellen sowie die Menge an zugegebenen Polykationen, verändert und angepasst. Die Transfektionseffizienz und die Zellviabilität werden mittels Durchflusszytometrie bestimmt. Die Bestimmung der Transfektionseffizienz erfolgt über die Detektion eines exprimierten fluoreszierenden Proteins, während die Zellviabilität mittels Propidiumiodid bestimmt wurde.

Unsere Ergebnisse zeigten, dass für eine effiziente Kondensation des genetischen Materials mit dem Nanostern-Polykation ein niedrigeres N/P-Verhältnis notwendig war als für l-PEI. Verschiedene Analysen, wie das Gel-Retardationsassay und Ethidiumbromid-Assay, wurden angewendet und zeigten, dass der Nanostern ab $N/P = 1$ und l-PEI ab $N/P = 3$ zuverlässig das gesamte genetische Material binden konnten.

Die Transfektion von ARPE-19-Zellen mit polykationischen Transfektionsagenzien unter Verwendung kommerziell erhältlicher Vektoren stellte bis heute eine bachtliche Herausforderung dar. Insbesondere die Nutzung von l-PEI, einem weit verbreiteten Polykation, erwies sich als nicht anwendbar. Im Gegensatz zur konventionellen Methodik, bei der die Menge des genetischen Materials konstant gehalten und die Menge des Polykations angepasst wird, um das gewünschte N/P-Verhältnis zu erreichen, befürworten die hier präsentierten Ergebnisse eine andere Strategie. Durch den Einsatz einer gleichbleibenden Menge an Polykation und Anpassung der Menge an genetischem Material konnten deutlich bessere Resultate erzielt werden.

Es wird angenommen, dass diese Änderung die zytotoxischen Effekte der Transfektion minimieren kann, da die Menge des zugegebenen Polykations die entscheidende Größe dafür sei. Diese Änderung stellte den ersten Schritt dar, um eine erhebliche Verbesserung der Transfektionseffizienz sowohl für das kommerziell erhältliche l-PEI als auch für den Nanostern zu erzielen. Weitere Modifikationen wie die Reduktion des Transfektionsvolumens auf 0.5 mL und die Verringerung der Kontaktzeit zwischen Polyplexen und Zellen auf 2 h führten zu weiteren Steigerungen der Transfektionseffizienz bei zufriedenstellender Zellviabilität. Optimale Ergebnisse mit l-PEI wurden bei 60 μg/10^6 Zellen für die mRNA-Transfektion und 40 μg/10^6 Zellen für die pDNA-Transfektion erzielt, beide bei einem N/P-Verhältnis von $\geq$ 10. Der Nanostern erreichte die besten Ergebnisse bei einem N/P-Verhältnis von 5 und einer Polymerdichte von 60 μg/10^6 Zellen, unabhängig vom verwendeten genetischen Material.

Für beide Polykationen waren Transfektionseffizienzen von etwa 70 % bei Verwendung von pDNA und einer Erholungszeit von 48 h nach Transfektion erreichbar, wobei die Zellviabilität bei etwa 80 % gehalten werden konnte. Diese Ergebnisse stellen eine erhebliche Verbesserung im Vergleich zu früheren Studien mit l-PEI dar und bedeuten einen vielversprechenden Fortschritt in der polykationischen Transfektion. Die weitere Nutzung dieser Methodik wurde für die Anwendung des CRISPR/Cas9-Systems getestet. Obwohl bestätigt wurde, dass das etablierte Verfahren transfizierte Zellen liefern konnte, wurde kein statistisch signifikanter Unterschied zwischen dem CRISPR-System und der Kontrollgruppe validiert. Der Ersatz von proprietären, hausintern synthetisierten Polymeren durch kommerziell erhältliches l-PEI in zukünftigen ARPE-19-Zelltransfektionsstudien könnte die Anwendbarkeit und Zugänglichkeit von genetisch modifizierten ARPE-19 Zellen erweitern.

Im Zuge der Fortschritte in Forschung und Entwicklung nicht-viraler Transfektionsmethoden bleibt der effiziente Transfer von Nukleinsäuren in Primärzellen, insbesondere Immunzellen, eine schwierige Herausforderung, die eine differenzierte Betrachtung erfordert. In dieser Studie wird der Nanostern für die Transfektion von primären humanen B-Zellen benutzt. Durch die Optimierung der Interaktion zwischen Polyplexen und Zellen, die Anpassung der Mengen von Polymer und Plasmid sowie die Feinabstimmung der Kulturbedingungen vor und nach der Transfektion erreichten wir eine Transfektionseffizienz von 40 % in humanen Tonsillar-B-Zellen bei gleichzeitig angemessener Zellviabilität von etwa 70 %. Eine bedeutende Erkenntnis der hier präsentierten Ergebnisse deutet darauf hin, dass die Komplexität und Verteilung der B-Zell-Subpopulationen vor und nach der Transfektion eine wichtige Rolle im Prozess spielen können. Insbesondere der Plasmazell-Subtyp zeigte sich für die Transfektion von besonderer

Bedeutung, es konnte durch Transfektion und anschließender Antikörperfärbung nachgewiesen werden, dass dieser Subtyp den präferenziell transfizierten Teil der B-Zellen darstellt. Nachfolgende Forschungen sollten sich auf den Einfluss der B-Zell-Subset-Dynamik vor und nach der Transfektion konzentrieren und eine Transfektionseffizienz-Abhängigkeit von der Plasmazellpopulation aufdecken. Zusätzlich wurde eine allgemeine Verbesserung der Zellviabilität untersucht, der bedeutsamste Effekt konnte beobachtet werden, als die Temperatur während der Transfektion auf 4 °C reduziert wurde. Diese Verbesserung ist wahrscheinlich auf Veränderungen in der Fluidität der Zellmembran und erhöhte Rigidität zurückzuführen. Diese Arbeit hat einen neuartigen Ansatz für die nicht-virale Transfektion von primären humanen B-Zellen entwickelt. Mehrere kritische Parameter wurden identifiziert, um den Bedarf an hoher TE und Zellviabilität anzusprechen. Zukünftige Studien sollten sich mehr auf die Transfektion spezifischer Subsets konzentrieren.

Abstract

This work evaluates the non-viral, polycationic transfection of ARPE-19 cells and primary human B cells. Two distinct polycations are utilized: the commercially available linear l-PEI and a nanostar synthesized at the department. The study's first focus is the polycations' ability to bind negatively charged polynucleic acids, such as pDNA or mRNA, into a polyplex. Quantifying the necessary ratio of genetic material to polycation using various standard methods to ensure complete complexation. Furthermore, many experimental parameters, such as transfection volume, contact time between polyplexes and cells, and the number of polycations added, are modified and adjusted to optimize transfection efficiency for both cell types, ARPE-19 and primary B cells. Transfection efficiency and cell viability were measured using flow cytometry. Transfection efficiency is determined by detecting an expressed fluorescent protein, while cell viability is determined using propidium iodide as the staining agent.

Our results indicate that for efficient condensation of genetic material with the nanostar polycation, a lower N/P ratio is required compared to l-PEI. Various analyses, such as gel retardation assay and ethidium bromide assay, were applied and showed that the nanostar could reliably bind the entire genetic material starting from an N/P ratio of 1 and l-PEI from an N/P ratio of 3.

Transfecting ARPE-19 cells with polycationic transfection agents using commercially available vectors has remained challenging and not feasible. Specifically, l-PEI, a widely used polycation, proved to be inapplicable. Unlike conventional methods, where the amount of genetic material is kept constant and the amount of polycation is adjusted to achieve the desired N/P ratio, the results presented here support a different strategy. By employing a continuous amount of polycation and adjusting the amount of genetic material, significantly better results were achieved. This change is believed to minimize the cytotoxic effects of transfection since the amount of added polycation is one of the crucial factors. This revision represented the first step in significantly improving transfection efficiency for commercially available l-PEI and the in-house synthesized nanostar. Further modifications, such as a reduced transfection volume to 0.5 mL and lowering the contact time between polyplexes and cells to 2 hours, increased transfection efficiency with a maintained robust cell viability. Optimal results with l-PEI were achieved at $60\,\mu g/10^6$ cells for mRNA transfection and $40\,\mu g/10^6$ cells for pDNA transfection, both at an N/P ratio of ≥ 10. The nanostar achieved the best results at an N/P ratio of 5 and a

polymer density of 60 µg/10^6 cells, regardless of the polynucleotide used. For both polycations, transfection efficiencies of about 70% were achievable using pDNA with a recovery time of 48 hours post-transfection while maintaining cell viability at about 80%. These results significantly improve over previous studies with l-PEI. Further utilization of this methodology was tested for applying the CRISPR/Cas9 system. Although it was confirmed that the established procedure could deliver transfected cells, no statistically significant difference between the CRISPR system and the control group was validated. Replacing proprietary, in-house synthesized polymers with commercially available l-PEI in future ARPE-19 cell transfection studies could enhance the applicability and accessibility of genetically modified ARPE-19 cells.

As advancements continue in research and development of non-viral transfection methods, the efficient transfer of nucleic acids into primary cells, particularly immune cells, remains challenging and requires in-depth consideration. This study uses the nanostar polycation to transfect primary human B cells. By optimizing the interaction between polyplexes and cells, adjusting the amounts of polymer and plasmid, and fine-tuning the culture conditions before and after transfection, a transfection efficiency of 40% was achieved in human tonsillar B cells while maintaining reasonable cell viability of about 70%.

A significant insight from the presented results suggests that the complexity and distribution of B cell subpopulations before and after transfection plays a crucial role in the process. The plasma cell subtype was identified as especially significant for transfection, demonstrated through transfection and subsequent antibody staining, indicating this subtype as the preferentially transfected portion of the B cells. Future research should focus on the influence of B cell subset dynamics before and after transfection. Additionally, a general improvement in cell viability was investigated, with the most significant effect observed when the temperature during transfection was reduced to 4 °C. This improvement is likely due to changes in cell membrane fluidity.

In summary, this work could significantly enhance the transfection outcomes for both cell types, primary human B cells and the retinal cell line ARPE-19, when polycations are used as transfection agents.

1 Introduction

Transport of genetic material, such as plasmid deoxyribonucleic acid (pDNA), messenger ribonucleic acid (mRNA), or other nucleic acids, in mammalian cells is a rapidly growing field of research that has the prospective to revolutionize medicine. Gene therapy, in particular, is a promising application of this research, as it has the potential to cure or alleviate diseases that currently have no or only limited treatment options.[1] This approach involves delivering functional copies of genes into cells to replace or supplement missing or malfunctioning genetic material. Although considerable advancements have been made over the last few years, numerous hurdles remain before this technology can be utilized broadly and effectively in clinical settings.[2]

Different methods are known by which genetic material can be transported into a cell; generally, they are distinguishable by the transportation method used, viral- and non-viral vectors.[3] Viral vectors utilize the mechanisms developed through millions of years of evolution to deliver genes to cells efficiently. Viral vectors are favored because of high transfection efficiency (TE), the capability to transduce dividing and non-dividing cells, and cell specificity through capsid modifications.[4] However, for a medical application, they are limited by the patient's immune system responses, trained to recognize and eliminate hostile viruses.[5,6] Therefore, the patient's immune system disrupts the transfection process and thereby eliminates all therapeutic effects. Additional limitations like size restrictions of the genetic cargo and immunogenicity resulted in a shift of interest in gene therapy research and brought non-viral vectors into the center of attention.[7–9] Synthetic vectors have been known since the 1960s, in which Spermine (**1;** Figure 1) was used successfully to transfect mammalian cells (D98S cell line).[10] In addition, other materials such as bioinspired molecules, polymers, lipids, and inorganic silica nanoparticles have also been investigated as potential vectors.[11] Polyethyleneimine (PEI, **2**), recognized as the "gold standard" among polycations, remains a preferred transfection agent and is even used today in clinical applications.[12] Lipids such as **3** and their derivatives experienced a surge in popularity because of their recent use in vaccines developed by Moderna® and BionTech® against the severe acute respiratory syndrome coronavirus 2 (SARS-CoV2).[13,14]
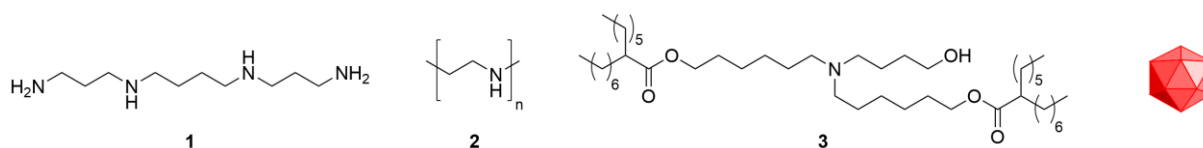

Figure 1: Selection of possible vectors. Spermine (**1**), l-PEI (**2**), ALC-0315 (**3**), and Adenovirus (schematic).

Non-viral vectors utilized in gene delivery are required to interact with the genetic cargo intended for transport. The negatively charged backbone of the genetic material interacts with the positively charged structure of the synthetic vector, which results in the formation of different aggregates (Figure 2).
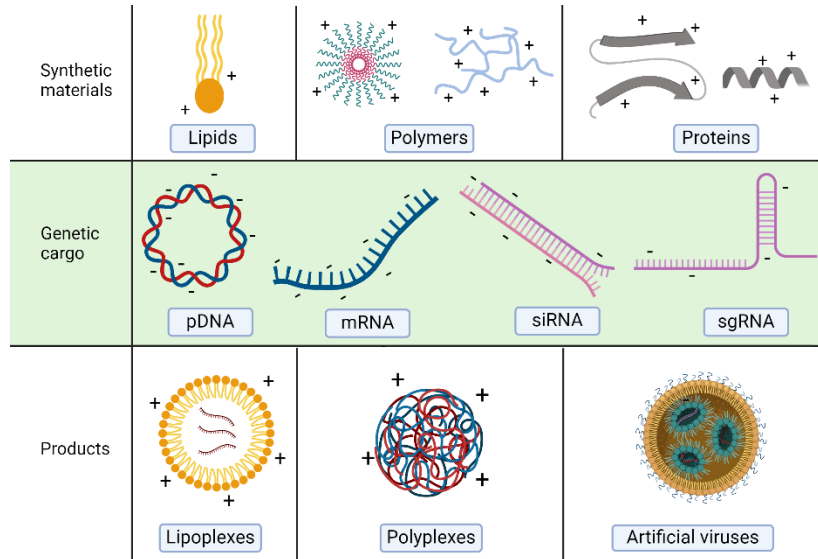

Figure 2: Selection of possible transfection agents and their interaction with genetic material.[15,16]

The resulting products protect the genetic material from nucleases and facilitate the uptake into the cell. Critical parameters, including size, charge, and chemical composition, must fall within an optimal range to ensure successful delivery and function.[3] Initial interaction between the resulting aggregates and a cell is believed to involve the cell membrane's negatively charged glucosamine chains.[17] However, the precise internalization mechanism into cells remains unclear, necessitating further research to understand the predominant pathways.[18] Despite the numerous advantageous properties of non-viral vectors, significant efforts are required to enhance their efficacy, particularly in comparison to viral vectors, which exhibit higher TE and, to some extent, lower cell mortality. This thesis aims to provide a comprehensive examination of transfection methods and offer novel insights for difficult-to-transfect cells when using polycationic non-viral vectors.

1.1   Transfection

Transportation of genetic material into a mammalian cell by itself is inefficient and virtually impossible. Electrostatic interaction between the negatively charged phosphate backbone of the polynucleotide and the negatively charged cell membrane repulse each other and makes internalization unlikely.[19] Furthermore, larger molecules such as proteins or polynucleotides cannot penetrate the cell membrane. To achieve internalization, specific active uptake mechanisms need to be utilized. In general, transfection can be categorized into three different methods, dependent on the mode of transportation: (1) viral transduction, which exploits the viral machinery (2) chemical methods, which use lipids, peptides, or polymers; and (3) physical methods, which utilize high energy densities to create pores in the cell membrane (Figure 3).[3] The optimal method depends on the experimental design and objective, as all the employed procedures have their advantages and disadvantages.[3,20]
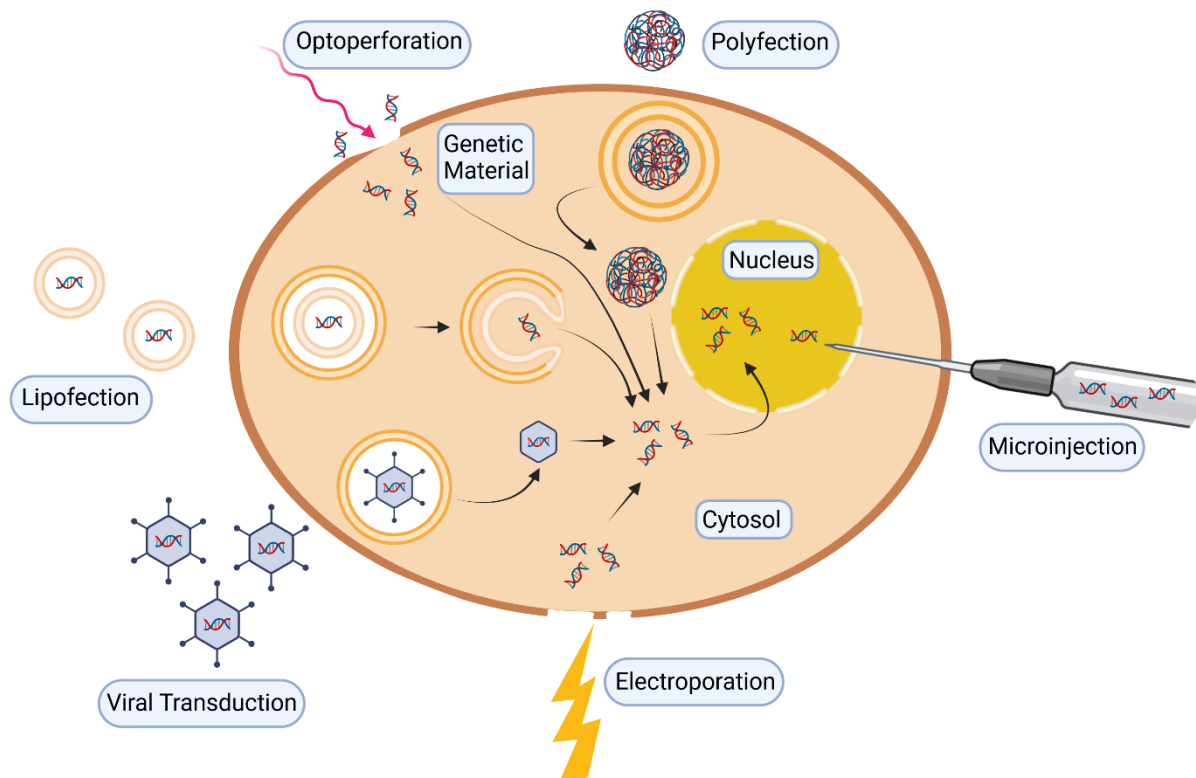

Figure 3:A selection of transfection methods.[16]

The transfection process can be compartmentalized into cargo preparation, cellular entry, cargo release, and transgene expression. For non-physical methods, the genetic material is condensed in size and thereby also shielded by its vector against DNases or RNases.[21,22] Entry methods vary depending on its carrier; while viruses can use receptor-mediated endocytosis, lipids allow fusion with the cell membrane or endosomes and deliver their cargo this way.[3,23]

Electroporation utilizes a strong electric field that perforates the cell membrane. This way, field-driven transport or diffusion can occur, and genetic material can enter the cell.[24–26] Releasing the genetic material to make it bioavailable is necessary for non-physical methods. Unpacking can be accomplished via different methods; conformational changes by pH-responsive moieties are most common.[27] The last step is transporting the bioavailable cargo to its destination: the cytosol for RNA and the nucleus for DNA. While viruses have developed a sophisticated mechanism to achieve their goal of delivering their cargo, chemically mediated methods rely mainly on inefficient stochastic processes.[23]

Once the cargo delivery is successful, two different modes of action are known by which protein expression occurs (Figure 4): stable and transient. Stable transfection results (Figure 4, A) in integrating genetic material into the host's genome, leading to long-term expression. Transient transfection (Figure 4, B) does not lead to integration, resulting in short-term transgene expression, which will cease entirely because of factors such as cell division and the degradation of the genetic material.[28,29]
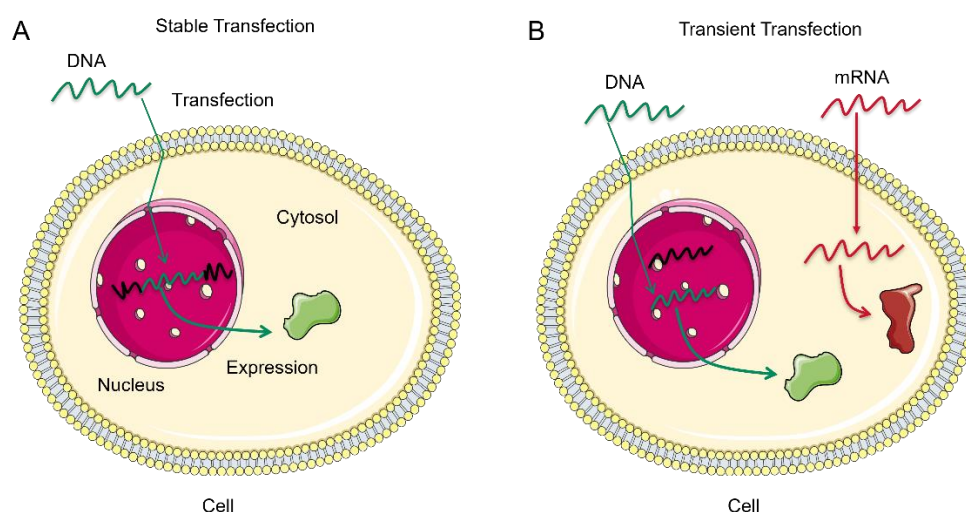

Figure 4: Schematic for (A) stable- and (B) transient transfection.[30]

While stable transfection can ensure stable protein production and is being applied in industry settings (e.g., production of monoclonal antibodies), transient transfection can be suitable for understanding some of the cell's metabolic pathways by knock-in and -out studies, or when only a short expression duration is desired (e.g., vaccination).[31,32]

1.1.1 Viral transfection

Viral vectors are modified viruses engineered to deliver genetic material into host cells without replicating.[33] Commonly used viral vectors include adenoviruses, adeno-associated viruses (AAVs), retroviruses, and lentiviruses.[34] These vectors exploit the natural ability of viruses to infect cells and release or integrate their genetic material into the host cell. They have emerged

as powerful tools for gene delivery in transfection, albeit with some safety concerns. The following section will discuss some basic principles, advantages, and disadvantages of viral vector-based transfection.

One of the most used viral vectors is the Adenovirus.[29] While its first clinical deployment in the 1990s led to the death of a young patient through systematic inflammatory response, generational improvements targeted immunogenicity and ensured better tolerability from the patient's immune system.[9,35] Retroviruses were one of the first clinically employed viral vectors to combat severe combined immunodeficiency (SCID). Most treatments were successful, but because of the integrating property of the retrovirus, some patients developed leukemia.[9,36,37]

Some viral vectors have restricted packaging capacity, limiting the size of the genetic cargo that can be delivered (Table 1). This constraint can be challenging when transferring large gene sequences or regulatory elements.[29] Specific viral vectors, like AAVs and lentiviruses, can mediate long-term gene expression due to their ability to integrate into the host genome.[29,38,39] This persistent expression is crucial for stable therapeutic effects in gene therapy. Using viral vectors in a clinical setting can trigger host immune responses, leading to neutralization and clearance of the viral particles. Pre-existing immunity in patients can further hinder efficiency, limiting or even nullifying therapeutic efficacy.[40,41]

Table 1: Overview of selected viral vectors and their transfection properties.

Virus	Insert Capacity	Features
Adenovirus	<7.5 kb	Broad host range
		Transient expression
		Strong immunogenicity
AAV	<4 kb	Broad host range
		Transient expression
		Strong immunogenicity
Retrovirus	8 kb	Transduces only in dividing cells
		Long-term expression
		Radom integration in the host genome
Lentivirus	8 kb	low cytotoxicity, integration
		long-term expression
		Broad host range

Viral vectors offer superior transduction efficiency, ensuring a higher percentage of target cells receive the desired genetic cargo. This high efficiency minimizes the amount of viral particles

required for successful transfection, reducing the potential for host immune responses. In addition, viral vectors can be engineered to target specific cell types by modifying the viral surface proteins (Figure 5). This specificity enables precise targeting of diseased or damaged cells, minimizing off-target effects and enhancing the therapeutic potential of gene therapies.[42,43]
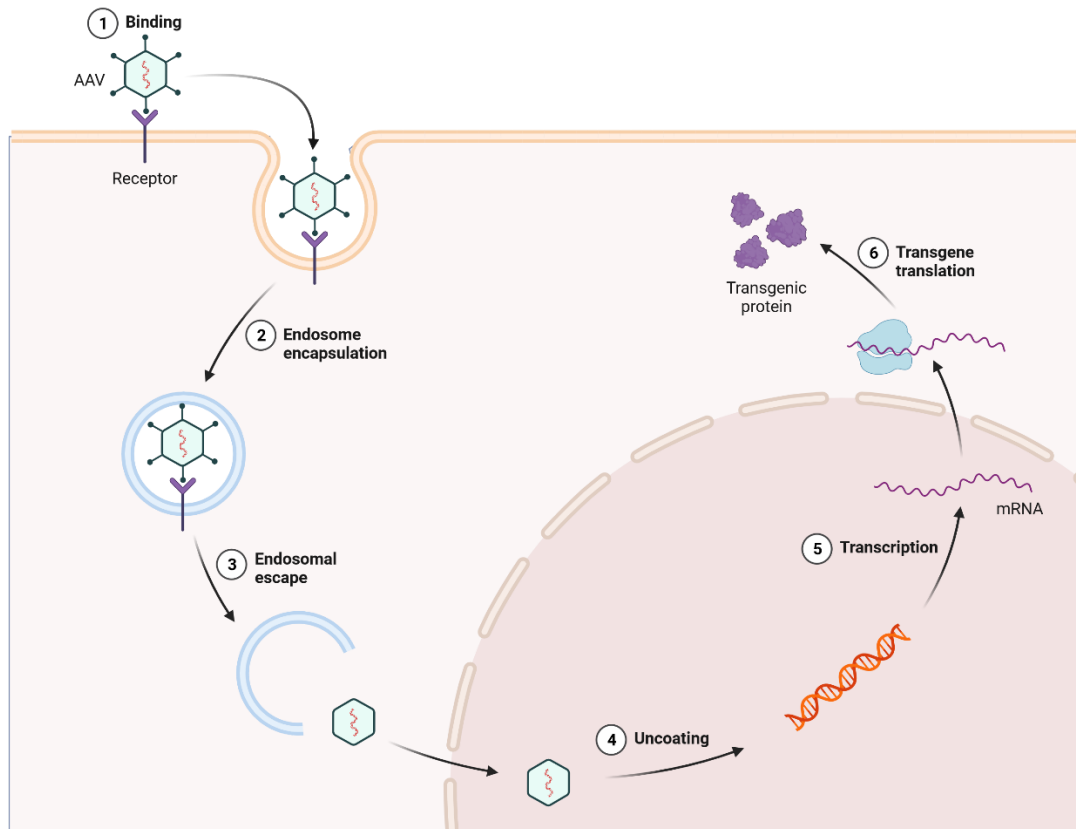

Figure 5:Viral, receptor-mediated transfection.[16]

Viral vectors, such as retroviruses, may pose a risk of insertional mutagenesis, wherein the viral DNA inserts into critical genomic regions, potentially leading to oncogenesis or disrupting essential gene functions.[29] Furthermore, vectors derived from pathogenic viruses may carry the risk of reversion to a virulent state, posing safety concerns for both researchers and patients.[44] Stringent safety measures are necessary to prevent accidental viral spread, thereby limiting such use in research.

Notable applications of viral vectors include the transduction of primary human T-cells to introduce the so-called CAR receptor, which enables T-cells to target cancerous human cells selectively.[4,45,46] This, in combination with traditional chemotherapy, shows great potential for future application in the treatment of cancer patients.[47] The widespread application was also introduced with the deployment of the COVID-19 vaccine of AstraZeneca in 2021, which used

a viral vector to induce protein production in the body.[48–50] Viral vectors in transfection represent a powerful tool in gene delivery with numerous advantages, including high transfection efficiency and cell-type specificity. However, the potential drawbacks, such as immunogenicity, risk of insertional mutagenesis, limited packaging capacity, and safety concerns, must be carefully considered.

1.1.2 Physical methods

Physical methods, such as electroporation, microinjection, and optoperforation, have gained prominence due to their high transfection efficiency. These techniques directly deliver nucleic acids into the cell cytoplasm or nucleus, bypassing the endosomal or other metabolic pathways.[20,51] One significant advantage of physical methods is their versatility, as they can be applied to a wide range of cell types, including primary and stem cells. Often, physical methods are employed when alternatives, such as chemical vectors, fail to achieve gene transfer or are accompanied by excessive cell death. This broad applicability makes physical methods suitable for various research areas and applications in molecular biology.[52] Moreover, physical methods offer a non-viral approach to transfection, alleviating concerns related to immune responses, insertional mutagenesis, and other safety issues associated with viral-based transfection techniques. However, drawbacks when using physical methods in transfection are not irrelevant. For instance, these techniques often require specialized equipment and technical expertise, which limit their accessibility and ease of use, especially for researchers without specialized training. Additionally, physical methods may have limitations concerning the size of genetic material that can be efficiently delivered into cells, as large polynucleotides pose challenges for some physical transfection techniques.[53] Furthermore, no *in-vivo* approach can be accomplished, limiting physical methods to *in-vitro* experiments.

Electroporation, the widest spread physical transfection method, relies on a high voltage applied to a buffer where the cells rest and can create pores on the cell membrane (Figure 6).[54] One significant disadvantage of this method is the high cell mortality paired with the substantial need for genetic material to accomplish successful transfection.[55]
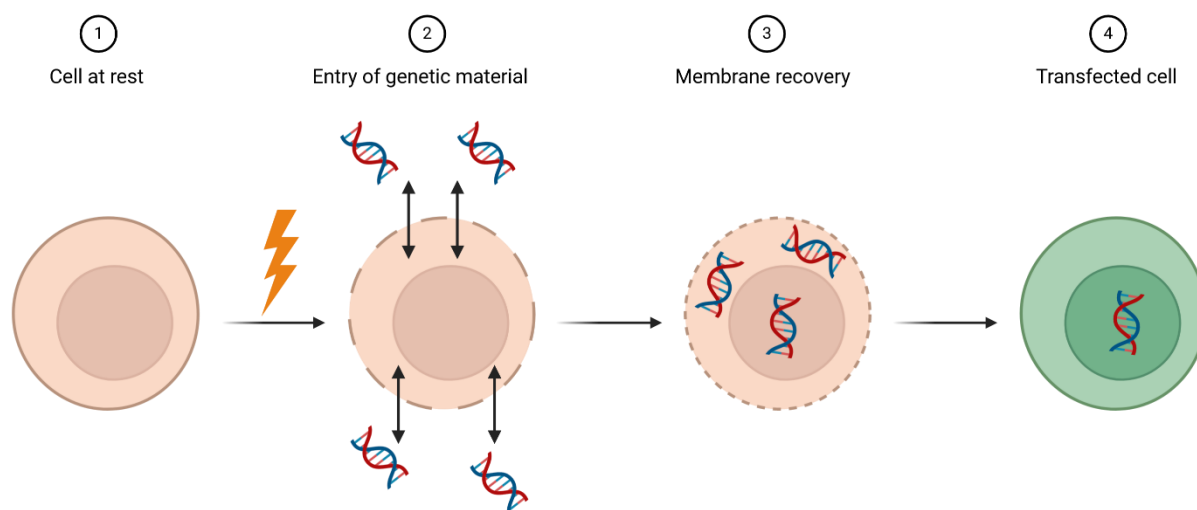
Figure 6: Electroporation Mechanism.[16]

Application of a high potential to cells creates holes in the cell membrane. It allows for diffusion-driven processes or an electrophoretic mobility shift to occur and genetic material to enter the cell. [56] Afterwards, regeneration of the cells`s plasma cell membrane takes place.

Physical methods offer higher efficiency and greater versatility regarding applicable cell types compared to other methods. Researchers can leverage these advantages in various research applications. However, careful consideration of the specific requirements of the experiment is essential to select the most suitable transfection method that balances efficiency, cell viability, and ease of use.

1.1.3 Chemical transfection

Non-viral transfection vectors offer a safer alternative to viral vectors, which can carry the risk of immunogenicity and integration into the host genome.[29] Among non-viral vectors, lipids and polycationic vectors are notable options due to their effectiveness and versatility.[57,58] Significant attention to the potential of non-viral delivery of polynucleotides was gathered because of the deployment of the COVID-19 vaccines of Moderna® and BioNTech® in which lipids delivered mRNA in human cells.[14,49]

To facilitate the delivery of genetic material into a cell, cationic lipids are utilized to form complexes with polynucleotides. This process involves the interaction between the negatively charged polynucleotide and the positively charged lipid, creating a structure known as a lipoplex. In initial interactions with the cellular membrane, it is hypothesized that the internalization of the lipoplex occurs through endocytosis, resulting in its encapsulation within an endosome (Figure 7). The escape from the endosome is a critical step to facilitate either transcription or translation of the encapsulated genetic material. It is theorized that endosomal

escape may occur through a fusion process between the lipoplex and the endosomal membrane, thereby releasing the genetic cargo into the cytosol.[59,60] Depending on the cargo used, pDNA or mRNA, further nuclear entry of the genetic material is necessary to transcribe the pDNA to mRNA and translate the mRNA to the protein of interest. Because of their simplistic structure, lipids are easily synthesized at a large scale and exhibit good stability during storage and transportation.[61,62] Lipoplexes can transfect various cell types, including non-dividing cells.[63]
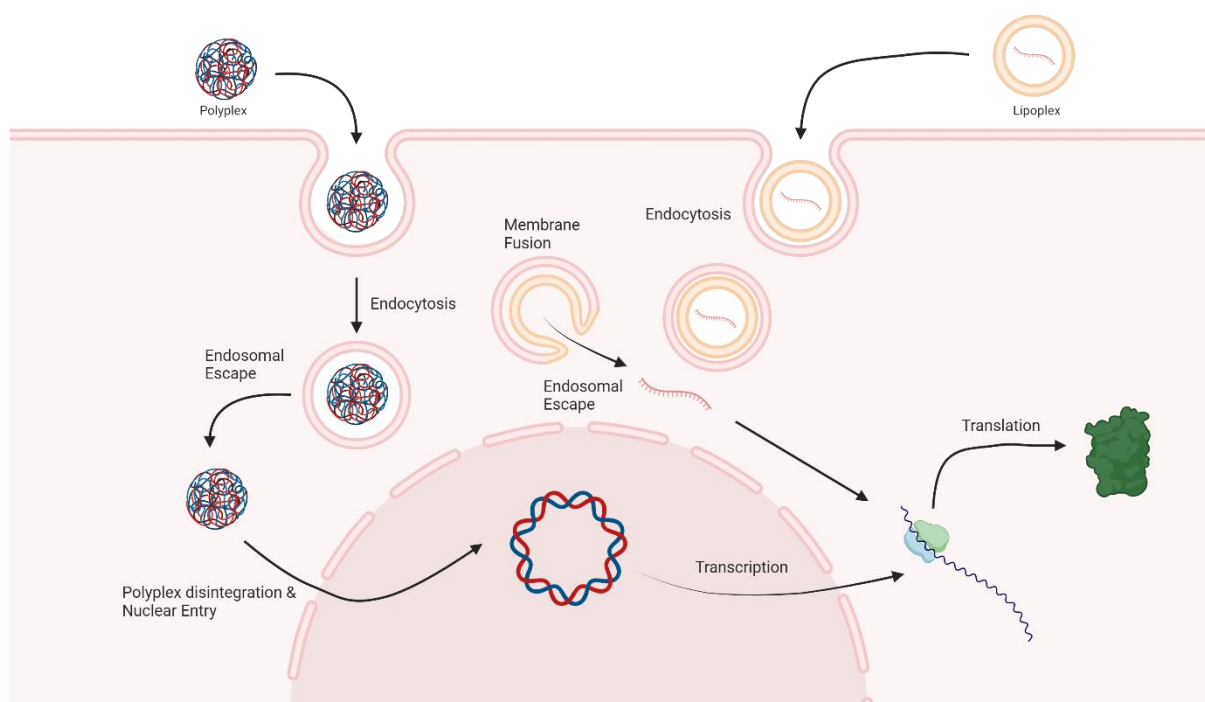

Figure 7: Entry of Poly/Lipoplex into a cell with protein expression.[16]

Similar to the mechanism observed with lipids, polymers that carry a positive charge can interact with genetic material to form a structure known as a polyplex through electrostatic interactions. In the first contact with the cell, the polyplex will be encapsulated within an endosome and internalized into the cell. Which internalization process is being employed depends on a multitude of parameters, such as size, charge, chemical composition, and the cell that's being targeted.[64–66]

Contrary to lipids, polymers lack the capability to interact with the endosomal membrane for fusion and subsequent cargo release. Instead, an alternative mechanism, known as the proton-sponge effect (PSE), is theorized to enable polyplex escape. This mechanism relies on the high proton buffer capacity of the polymer, which induces osmotic swelling of the endosome, ultimately leading to its rupture and the release of the encapsulated nucleic acids. (Figure 8).[67,68]
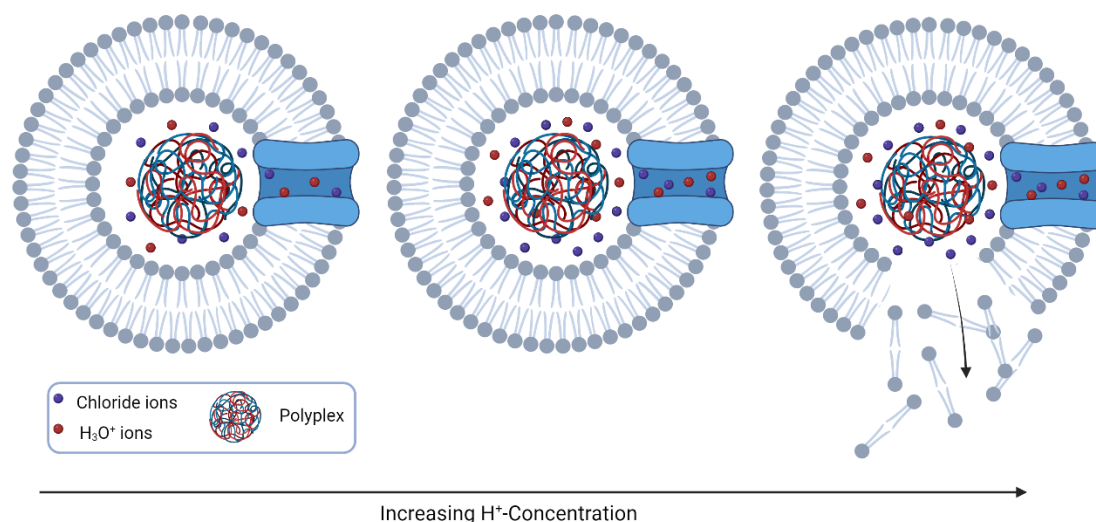
Figure 8: Mechanism of the PSE, a gradual increase of the H_3O^+ concentration results in swelling of the endosome and eventual rupture with polyplex release into the cytosol.[16]

This process is considered particularly relevant for polymers like polyethyleneimine, which can capture protons and buffer the endosomal pH, thus facilitating the escape process.[67] However, the validity of the proton sponge hypothesis has been a subject of debate within the scientific community, with various conflicting reports and no unified conclusion reached.[67–70] Alternative theories have been proposed, such as the direct interaction of cationic polyplexes or free polymer with the endosomal membrane, causing destabilization, increased permeability, or polymer-supported nanoscale hole formation.[66,71] These alternative endosomal escape mechanisms are considered more closely related to viral-mediated escape methods than the proton sponge effect. Despite the ongoing debate and research into the exact mechanisms, it is clear that the efficient escape from endo-lysosomal compartments is a significant barrier in gene therapy, and understanding these mechanisms is crucial for improving the efficacy of non-viral vectors in therapeutic applications.

Lipid- and polymer-based transfection vectors hold promise for gene delivery in research and clinical applications. Lipid-based vectors offer low immunogenicity, scalability, and broad cell-type compatibility, while polycationic vectors excel in nucleic acid binding, endosomal escape, high transfection efficiency, and prolonged gene expression.[72] As research advances, optimizing these vectors will enhance their safety and efficacy, expanding their utility in gene therapy and other biomedical applications.

The next chapter will provide a more detailed overview of polycations in transfection.

1.2 Polymers in transfection

Over the years, numerous polymers have been synthesized and found to be used as transfection agents.[73] An ionizable functional group, mostly nitrogen or sulfur, is a common motif in their structure.[67] Depending on the incorporation and density of these groups, a highly chargeable polymer can be synthesized (Figure 9).
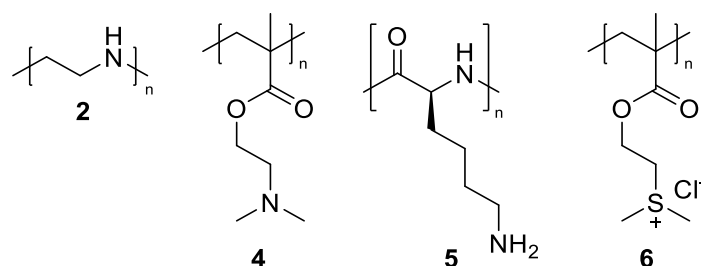
Figure 9: Structures of l-PEI (**2**), poly-2-(Dimethylamino)ethyl methacrylate (pDMAEMA, **4**), poly-Lysine (**5**), poly-(2-(methacryloyloxy)ethyl)dimethylsulfonium chloride (**6**)

As the gold standard for polycationic transfection, l-PEI (**2**) seems the obvious choice to modify further and enhance the transfection capabilities of the polymer. However, drawbacks like high cytotoxicity challenges to alter the structure and poor transfection results in hard-to-transfect cells render future improvements hard to justify because of inherent problems and more promising alternatives.[74] Branching out to acrylates seems beneficial because of their wide range of structural and functional variety, which, at the same time, can be easily modified post-polymerization. As such, pDMAEMA (**4**) or derivatives with different structural motifs have shown high transfection efficiency in the past, even in hard-to-transfect cells.[75–78] Structural changes by elongating the distance between the electron-withdrawing and electron-donor group, changing the electron-donor affinity, and altering the steric hindrance profoundly influenced polyplex stability and transfection efficiency (Figure 10).[79]
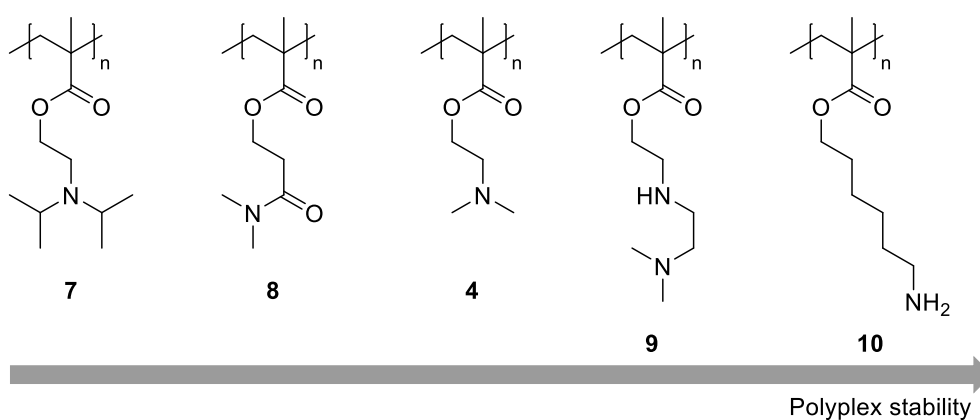
Polyplex stability

Figure 10: Possible changes in pDMAEMA (**4**) derivatives and their influence on polyplex stability.

Beyond internal charges, the architecture of polymers plays a fundamental role in influencing their transfection capabilities. The structural architecture of polymers, including their branching, size, shape, and molecular weight, significantly affects their ability to condense genetic material, interact with cell membranes, and facilitate endosomal escape, ultimately impacting gene delivery efficiency.[80–82] As highlighted in the review by RINKENAUER et al., there is a discernible correlation between the transfection efficiency and the structural geometry of the polymer, which can be adjusted through synthetic methods.[73] The morphological forms of the polymer can be broadly categorized into three distinct geometries: star-shaped, comb-shaped, and linear-shaped (Figure 11). Additionally, it is possible to further subdivide each of these categories for a more detailed analysis
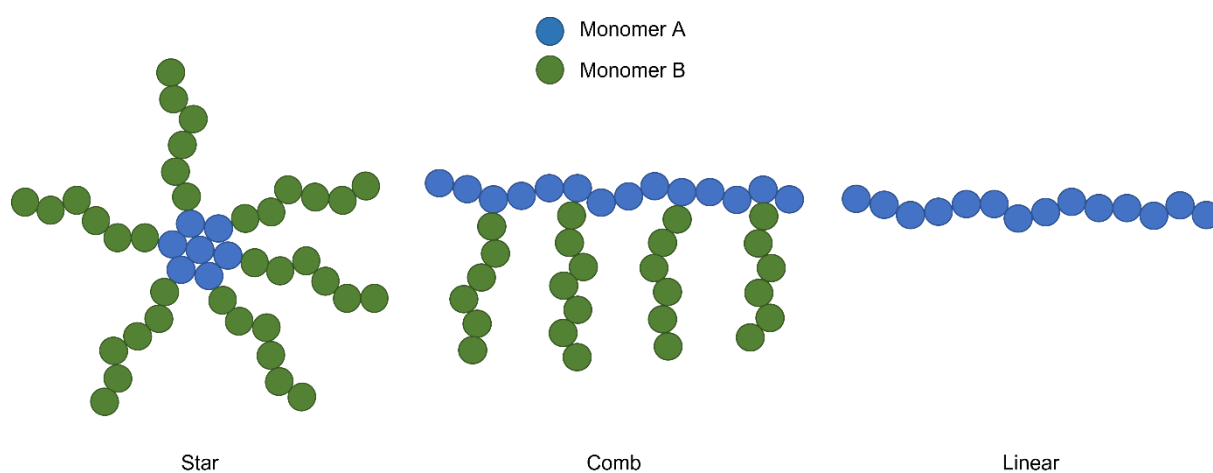

Figure 11: Polymer architecture archetypes.

Other characteristics, such as charge density or hydrophobic interaction with the genetic material, can be adjusted depending on the polymer's chosen geometry. A general trend observed seems to favor more complex structures to enhance transfection capabilities and stronger polyplex formation.[73]

The positive ζ–potential of polyplexes is a crucial factor for their internalization by cells. However, the presence of negatively charged proteins in the growth medium of cells can impede transfection efficiency by promoting aggregation of polyplexes and neutralizing their positive charge. To circumvent this issue, the use of polymers such as polyethylene glycol (PEG, **11**), poly-2-(2-Methoxyethoxy)-ethyl-methacrylate (pDEGMA, **12**), or poly(2-oxazoline) (pOx, **13**) as charge shielding agents have been proposed (Figure 12).[83,84] These polymers can effectively protect the positive charge of polyplexes, thereby reducing the likelihood of aggregation with negatively charged proteins and increasing the efficiency of polyplex internalization by cells.[85,86]
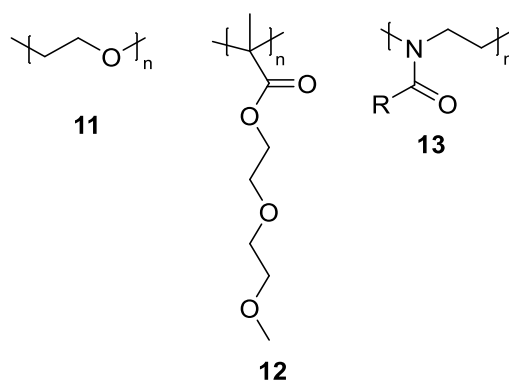
Figure 12: Structures of PEG (**11**), pDEGMA (**12**) PMeOx (**13**).

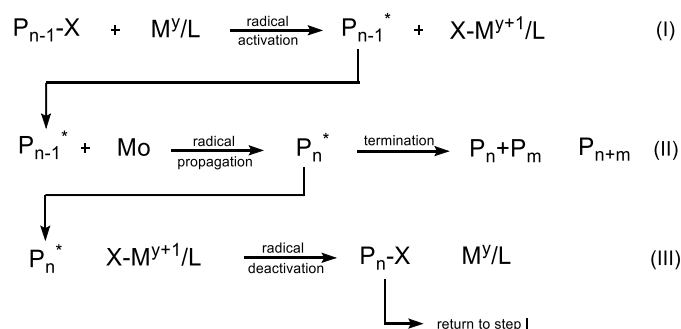## 1.2.1 Synthesis of polymers for transfection

A critical condition in polymeric transfection that ensures reliable and reproducible results is the polydispersity index (PDI), defined by M_w/M_n.[87] Traditionally used methods for polymerization, like radical polymerization, deliver an extensive range of polymers with various chain lengths and molecular weights. In the last few decades, multiple new or modified concepts were developed to control the PDI, ensuring a narrow distribution of polymer chains. Controlled living radical polymerization is one method that can be further subdivided depending on what reagents are employed: atom transfer radical polymerization (ATRP) or reversible-addition-fragmentation chain-transfer polymerization (RAFT).[88–90] A more detailed look at ATRP is provided in the following.

ATRP can be utilized to synthesize complex structures under mild conditions and with excellent control of the PDI.[91] It involves the initiation of polymerization by a transition metal complex, typically copper, which acts as both a catalyst and a reducing agent. The process proceeds through a series of steps, including initiation, propagation, and termination. During initiation, the transition metal complex generates a radical species, which then reacts with the monomer to form a growing polymer chain. The propagation step involves the transfer of the radical species from the transition metal complex to the growing polymer chain, allowing for the addition of monomer units to the chain. The decisive difference to conventional radical polymerization is a reversible deactivation of the active chains, which significantly hinders the diffusion-dominated process of chain deactivation and, subsequently, poor control of the PDI within the reaction (Equation 1).

$$P_n\text{-}X + M^y/L \underset{k_{deact}}{\overset{k_{act}}{\rightleftharpoons}} P_n^* + X\text{-}M^{y+1}/L$$
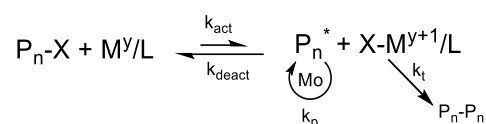
Equation 1: General mechanism of ATRP. Where P_n-X is the dormant alkyl halide, X is the halide, M^y is a transition metal, L is a ligand, P_n^* active radical, and Mo is an additional monomer.

In order to utilize the ATRP method, several key parameters must be taken into account. These include the use of an alkyl halide (Pn-X) and a transition metal catalyst, which are necessary for the initiation of the radical polymerization reaction (Equation 2, (I)). The active radical reacts with the chosen monomer, which starts the chain growth reaction (Equation 2, (II)). At this moment, termination of the reaction is possible, but because of the controlled manner of ATRP, it is unlikely. Radical deactivation in ATRP often occurs through the reformation of the alkyl halide species, which is in equilibrium with the transition metal catalyst utilized in the polymerization process (Equation 2, (III)).

$$P_{n-1}\text{-}X \quad + \quad M^y/L \xrightarrow[\text{activation}]{\text{radical}} P_{n-1}^* \quad + \quad X\text{-}M^{y+1}/L \qquad \text{(I)}$$

$$P_{n-1}^* \quad + \quad Mo \xrightarrow[\text{propagation}]{\text{radical}} P_n^* \xrightarrow{\text{termination}} P_n + P_m \quad P_{n+m} \quad \text{(II)}$$

$$P_n^* \quad X\text{-}M^{y+1}/L \xrightarrow[\text{deactivation}]{\text{radical}} P_n\text{-}X \quad M^y/L \qquad \text{(III)}$$

return to step I

Equation 2: Detailed mechanism of ATRP. Where P_{n-1}-X is the dormant alkyl halide, X is the halide, M^y is a transition metal, L is a ligand, and P_{n-1}^* is an active radical.

The reactivity of the alkyl halide is a critical determinant of the efficiency of the initiation step in ATRP. Alkyl halides with a tertiary carbon atom in proximity to the halide group exhibit the highest reactivity. Secondary and primary alkyl halides follow in decreasing order of reactivity. This reactivity trend directly results from the relative stability of the radical species formed from the alkyl halides (Figure 13).
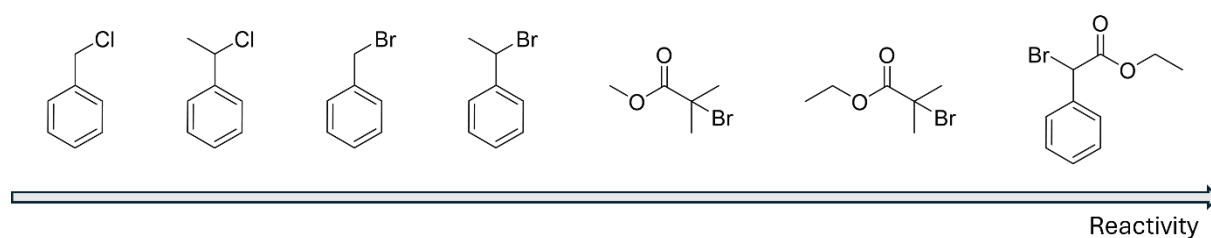
Reactivity

Figure 13: Selection of ATRP initiators sorted for their reactivity with Cu^IX/PMDETA (X = Br or Cl) in MeCN at 35 °C.[92]

Depending on the reactivity of this molecule, the rest of the reaction conditions can be chosen. Another critical part is the ligand chosen for the complexation of the metal ion. The group of MATYJASZWSKI went to great lengths to determine the reactivity of the most common ligands for ATRP (Figure 14).
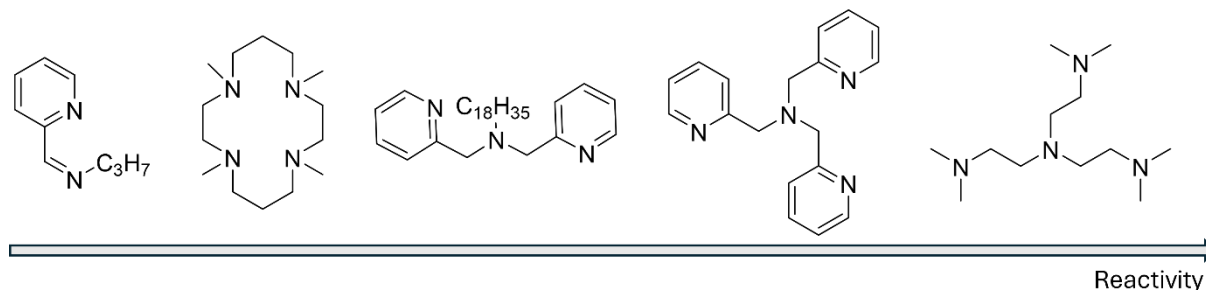

Reactivity

Figure 14: Selection of ATRP ligands sorted for their reactivity with EtBriB in the presence of Cu^{I}Br in MeCN at 35°C.[92]

When carefully chosen and controlled, both parameters can help ensure successful polymerization and a narrow PDI, even for multi-block polymers. Additional factors such as solvent polarity and temperature can also play a role in polymerization, but they may have a lesser impact than previously mentioned parameters. The effect of these factors can vary depending on the specific polymerization process and the type of monomers being used.[93]

1.3   Polyplex characterization

A polyplex is a complex formed between a polycation and a nucleic acid, such as DNA or RNA. Polyplexes are of particular interest in the field of gene therapy, as they can be used to deliver genetic material to cells in an efficient manner. The characterization of polyplexes is a fundamental step in elucidating the mechanisms underlying transfection. Critical attributes of polyplexes, including their surface charge (ζ-potential) and hydrodynamic radius (Rh), provide essential insights.
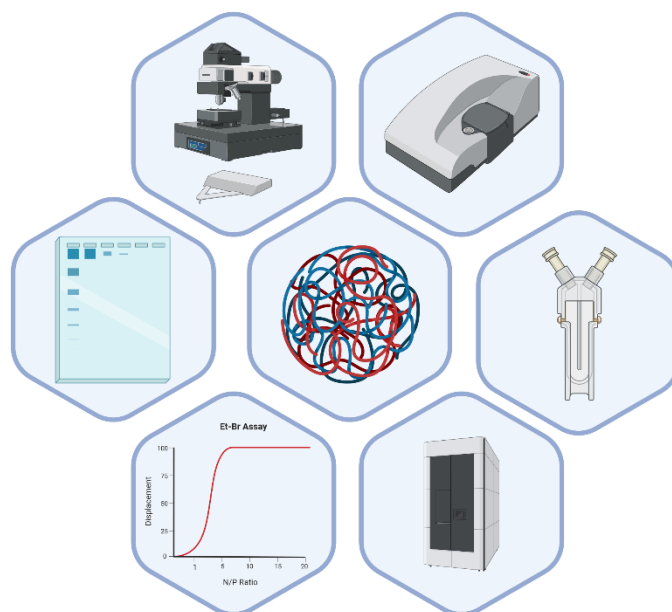
Figure 15: Overview of various analytical methods.[16]

The internalization depends on these parameters, with a positive surface charge necessary for electrostatic interaction with the negatively charged cell membrane.[94] The most commonly employed method to establish the desired charge of a polyplex involves adjusting the ratio of polycation to polynucleotide mixed. This parameter is referred to as the N/P ratio, where "N" denotes the nitrogen-containing, positively charged polycation, and "P" represents the negatively charged polynucleotide phosphate backbone. The N/P ratio is a critical factor of the polyplex's physicochemical properties, including its size, charge, stability, and, ultimately, transfection efficiency. Two prevalent techniques are utilized for this purpose: The first approach involves using a fixed quantity of genetic material to achieve a designated N/P ratio. In contrast, the second method maintains a constant quantity of polycation, allowing for variations in the amount of genetic material. These distinct approaches are instrumental in modulating the physical and chemical properties of polyplexes, thereby impacting their cellular uptake and overall transfection efficiency. In addition to surface charge, polyplex size is equally important. It is believed that 120 nm is the maximum size to be internalized via clathrin-mediated endocytosis.[95] Exceeding this threshold can limit the polyplex uptake and hinder the transfection's efficacy. Various other size limits apply to different internalization pathways; a smaller size generally seems beneficial for internalization.[96] Many established methods, such as dynamic light scattering (DLS) and zeta potential measurements, are used to elucidate these characteristics. Next to those conventional techniques, more size-determining procedures can be used, such as small-angle X-ray scattering (SAXS) and atomic force microscopy (AFM).[97–100] These procedures could deliver a more detailed insight into sub-100 nm structures in a polyplex solution. This way, other interesting parameters such as free, not bound to genetic

material polymer could be identified. The methodology employed in polyplex formation significantly influences the polyplexes' characteristics, which in turn affects their internalization mechanism.

1.4   Mammalian cells

Understanding the cellular side is essential for gene delivery and efficient transfection. However, not all mammalian cells respond equally to transfection methods, leading to varying levels of success. This discrepancy arises from inherent cellular characteristics and unique cellular functions that either facilitate or hinder the uptake and integration of genetic material.[53,79] Cells exhibit remarkable diversity in origin, structure, and function. Different cell types may originate from distinct tissues, organs, or organisms, leading to variations in membrane properties and internal machinery.

Consequently, the physicochemical properties of the cellular membrane, such as surface charge and lipid composition, can significantly influence transfection efficiency. Various transfection techniques exist, such as chemical, physical, and viral-mediated methods. Each method has its strengths and limitations, with some being more suitable for specific cell types than others. For instance, lipofection, a chemical-based method, is effective for many adherent cells but might not work as well for certain suspension cell lines. Similarly, electroporation, a physical transfection approach, is advantageous for delivering nucleic acids into difficult-to-transfect primary cells but may not yield optimal results in immortalized cell lines.

Cells have evolved intricate defense mechanisms to protect themselves from foreign entities, including nucleic acids, that could disrupt cellular homeostasis or promote harmful effects. For example, the presence of nucleases can degrade exogenous genetic material before it has a chance to be transcribed or translated. Additionally, endocytosis, a cellular uptake mechanism, can internalize and degrade foreign nucleic acids before they reach the cell's nucleus, rendering them ineffective in altering gene expression. The cell's state in the cell cycle and its level of differentiation can impact transfection efficiency. Cells in specific cell cycle phases, such as S-phase, may exhibit increased accessibility to transfection due to their heightened metabolic and replicative activity. Additionally, less differentiated or stem-like cells often display increased transfection efficiency due to their greater plasticity and more accessible chromatin structure.

Despite the challenges posed by varying cell types, the rationality of transfecting different cells lies in its potential to uncover crucial biological insights and applications. Given the distinct roles of various cell types in bodily functions, elucidating the genetic functions is necessary for

advancing biomedical research and therapeutic interventions. Specifically, the targeted transfection of select cell types is crucial for developing gene therapies to correct genetic anomalies and treat cellular diseases. Moreover, transfection techniques are instrumental in bioprocessing applications, where cells are genetically engineered to augment protein production, showcasing the technique's versatility in both research and therapeutic contexts.

1.4.1 ARPE-19 cells

The outermost layer of the retina, the retinal pigment epithelium (RPE), has been shown to play a critical role in the physiology of the underlying photoreceptors.[101] Age-related macular degeneration (AMD) is one of the most common causes of irreversible blindness in the elderly.[102,103] Approximately 200 million people worldwide are affected by one form of AMD.[104] Generally, AMD can be categorized into early-, intermediate-, and late stages. The latter is further subdivided into the "dry" and "wet" forms of the illness.[102–104] The "wet" condition is treated by injecting a VEGF inhibitor into the eye monthly, while no known therapy is applicable for the "dry" form, which makes up about 90% of all late-stage AMDs.[102,104,105]

Therefore, a need for new and reliable treatment methods is in high demand. One promising approach relies on gene therapy, which has become one of the most impactful research topics of our time. In the context of AMD, this kind of care can involve genetically modified RPE cells, which constantly express various proteins that ensure the cell's survival and retain their functionality. The first steps for this kind of treatment must be done on adequate model cells to ensure feasible genetic modification. One potential model is the ARPE-19 cell line, derived post-mortem from a male human donor. It still carries many properties of primary RPE cells, such as their growth behavior (monolayer), morphology (cobblestone), and selective RPE makers (CRALBP).[106] Furthermore, replacing primary RPE cells in animals with ARPE-19 cells showed functional compatibility and strengthened their role as potential model cells.[107] ARPE-19 cells are known to be challenging to transfect and need additional optimization of the transfection parameters combined with a suitable vector.[108–110] Although various groups have successfully transfected ARPE-19 cells, no commercially available vector could achieve transfection efficiencies $> 58\%$.[111,112] Physical methods such as nucleofection used by THUMANN et al. achieved the best results with a transfection efficiency of $\approx 80\%$ but with no information on cell viability (CV).[113] Polymeric vectors were used by SUNSHINE et al. and could reach a TE of 44% while maintaining a CV of 77%.[108] SUN et al. could achieve 80% TE and high CV with a polymer-lipid formulation that could transfect ARPE-19 cells in a serum-containing medium.[114] While these results are noteworthy, the transfection agents were

specially prepared in-house and are not as easily replicated, which makes application outside the lab difficult.[108,115]

Despite the challenges, the immortalized cell line ARPE-19 is a viable alternative for primary human cells for research applications. Given this, refining the transfection approach by incorporating a readily available transfection agent becomes crucial.

1.4.2 B cells

B-lymphocytes, also known as B cells, are a critical component of the adaptive immune system, playing multifaceted roles in immune defense, regulation, and homeostasis. These cells are primarily recognized for their capacity to produce antibodies, which are crucial for neutralizing pathogens and facilitating their clearance by other immune cells.[116,117] Beyond antibody production, B cells exert regulatory functions through cytokine secretion, antigen presentation, and the modulation of T-cell responses, thereby influencing both innate and adaptive immunity.[118–120] Given the diverse functions of B cells within the human body, it is anticipated that differentiation occurs during their maturation process (Figure 16). This differentiation can be replicated *in-vitro* by culturing B cells in a medium supplemented with CD-40 ligand (CD-40L).
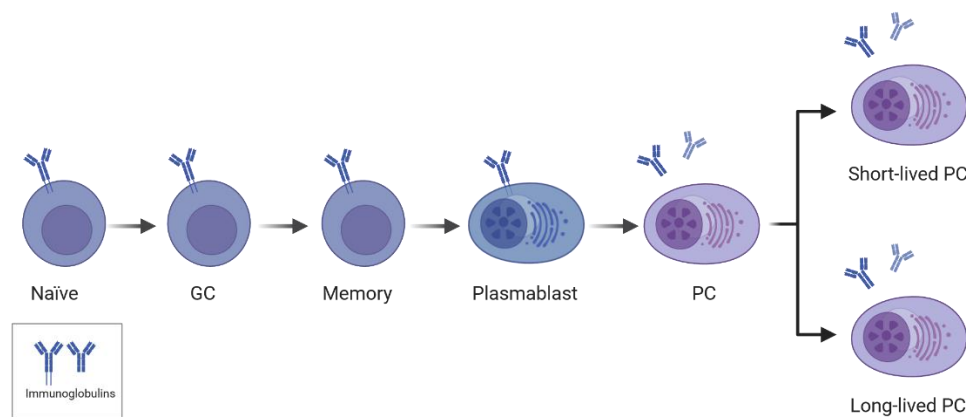

Figure 16: Differentiation pathway of B cells.[16,121]

Through this process, B cells differentiate into multiple subclasses, namely naïve-, memory-, germinal center- (GC), and plasma-cells (PC), which can be discriminated by their clusters of differentiation (CD).[122,123] All B cells express CD-19 and can thereby be unmistakably classified as such.[124] Other CD markers include CD-20, CD-27, and CD-38, which can be used to further classify B cells into the subclasses mentioned above (Table 2). Immunophenotyping makes it possible to distinguish various CD-markers in flow cytometric measurements.

Table 2: B cell subclasses and their respective CD-marker differentiation.

Subclasses	Classification[1]
CD20$^+$CD27$^-$CD38$^{-/+}$	Naive
CD20$^+$CD27$^+$CD38$^-$	Memory
CD20$^{-/+}$CD27$^+$CD38$^+$	GC
CD20$^-$CD27^{++}CD38^{++}	Plasma

[1] Classification according to JACKSON et al.[125,126]

For transfection purposes, it is advantageous for the transfected cell to produce large quantities of protein consistently, irrespective of the cell type. PC, also known as antibody-producing cells (APC), are particularly well-suited for this role. Within the organism, these cells are tasked with synthesizing antibodies, indicating that they are already equipped with the required machinery for efficient protein production. Consequently, genetically modified plasma cells represent optimal candidates for producing desired proteins, utilizing their intrinsic capabilities for high-level protein synthesis.

1.5   CRISPR/Cas

The discovery and development of the clustered, regularly interspaced short palindromic repeats (CRISPR) CRISPR/Cas system has ushered in a new era of genome editing and genetic research.[127] Based on bacteria's natural immune defense mechanisms, this technology has been harnessed as a powerful tool for precise and efficient genome editing in various organisms, including humans.[128,129] Of the various CRISPR/Cas systems discovered, the CRISPR/Cas9 system has emerged as the most widely used genome editing due to its simplicity and versatility. The Cas9 protein acts as a molecular scalpel that can precisely cut DNA at specific locations guided by a synthetic RNA molecule known as single-guide RNA (sgRNA). The sgRNA is designed to be complementary to the target DNA sequence, directing Cas9 to the desired genomic location. Once the Cas9 protein locates the target, it generates double-strand breaks (DSBs) in the DNA, triggering the cell's repair machinery (Figure 17).[130]

In transfection studies, researchers utilize the CRISPR/Cas9 system to introduce specific genetic alterations into the genome of target cells. This process involves the delivery of the CRISPR/Cas9 components into the cells. Once inside the cell, the CRISPR/Cas9 system guides the Cas9 protein to the target DNA sequence, where it introduces DSBs. The cell's natural DNA repair mechanisms, namely non-homologous end joining (NHEJ) and homology-directed repair (HDR), are then activated to fix the damage and introduce the genetic cargo directly into the double-strand.
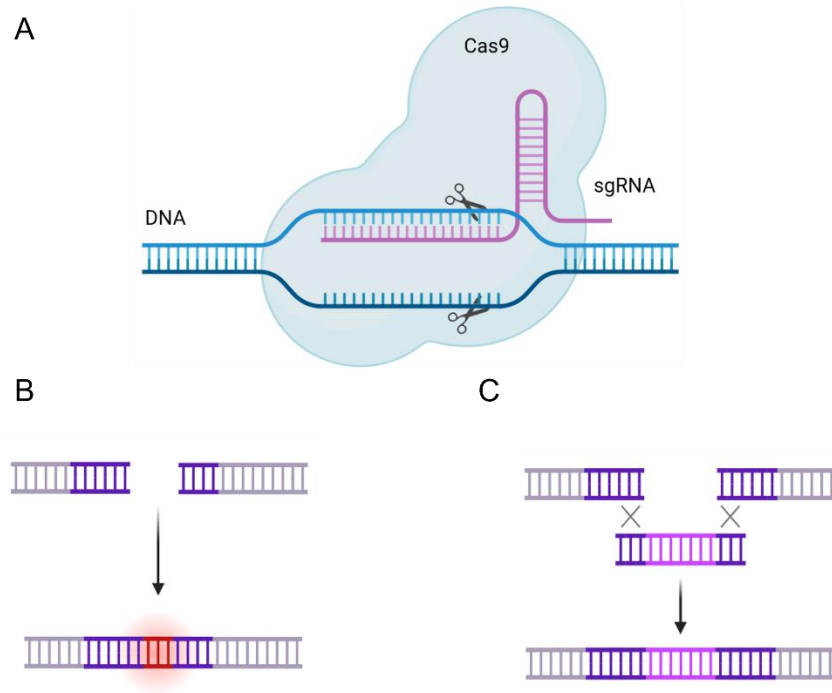
Figure 17:(A) CRISPR/Cas9 mechanism, (B) NHEJ, (C) HDR.[16]

NHEJ is the primary repair mechanism for DSBs and involves directly ligating the broken ends back together. While this process is error-prone and can result in small insertions or deletions (indels) at the repair site, it is highly efficient. However, HDR relies on a DNA template, often a donor DNA molecule, to guide repair. This process can be harnessed to introduce precise genetic changes, such as specific base substitutions or the insertion of new sequences. However, HDR occurs at a lower frequency than NHEJ. [131,132]

1.6 Objective of this work

A profound understanding of cells is indispensable for addressing the growing demands of medical and biotechnological applications. Transfection serves as a fundamental tool in manipulating cellular processes; successfully employed, it enables the management of metabolic pathways through molecules like siRNA or incorporating novel gene sequences via CRISPR-Cas9. Nonetheless, uniform transfection efficiency is not guaranteed across all cell types — primary cells, in particular, present challenges, necessitating meticulous optimization for reliable outcomes. Many parameters, such as the polycation dose or contact time between cells and polyplexes, must be evaluated to improve transfection outcomes (Figure 18).
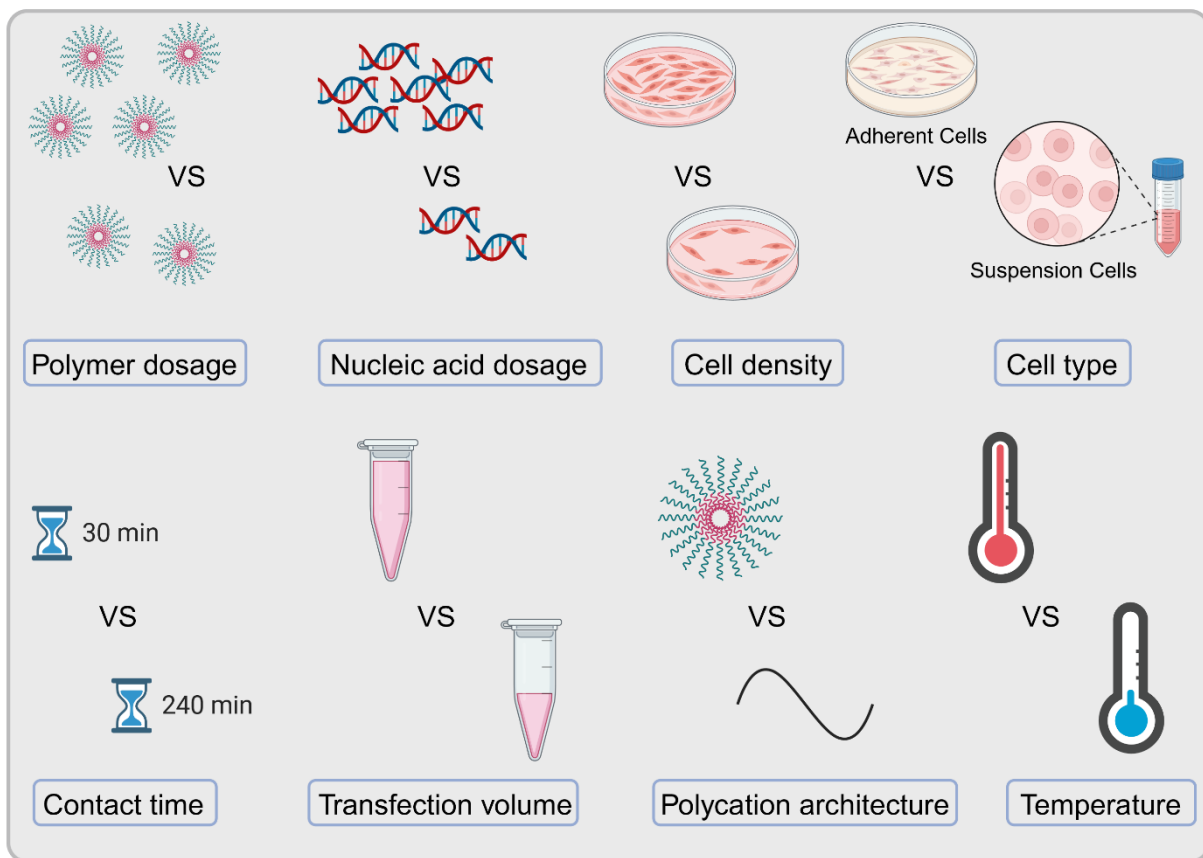

Figure 18: Various parameters influencing transfection outcome.[16]

This study aims to enhance our understanding of the transfection process in primary human B cells and the ARPE-19 cell line. Both cell types are considered hard to transfect, particularly when utilizing polycations. A multiparametric approach will be employed to achieve higher than previously reported transfection efficiencies while ensuring satisfactory cell viability.

2 Materials & Methods

2.1 Materials

If not otherwise indicated, Greiner Bio-One (Frickenhausen, Germany) was used as the supplier for cell culture materials and Sigma-Aldrich (Taufkirchen, Germany) as chemicals. Linear PEI (l-PEI, 25 kDa) was from Polysciences (Polysciences Europe GmbH, Eppenheim, Germany). The "nanostar" was kindly provided by Dr. C.V. Synatschke (Max Planck Institute for Polymer Research, Mainz, Germany). This transfection agent is not commercially available but can be synthesized following a published protocol.[133] Fetal calf serum (FCS) was from Biochrom (Biochrom AG, Berlin, Germany). Dulbecco's Modified Eagle's Medium (DMEM) was from VWR (Ismaning, Germany). Dulbecco's phosphate-buffered saline (DPBS) without Ca^{2+} and Mg^{2+}, Trypsin/EDTA, and penicillin/streptomycin were from Lonza (Visp, Switzerland). Amphotericin B was from Corning (NY, USA). L-Glutamine was from Gibco (Fisher Scientific, Schwerte, Germany). HBG buffer (20 mM Hepes, 5 wt % glucose, pH 5.5) was prepared in-house and sterilized by filtration (Chromafil®, CA-20/25(S), 0.2 µm; VWR, Ismaning, Germany). OPTI-MEM culture medium supplemented with GlutaMAX was from ThermoFisher Scientific (Dreieich, Germany). The staining dye peqGREEN was from VWR (Ismaning, Germany). Primers for cDNA synthesis were from Microsynth AG (Balgach, Switzerland). Sterile ultra-pure PCR water was from Sigma-Aldrich (Taufkirchen, Germany). For pre-equilibration, media were incubated for 1 h in a standard mammalian cell culture incubator (37 °C, 5% CO_2, 95% humidity). For induction of the B cell proliferation, the following medium was used (referred to as "B cell growth medium": 88% IMDM medium, 10% human AB serum, Cyclosporin A (CsA, 1 µg/mL) all from Sigma-Aldrich (Taufkirchen, Germany), 1% Ultraglutamine (200 mM, Lonza, Visp, Switzerland), ITS-G (100×, ThermoFisher, Dreieich, Germany), Interleukin-4 (rhIL-4, 10 ng/mL), Interleukin-21 (rhIL-21, 20 ng/mL), B cell activating factor (rhBAFF, 4 ng/mL), rhCD40L (400 ng/mL) all from Miltenyi Biotec (Gladbach, Germany). Tonsillar tissue as the source for the B cells was obtained during routine tonsillectomy (complete removal of the tonsillar tissue) (Gemeinschaftspraxis Gollner, Kulmbach, Germany). Written consent for the intended utilization was obtained, after verbal and written information on research goals, as approved by the ethical review committee from the University of Bayreuth, Germany (written approval #O 1305/1-GB, 2018).

2.2 Methods

2.2.1 Cell culture

ARPE-19 cells

The ARPE-19 cell line (immortalized retinal pigmented epithelial cells (RPE), ATTC, CRL-2302) was cultured in DMEM supplemented with 10% (v/v) FCS, 4 mM L-Glutamine, 100 U/mL penicillin/streptomycin, and 2.5 µg/mL amphotericin B. This medium is referred to as D10. The cells were passaged twice per week for cell maintenance with a starting cell density of 50,000 cells/mL. The cells were collected by trypsinization (5 min incubation time, 37 °C, 5% CO_2, 95% humidity).

B-Lymphocytes

B cells were isolated as previously described.[122] Briefly, after removal by surgery, tonsillar tissue was immediately transferred into an ice-cold buffer (HBSS containing 100 U mL^{-1} penicillin, 100 µg/mL streptomycin, 2.5 µg/mL amphotericin B, 2mM Ethylenediaminetetraacetic acid (EDTA), and 0.5% (w/v) bovine serum albumin (BSA)) and placed on ice for the transport. Upon receiving the tonsillar tissue in the laboratory, it was transferred to RPMI1640 culture medium and segmented into fine sections. These sections were then applied to a 70 µm cell strainer (Greiner Bio-One, Frickenhausen, Germany) positioned atop a 50 mL centrifuge tube. The tissue fragments were forced through the strainer's mesh using a syringe plunger for assistance. The remaining erythrocytes were incubated in an Erylysis buffer (1×) for 5 min. According to the supplier's instructions, cell debris, and any remaining red cells were removed by density gradient centrifugation (Ficoll LSM 1077; PAA Laboratories GmbH, Pasching, Austria). Mononuclear cells were collected and resuspended in HBSS containing 10% (v/v) heat-inactivated FCS ("HBSS-FCS"). A maximum of 4×10^8 cells in 4 mL HBSS-FCS were filled into a sterilized 20 mL syringe column (B. Braun, Melsungen, Germany) packed with 1 g sterile nylon wool (Polysciences Inc., Hirschberg an der Bergstrasse, Germany) and incubated upright for 1 h in the cell culture incubator (37 °C, 95% humidity, 5% CO_2). Afterward, the non-bound cells (mainly T cells) were eluted by gently rinsing the wool twice with one column volume of HBSS-FCS. The B cells were collected by filling the column with fresh HBSS-FCS, followed by mechanical agitation to detach the cells. Subsequently, the wool was squeezed by pushing down the syringe piston to flush out the B cells. This step was repeated twice. B cells were recovered by centrifugation (300×g, 5 min) and resuspended in cryo-medium (90% FCS-10% DMSO) before cryopreservation. For the experiments, cells were

thawed, and 1 mL of the obtained B cell suspension was washed with 9 mL DPBS. The cells were recovered by centrifugation (400×g, 10 min), the supernatant was discarded, and the cell pellet was resuspended in B cell growth medium. The cells were then seeded at a cell density of 10^6 cells mL^{-1} into tissue culture plates (10 cm Petri dish) for expansion. Before transfection, the B cells were incubated (37 °C, 95% humidity, 5% CO_2) in the B cell growth medium with medium change every 4 days for up to 8 days to induce proliferation.

2.2.2 Polynucleotides

Plasmids

Plasmid pEGFP-N1 (4.7 kbp) was used for polyplex formation by Clontech Laboratories, Inc. (Mountain View, CA, USA). The plasmid encodes for an enhanced Green Fluorescent Protein (referred to as GFP) and was amplified in *Escherichia coli* using standard laboratory techniques (LB medium supplemented with 30 µg/mL kanamycin). The EndoFree Plasmid Kit (Giga Prep/Maxi Prep) from QIAGEN (Hilden, Germany) was used for plasmid preparation (quality control: >80% supercoiled topology (agarose gel) and $A_{260}/A_{280} \geq 1.8$). Purified plasmids were solubilized in sterile ultrapure PCR-water (Sigma-Aldrich, Taufkirchen, Germany).

Plasmid pAAVS1 (5.4 kbp) was used for polyplex formation by VectorBuilder GmbH (Neu-Isenburg, Germany). The plasmid encodes for an enhanced Green Fluorescent Protein (referred to as EGFP), a left-homology arm (L-HA), and a right-homology arm (R-HA) in analogy to the AAVS1 locus and was amplified in *Escherichia coli* using standard laboratory techniques (LB medium supplemented with 50 µg mL^{-1} ampicillin). The EndoFree Plasmid Kit (Giga Prep/Maxi Prep) from QIAGEN (Hilden, Germany) was used for plasmid preparation (quality control: >80% supercoiled topology (agarose gel) and $A_{260}/A_{280} \geq 1.8$). Purified plasmids were solubilized in sterile ultrapure PCR-water (Sigma-Aldrich, Taufkirchen, Germany).

mRNA

EGFP mRNA was synthesized from complementary DNA (cDNA) produced via PCR using pEGFP-N1 as a template and primers adapted from Herb *et al.*.[134] Briefly, 100 ng pEGFP-N1 was mixed with 10 µM of each primer (eGFP$_{for}$: 5'-GAAATTAATACGACTCACTATAGGGATCCATCGCCACCATGGTGAGCAAGG-', 51 nt, Tm: 73 °C; eGFP$_{rev}$: 5'-TGGTATGGCTGATTATGATCTAGAGTCG-', 28 nt, Tm: 67 °C), as well as Q5® High-Fidelity 2X Master Mix (New England Biolabs GmbH, Frankfurt am Main, Germany) in a total volume of 50 µL, and pulse-spun in a microfuge at

2000 g. Afterward, the PCR program was run in a Thermocycler (Thermo Scientific Hybaid PX2 thermal cycler, Cole-Parmer® GmbH, Wertheim, Germany). The PCR conditions were (1) initial denaturation cycle at 98 °C for 30 s, (2) denaturation cycle at 98 °C for 10 s, (3) annealing cycle at 70 °C for 30 s, (4) elongation cycle at 72 °C for 2 min and (5) final elongation cycle at 72 °C for 2 min. Steps (2) to (4) were repeated 35 times. Amplification was checked by agarose gel electrophoresis of the PCR product, analyzing 15 µL of PCR mixture with 6X Orange Loading Dye (Fermentas, Waltham, MA, USA). The 1% agarose gel was run at 90 V/60 min in 1X Tris-acetate-EDTA (TAE) buffer. The PCR product was purified via ethanol precipitation by adding 5 µL 3 M sodium acetate and 150 µL ice-cold ethanol absolute to precipitate the cDNA at -20 °C for at least 16 h. The DNA was centrifuged (30 min., 4 °C, 16.060 g) (Heraeus Biofuge Pico, Heraeus, Hanau, Germany) and the pellet was washed twice in ice-cold 70%-ethanol (10 min., 4 °C, 16.060 g). Afterward, the pellet was resuspended in sterile ultra-pure PCR water. The quality of the cDNA was analyzed via spectrophotometry ($A_{260/280} \geq 1.8$) using a NanoDrop^{TM} 2000 (Thermo Fisher Scientific, Dreieich, Germany).

mRNA was prepared from the cDNA using the HiScribe™ T7 ARCA mRNA Kit (New England Biolabs GmbH, Frankfurt am Main, Germany). We slightly modified the manufacturer's protocol by carrying out all incubation steps at 37 °C and 300 rpm. Precipitation was performed overnight (24 h) at -20 °C. mRNA quality was analyzed by 1% agarose gel electrophoresis (90 min., 65 V) in 1X Tris-acetate-EDTA (TAE) buffer and spectrophotometry ($A_{260/280} \geq 2.0$, $A_{260/230} = 2.3$-2.4).

CleanCap Cas9 mRNA was purchased from Tebubio GmbH (Offenbach, Germany). The mRNA encodes a variant of the Cas9 protein from Streptococcus pyogenes SF370, known as CRISPR Associated Protein 9.

sgRNA

The sgRNA was from Thermo Fisher (TrueGuide™ sgRNA Positive Control, AAVS1 (human)) with a matching AAVS1 sequence (GCCAGUAGCCAGCCCCGUCC).

2.2.4 Transfection

Polycationic transfection agents

Besides the l-PEI from Polysciences, a well-defined star-shaped polymer (referred to as nanostar) synthesized in-house via atom-transfer radical polymerization (ATRP) of DMAEMA was used as a polycationic transfection agent. Synthesis and characterization of the nanostar have been described previously.[135] An average nanostar consists of an inorganic core decorated with 24 polycationic PDMAEMA arms, each with an average length of 230 monomeric units; see structure below. The construct's average molecular weight, M_n, was 755 kDa, and the polydispersity (M_w/M_n) was <1.21.
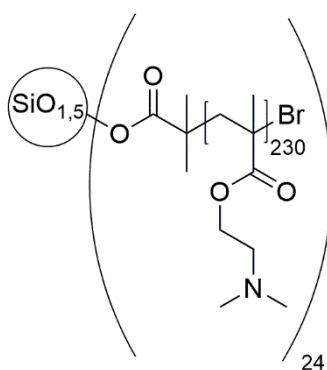
Polymer stock solutions were prepared in sterile ultrapure PCR-water (Sigma-Aldrich, Taufkirchen, Germany) as 1.25 mg/mL (l-PEI) and 1.82 mg/mL (nanostar) and diluted for use as indicated. LD_{50} values were 12.1 µg/mL for l-PEI and 500 µg/mL for nanostar, as previously determined by a standard MTT assay using L929 cells.[133,136]

N/P-Ratio Calculation

N/P-ratios were calculated according to:

$$N/P = \frac{(\mu L\ polycation\ stock\ solution * N)}{(\mu g\ pDNA * p)}$$

Equation 3: With N = concentration (mM) of nitrogen residues in the transfection agent and p = nmoles phosphate in genetic material. Note: 1 µg of DNA and mRNA containing 3 nmoles and 3.11 nmoles of anionic phosphate, respectively

Transfection Protocols

Adherent cells

For transfection, cells were harvested by trypsinization, seeded at the desired concentration in the plate (6- or 12-well), and incubated for 24 h in the cell culture incubator. For polyplexes preparation, the N/P ratio was set either by using a constant amount of polynucleotide while adjusting the polymer concentration or by using a constant amount of polymer while adjusting the polynucleotide concentration. On the day of transfection, polyplex was prepared by first diluting a suitable amount of genetic material in HBG buffer. The mixture was vortexed for approximately 1 sec before the required amount of transfection agent was added in a single drop. Immediately after, the polyplex solution (200 µL for transfection in 6-well plates; 50 µL for transfection in 12-well plates) was vortexed for precisely 10 sec at 2200 rpm. The mixture was incubated at room temperature for 20 min, followed by the addition of Opti-MEM (450 µL per 50 µL of polyplex solution). This was followed by another 10 min incubation at room temperature. After that, cells were washed twice with DPBS, and the polyplex solution was added. Polyplexes were spread by gentle mixing before placing the plates in the cell culture incubator (37 °C, 95% humidity, 5% CO_2) for up to 4 h. After the indicated period, the polyplex solution was discarded and replaced by 1 mL (12-well plate) or 2 mL (6-well plate) D10-medium before placing the cells back into the cell culture incubator (37 °C, 95% humidity, 5% CO_2) for up to 48 h. As a negative control, the cells were also put through a mock transfection ("Mock"), i.e., solely incubated with the complexation buffer. For analysis by flow cytometry, the cells were harvested by trypsinization and centrifugation (300×g, 5 min) and resuspended in DPBS supplemented with propidium iodide (PI, 1 µg/mL) to counterstain dead cells.
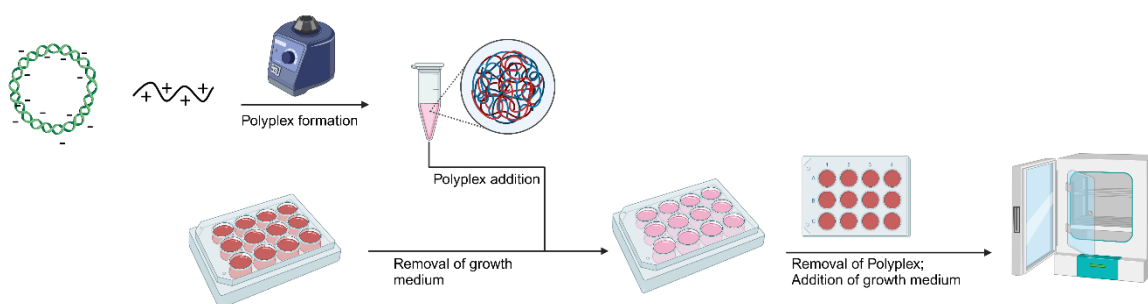

Figure 19: Plate-transfection procedure.

Suspension cells

Before transfection, B cells were cultivated in growth medium to induce the proliferation. Usually, 3 to 6 days were necessary to produce a sufficient number of cells for transfection. On the day of transfection, the cells were collected by centrifugation (400×g, 10 min) and washed twice with 10 mL DPBS. After resuspension in Opti-MEM, cell count and viability were determined with a LUNA-FL™ Dual Fluorescence Cell Counter (Logos Biosystems, Gyeonggi-do, South Korea). Thereafter, the cells were transfected with l-PEI or nanostars according to the procedures described below.

Well plate transfection protocol

1 mL of the cell suspension (2×10^5 cells/mL in OPTI-MEM) was transferred into a well of a 6-well plate and incubated (37 °C, 95% humidity, 5 % CO_2) while the polyplexes were being prepared. For polyplex preparation, the first 3 µg of pDNA was mixed with HBG-buffer unless otherwise mentioned. The mixture was vortexed for approximately 1 sec before the amount of polymer needed for the intended N/P ratio was added in a single drop. Immediately after, the mixture (200 µL) was vortexed for precisely 10 sec at 2200 rpm and incubated at room temperature. After 20 min of incubation, 800 µL of OPTI-MEM was added per 200 µL of polyplex solution, followed by incubation for 10 additional min at room temperature. 1 mL of the polyplex solution was added to the cell suspension in the 6-well plate (total volume per well then: 2 mL) and incubated (37 °C, 95% humidity, 5% CO_2) for 240 min. Afterward, the cell/polyplex mixture was transferred to a micro-tube, and the cells were separated from the supernatant by centrifugation (400×g, 10 min). The supernatant was discarded, and the cell pellet was suspended in 500 µL of growth medium by gently pipetting up and down and transferred to the well of a 24-well plate. The tube was then rinsed with 500 µL growth medium, which was added to the corresponding well (total cultivation volume: 1 mL). The plate was placed in the cell culture incubator (37 °C, 95% humidity, 5% CO_2) for up to 48 h.
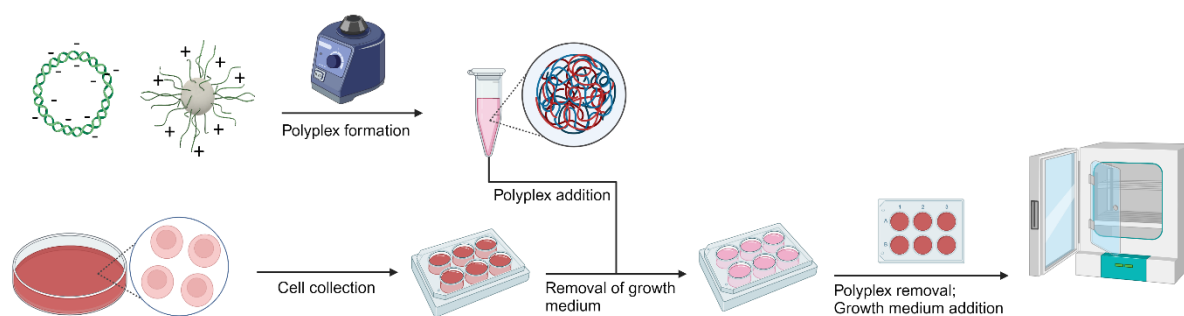
Figure 20: Well plate protocol

Tube transfection protocol

1 mL of the cell suspension (2×10^5 cells/mL in OPTI-MEM) was transferred into a micro-tube and stored on ice while the polyplexes were prepared. In this protocol, the N/P ratio was adjusted by varying the amount of pDNA while keeping the polymer amount constant. For polyplex preparation, an HBG buffer was first added, followed by a suitable amount of pDNA needed for the intended N/P ratio. The mixture was vortexed for approximately 1 sec before the required amount of transfection agent was added in a single drop. Immediately after, the polyplex solution (50 µL) was vortexed for precisely 10 sec at 2200 rpm. The mixture was incubated at room temperature for 20 min, followed by the addition of 450 µL of Opti-MEM per 50 µL of polyplex solution. This was followed by another 10 min incubation at room temperature. The cells stored on ice were recovered by centrifuging ($400 \times g$, 10 min), and the supernatant was discarded. The cell pellet was mechanically dislocated before adding the polyplex/OPTI-MEM mixture. Cells and polyplexes were gently mixed before placing the tube upright in the cell culture incubator (37 °C, 95% humidity, 5% CO_2) for up to 90 min. After the indicated time span, the cells were recovered by centrifugation ($400 \times g$, 10 min), the supernatant was discarded, and the cell pellet was resuspended in 500 µL of growth medium. After mixing in by gently pipetting up and down, the cell suspension was transferred into the well of a 24-well plate. The tube was then rinsed with 500 µL growth medium, which was added to the corresponding well (total cultivation volume: 1 mL). The plate was placed in the cell culture incubator (37 °C, 95% humidity, 5% CO_2) for up to 48 h. To investigate the influence of the transfection procedure per se, aliquots of the cells were always put through a mock transfection (referred to as "Mock"), i.e., were solely incubated with the complexation buffer.
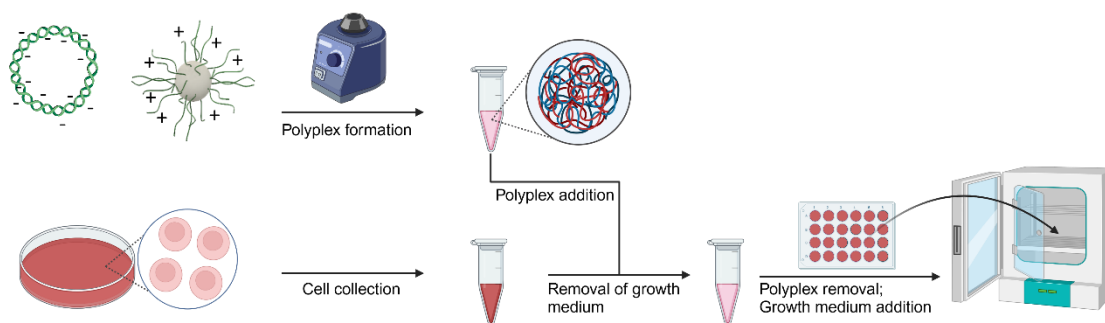
Figure 21: Tube-transfection procedure.

2.2.5 Analytics

Determination of cell number and viability

A LUNA-FL™ Dual Fluorescence Cell Counter (Logos Biosystems, Gyeonggi-do, South Korea) was used to determine the number and viability of the cells. For this purpose, the cells were stained with an Acridine Orange (AO, staining all cells)/Propidium Iodide (PI, staining dead cells) solution (Logos Biosystems, Gyeonggi-do, South Korea) according to the supplier's instructions.

Determination of the transfection efficiency (EGFP fluorescence) and survival rate

The transfection efficiency (TE) was assessed via the EGFP fluorescence by flow cytometry (Cytomics FC500; dual laser (488 nm, 635 nm); Beckman Coulter, Krefeld, Germany). Forward scatter (FSC), side scatter (SSC), green fluorescence (GFP, em 525 nm), and red fluorescence (PI, em 620 nm) were recorded. Negative controls, i.e., mock-transfected cells, were used to set the measurement parameters. Data were collected from at least 30,000 events. Cells were initially evaluated by scatter properties (FSC/SSC) to select the appropriate population (Gate: "ARPE-19" or "Lymphocytes") and to exclude aggregates and apoptotic cells. The relative EGFP fluorescence of the gated cells was measured, allowing a statistical quantification of the percentage of transfected cells "transfection efficiency", TE) in the appropriate population. We defined EGFP-expressing cells as cells having a higher fluorescence than the mock-transfected cells (i.e., autofluorescence of the cells). This cell population was consequently analyzed for red fluorescence intensity (PI) to determine cell viability. Histogram plots of the respective fluorescence intensities (log scale) were used to estimate the percentage of transfected cells and the expression level distribution according to: low producers (Low), fluorescence intensity between 10^3 a u and 10^4 a u.; middle producers (Middle), fluorescence intensity between 10^4 a u and 10^5 a u.; high producers (High),

fluorescence intensity $>10^5$ a u., in the gate: "ARPE-19". The gating strategy for analyzing the transfected ARPE-19 cells is presented in Figure 22. Flow cytometry data were evaluated using FlowJo software v 10.9.1 (Tree Star, Stanford University, Stanford, CA, USA, 2016).
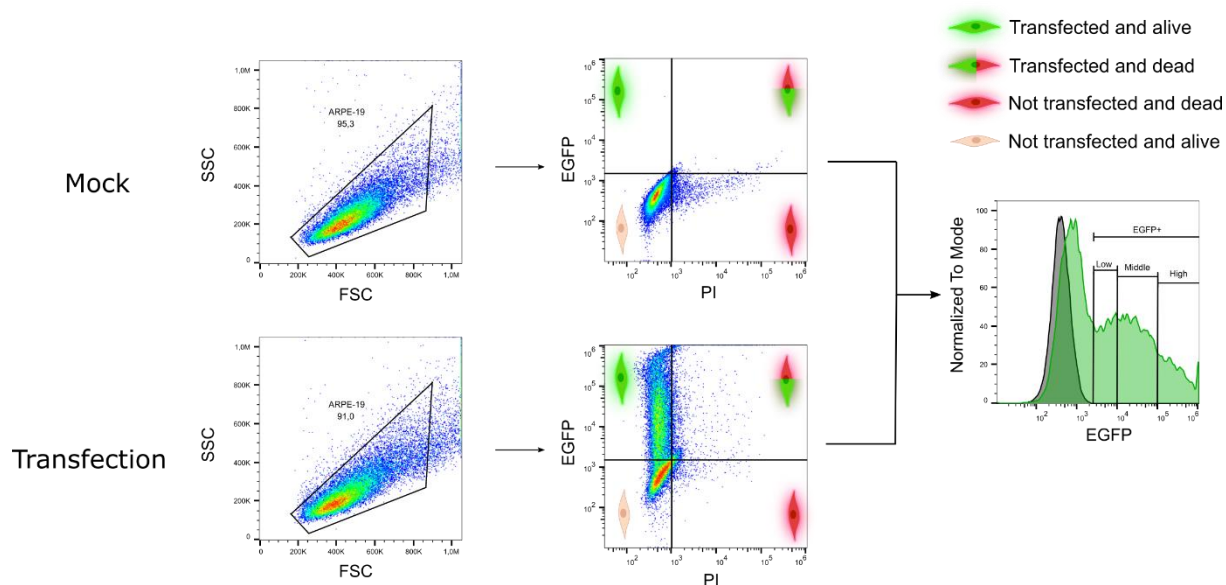

Figure 22: Gating strategy for ARPE-19 cells.

B cells subclasses

For phenotyping B cell subsets, the cell surface markers CD19, CD20, CD27, and CD38 were evaluated utilizing flow cytometry (Cytomics FC500; dual laser (488 nm, 635 nm); Beckman Coulter, Krefeld, Germany). This assessment was conducted following the cell staining process with murine antibodies specific to each CD marker (anti-CD19-APC, catalog #302212; anti-CD20-PE, catalog #302306; anti-CD27-PE-Cy7, catalog #356412; anti-CD38-FITC, catalog #356610; all sourced from BioLegend, San Diego, California, USA), adhering to the guidelines provided by the manufacturer. Briefly, 0.5 x 10^6 cells were washed twice using 1 mL of PBS (400 g, 5 min.) and resuspended in 100 µL of PBS. This was followed by a 30-minute incubation period with the antibodies at 0°C. After the incubation, the cells underwent two additional washes with 1 mL of PBS (400 g, 5 min.) and were then resuspended in 500 µL of PBS for flow cytometry analysis. The flow cytometer settings were adjusted to record 80,000 events per sample. Control samples, which underwent a mock immunostaining procedure, were employed to calibrate the measurement parameters. Data recorded included forward scatter (FSC), side scatter (SSC), and fluorescence intensity measurements for FITC (emission at 525 nm), PE (emission at 575 nm), APC (emission at 655 nm), and PE-Cy7 (emission at 750 nm). Spillover compensation for each antibody was determined using single stains with OneComp eBeads (ThermoFisher, Waltham, Massachusetts, USA).

Gel-retardation-assay

For the gel retardation assay, polyplexes were produced in 50 µL HBG using 2 µg of genetic material and varying amounts of polycationic solution to reach the indicated N/P ratio. Mixtures were vortexed for 10 sec and incubated at room temperature for polyplex formation and maturation. After 20 min of incubation, 5 µL 10X loading buffer (60% glycerol, 10 mM Tris-HCl pH 7.6, 60 mM EDTA, 0.03% bromophenol blue) was added. To analyze mRNA polyplexes, 5 µL of 2X RNAse-free loading buffer (95% formamide, 18 mM EDTA, and 0.025% SDS, 0.15% bromophenol blue) was used instead. Then, 15 µL of these mixtures were analyzed in 1% (w/v) agarose gels with Tris-acetate-EDTA as running buffer (running time 90 min, applied voltage 90 V). Gels were stained with peqGREEN (60 ng/mL), and the genetic material was visualized under ultraviolet (UV) light (254 nm).

Ethidium bromide displacement assay

For the ethidium bromide (EtBr) assay, a constant amount of nucleic acid (2 µg) was used. The genetic material (pDNA, mRNA) was diluted with HBG buffer in a total volume of 100 µL, and 1 µL EtBr (0.1 mg/mL) was added to the mixture. Afterward, the necessary polymer amount was added to achieve the desired N/P ratio, as described above (Equation 3). After brief vortexing (10 s, 2500 rpm), the polyplexes were incubated in the dark for 30 min. The mixture was pipetted into a black 96-well plate and analyzed in a plate reader (GENios Pro, Tecan, Männedorf, Switzerland). As a control, we used HBG with EtBr (background fluorescence of the assay). Also, genetic material (pDNA, mRNA) with EtBr without polymer was measured (maximal achievable fluorescence for the assay). The relative displacement of ethidium bromide was calculated using the following Equation 4.

$$relative\ displacement = 1 - \frac{F_{Obs} - F_0}{F_{NA} - F_0}$$

Equation 4: F_{obs} = fluorescence intensity of the sample, F_{NA} = maximal fluorescence intensity of the nucleic acid, and F_0 = background fluorescence intensity of ethidium bromide in HBG.

2.2.6 Statistical analysis

Group data are reported as mean ± standard deviation. If not otherwise stated, n represents the number of independent experiments. OriginPro software (version 2023, OriginLab, Northampton, MA, USA) was used for one-way and two-way ANOVA with Bonferroni multiple comparison tests to determine whether data groups differed significantly. Statistical significance was defined as $*p < 0.05$, $**p < 0.01$, $*** p < 0.001$, if not otherwise indicated.

2.2.7 Licence agreement

Parts of the schemes and figures were drawn using pictures from Servier Medical Art. Servier Medical art by Servier is licensed under a Creative Commons Attribution 3.0 Unported License (https://creativecommons.org/licenses/by/3.0/).

3   Results and discussion

Delivering genetic material into mammalian cells poses challenges, which can be cell-type-specific. The general assumption is to categorize cells into two broad categories: easy-to-transfect and hard-to-transfect. As the name implies, easy-to-transfect cells can easily internalize genetic material carried by a vector. The reason why some cells are more susceptible to transfection is not yet known. Cell lines, such as Chinese hamster ovary-(CHO) or human embryo kidney-(HEK) cells, are considered to take up genetic material efficiently. In contrast, primary human cells, such as primary B or T cells, and some cell lines, e.g., ARPE-19, seem less prone to transfection.[137] In the following, the transfection of multiple hard-to-transfect cell types will be explored and evaluated for their transfection efficiency (TE) and cell viability (CV).

3.1   Polyplex validation

As mentioned, genetic material cannot pass the cell membrane independently and needs assistance from a suitable vector to be protected from nucleases and mask its negative charge. A more detailed look at polyelectrolyte complexes of genetic material and polycations (polyplexes) will be provided in the following. For successful transfection, several critical physicochemical properties of the polyplex must be aligned. These properties include but are not limited to size and charge. Multiple analysis methods are known by which these properties can be evaluated. A standard technique is the so-called gel retardation assay (GRA); here, polyplexes with varying N/P ratios are prepared and analyzed via gel electrophoresis. Genetic material can be detected via an intercalating dye that exhibits fluorescence under UV light. Once the genetic material is bound in a polyplex, it is shielded from nucleases and intercalating agents such as PeqGreen® or ethidium bromide, thereby evading detection (Figure 23).
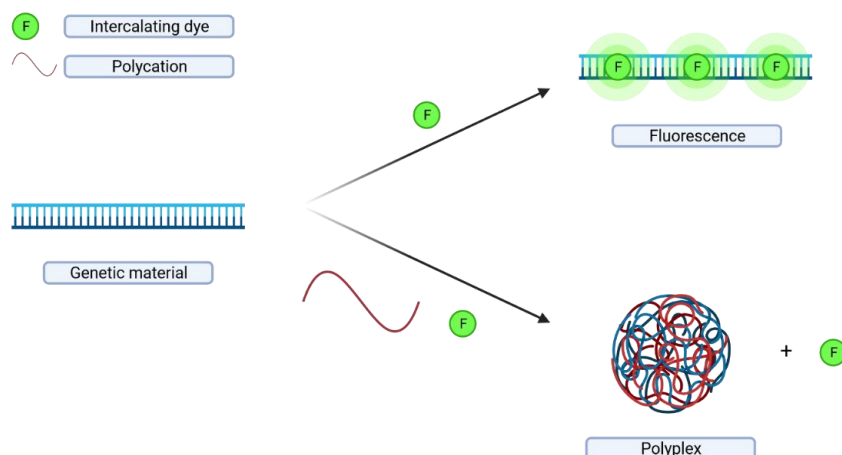
Figure 23:Gel retardation assay outcomes with and without polycation.

The polyplex formation depends on the amount of polycation in relation to the genetic material. While, in theory, an N/P ratio of 1 should be sufficient to bind all genetic material in a polyplex, this is not always the case, most likely attributed to steric hindrance and reachability.[138,139] For l-PEI (25 kDa) and the Nanostar, a complete complexation can be observed above an N/P ratio of 5 and 3, respectively, recognizable by the lack of a fluorescent signal (Figure 24).
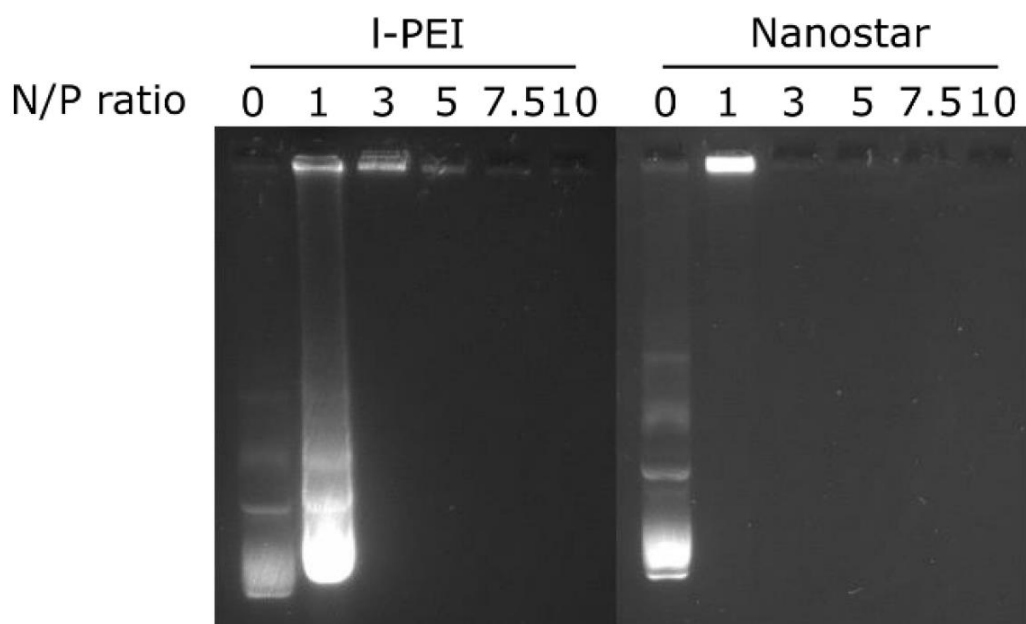
Figure 24: GRA for l-PEI and Nanostar. N/P ratio = 0, represents pDNA only.

This assay is helpful in the determination of which N/P ratios are feasible for transfection and is recommended to perform for every polycation/genetic material combination that will be used in transfection experiments. Due to the comparatively lower stability of mRNA compared to pDNA or other double-stranded polynucleotides, precautions must be taken when conducting the assay for mRNA.[140] For this, the composition of the gel matrix was altered (addition of

formaldehyde) so that degradation of mRNA was limited, and a comprehensive assessment of its complexation with l-PEI and the Nanostar polycation could be conducted (Figure 25).[141]
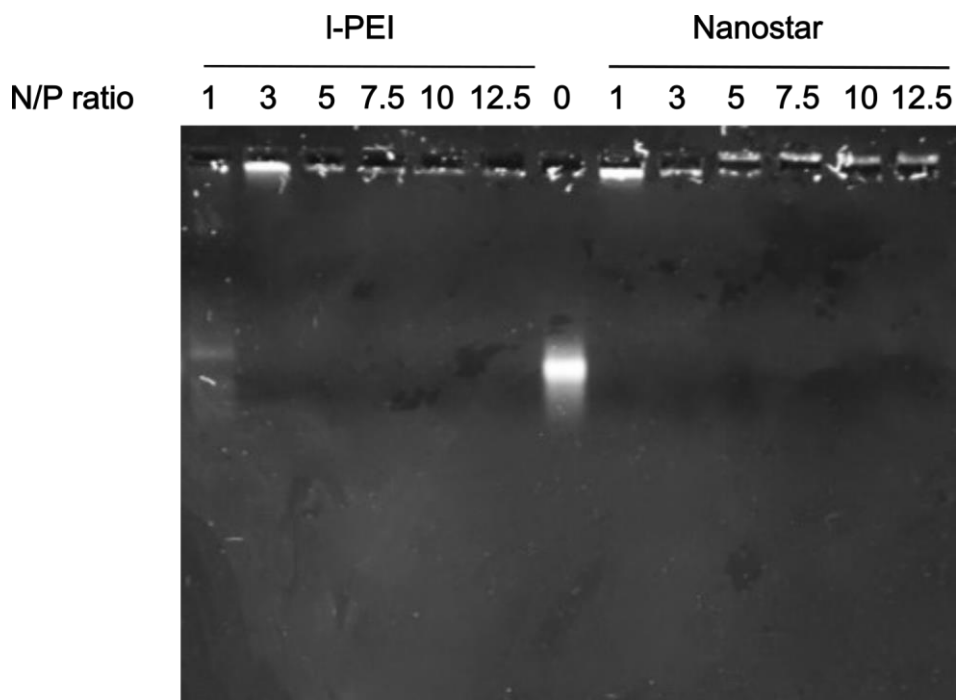
Figure 25: GRA using EGFP-mRNA and l-PEI/Nanostar polycations.

Similar to the GRA using pDNA, mRNA was successfully complexed at an N/P ratio of >3 for l-PEI and >1 for the nanostar polycation.

Since the results of the GRA were cumbersome to obtain when using mRNA (gel preparation), another method was employed in which the complexation of the genetic material could be analyzed. Here, we used an ethidium bromide displacement assay, in which the genetic material is first mixed with the intercalating dye (EtBr), incubated, and then polycation is added. Polyplex formation should start and displace EtBr, after which no fluorescence signal should be detected (Figure 26).
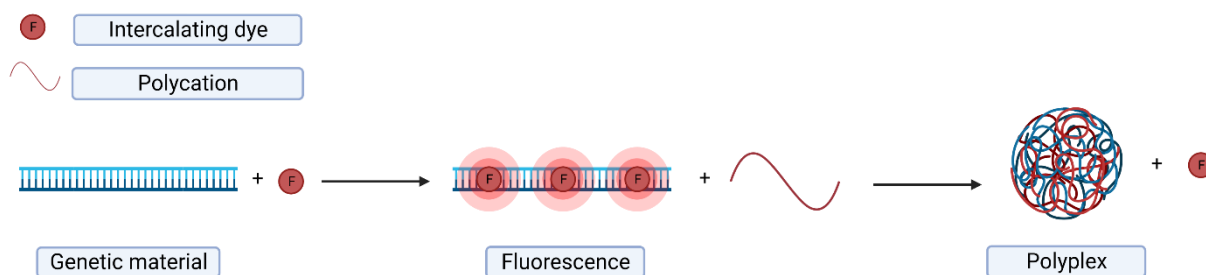
Figure 26: Ethidium bromide assay.

As soon as a plateau can be observed in the ethidium bromide assay, one can assume complete complexation of the genetic material.

Analysis of the EtBr assay shows similar behavior to the GRA. The nanostar polycation can fully complex at an N/P ratio of >1 for pDNA and mRNA. Using l-PEI, one can observe a similar trend as in the GRA in which l-PEI seems to need higher N/P ratios compared to the Nanostar and achieves complete complexation of the genetic material at an N/P ratio of >3 (Figure 27).
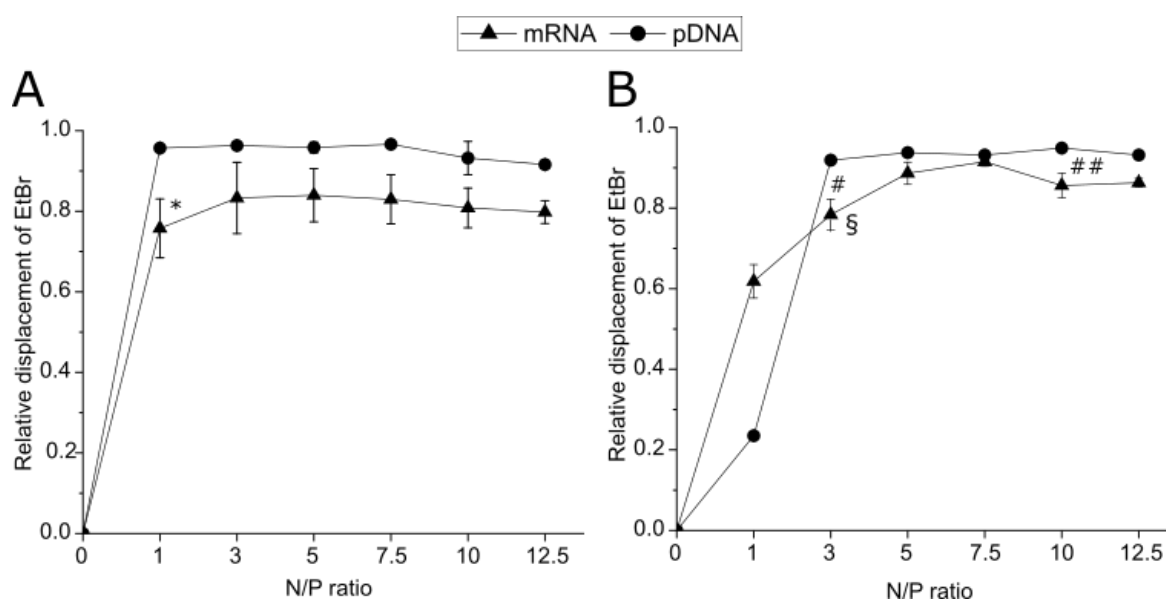

Figure 27:EtBr displacement Assay (A) Nanostar; (B) l-PEI. Statistical significance between N/P 1 mRNA and N/P 1 pDNA for nanostar-based complexation is indicated as * ($p < 0.01$). For PEI-based complexation, statistical significance between N/P 3 pDNA and N/P 3 mRNA is # ($p < 0.001$), between N/P 10 pDNA and N/P 10 mRNA is ## ($p < 0.05$), and between N/P 3 mRNA and N/P 5 mRNA is § ($p < 0.01$). Data represent the mean ± SD, $n \geq 2$.

In general, mRNA fluorescence is lower than pDNA fluorescence, which can be explained by the tendency of EtBr to bind only with double-stranded molecules. In contrast, mRNA is single-stranded; stacked base domains are thought to be necessary for EtBr to intercalate. Since such domains are not the predominant form of the molecule, the overall fluorescence intensity is lower when compared to double-stranded pDNA.[142] Nonetheless, a qualitative assessment can be drawn from this analysis, aligning with the GRA, and can be used as guidance for future N/P ratio evaluation in transfection experiments.

An essential characteristic of polyplexes is their size, with dimensions below 200 nm deemed optimal for endocytotic uptake.[143] The size of these polyplexes is influenced by various parameters, including the composition of the complexation matrix (e.g., 150 mM NaCl, OPTI-MEM, or culture medium), surface charge, and, to a certain extent, the N/P ratio. Analytical

techniques such as Dynamic Light Scattering (DLS) for size determination and ζ-potential measurements for surface charge assessment can be employed.

Previous investigations have demonstrated that the nanostar polycation of approximately 160 nm, corresponding to an N/P ratio of 20, aligns with the optimal range for transfection vectors.[144]
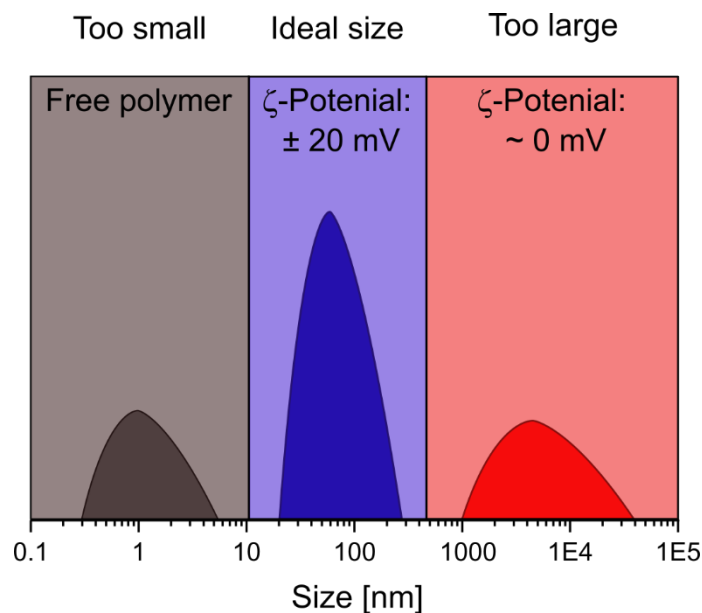

Figure 28: Size dependency of the polyplexes in relation to the zeta potential.

We assumed that a ζ-potential around 0 mV could lead to aggregation and, therefore, bigger polyplexes that the cells could not internalize (Figure 28). This would align with previously reported results that an N/P ratio-dependent size distribution exists for l-PEI and the nanostar polycation.[144]

3.2 Transfection of ARPE-19-cells

The ARPE-19 cell line is a commonly used *in vitro* model for research in ophthalmology and retinal biology. Derived from human retinal pigment epithelial (RPE) cells, ARPE-19 cells are a valuable tool for studying various aspects of retinal function, metabolism, cell physiology, and responses to different stimuli.[101] Dysfunctions in RPE cells are associated with various retinal diseases. ARPE-19 cells serve as a valuable surrogate for primary human RPE cells due to their closely mimicked properties and functions in the retina. Given the limited availability of primary RPE cells, using the ARPE-19 cell line becomes essential, rendering these cells valuable for investigating relevant conditions such as age-related macular degeneration (AMD) or diabetic retinopathy within retinal research.[101,103,145,146] Transfecting these cells allows researchers to study disease-associated genes or the effects of potential therapeutic interventions. Scientists can gain insights into these conditions' mechanisms by introducing specific genes or gene-silencing constructs. In the context of gene therapy research, transfection of ARPE-19 cells can be an initial step to assess the feasibility and efficacy of gene delivery approaches for treating retinal disorders.

The transfection of ARPE-19 cells employing commercially available vectors has been observed to be inefficient. Lipofectamine2000™ has shown moderate success, whereas polycationic agents have presented comparatively lower efficacy, with the commonly recognized "gold standard," polyethyleneimine (PEI), achieving single-digit efficiencies.[147,148] However, researchers have developed in-house synthesized polycations, which have demonstrated satisfactory TE and CV outcomes (Figure 29).[108,114]
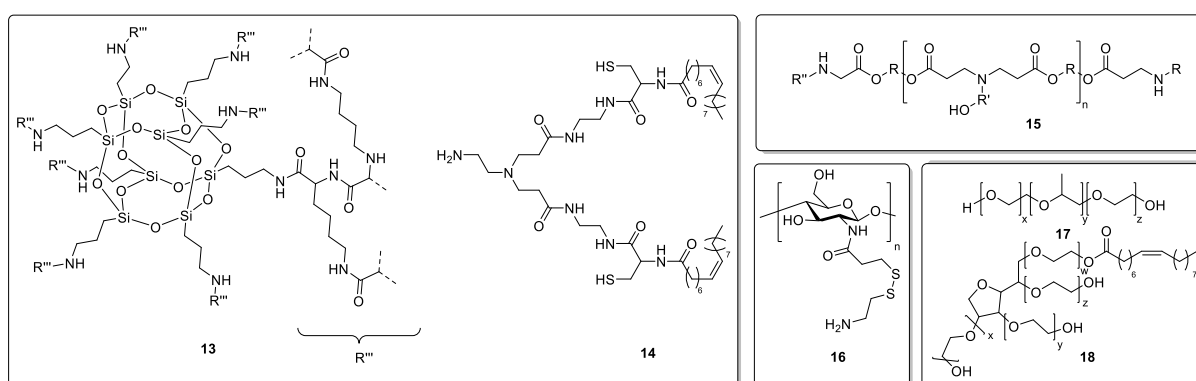

Figure 29: Polycation structures for gene delivery in ARPE-19 cells. [149]

The enhanced efficiency in genetic material delivery observed with the custom polycation is likely attributable to its more intricate molecular structure. Previous studies have indicated that star-shaped polymers exhibit superior TE compared to their linear counterparts.[73] In particular,

S<small>UN</small> et al. achieved a remarkable TE of approximately 80% while maintaining high cell viability by utilizing a core-shell dendrimeric-lipid formulation **14**. However, it is noteworthy that the synthesis of the polycation **15** is complex, rendering it inaccessible to researchers without access to an advanced chemical synthesis laboratory. Similarly, the branched polyester structure **16**, proposed by S<small>UNSHINE</small> et al., has demonstrated promising results with a TE of around 44%, albeit facing synthetic challenges similar to **15**. Efforts to enhance transfection efficiency by incorporating additives such as Polysorbate 80 (**18**) or Polyoxamer 188 (**17**) have been underway, but these approaches have shown limited success in overcoming the observed hurdles.[108,114,150]

The demand for easily accessible polycationic transfection agents is apparent. The following section will evaluate currently employed methods for ARPE-19 transfection, particularly emphasizing the employment of commercially obtainable l-PEI.

3.2.1 Literature approach

Certain "standard conditions" have been established for the transfection of adherent cells. A constant amount of genetic material, usually 3 µg, will be utilized. Consequently, the polycation will be varied to achieve charge compensation and facilitate polyplex formation, thereby setting up the desired N/P ratio. This method's advantage is cost predictability, which is achieved by using a constant amount of genetic cargo, given the relatively high cost of pDNA or mRNA compared to the polycation.[151] However, it has been observed that this method may not be the most efficient when attempting to transfect "hard-to-transfect" cells. The polycation, primarily responsible for cytotoxicity and subject to change with varying N/P ratios, is a parameter prone to fluctuations during optimization trials. Maintaining a constant polycation concentration across different N/P ratios is suggested to allow for more predictable TE and CV outcomes.

In the preliminary assessment of ARPE-19 cell transfectability, two distinct polycations were employed: commercially available l-PEI (25 kDa), recognized as the benchmark in polycationic transfection, and an in-house synthesized 24-arm pDMAEMA-nanostar with a well-defined structure. Polyplexes for transfection were initially prepared with a consistent amount of pDNA (3 µg), while varying quantities of polycation were utilized to achieve the desired N/P ratio, aligning with the established methodology in the relevant literature.[152] Transfection was conducted in 6-well plates with a cell density of 2×10^5 cells/well, following an incubation period of 4 hours between polyplexes and cells. The results depicting TE and cell viability 24 hours post-transfection are illustrated in Figure 30.
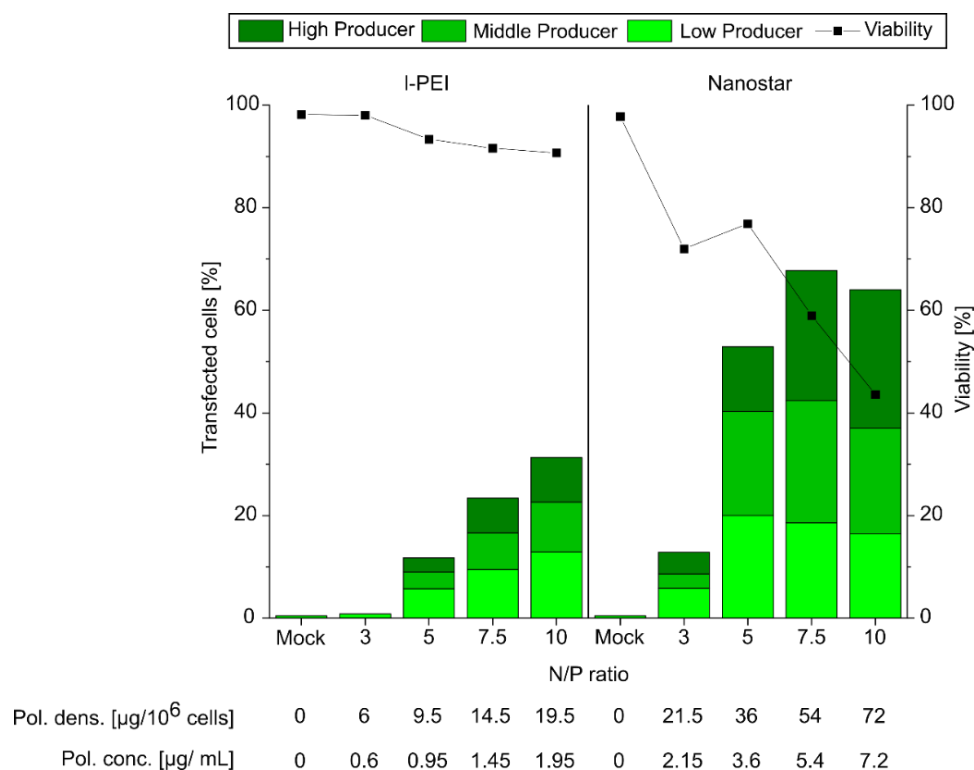
Figure 30: Transfection of ARPE-19 cells using the standard methodology. Total cells: 2×10^5, 6-well plates, transfection volume 2 mL (0.2 mL polyplex solution), and 3 µg pDNA. Analysis was conducted after 24h of recovery time post-transfection. Bars represent percentages of transfected cells within the viable cell population. Lines are guides to the eye.

For l-PEI, the TE remained at or below 30% while maintaining a high cell viability of over 90%. These values align with previously documented outcomes for l-PEI and jetPEI® in ARPE-19 cells, where TE was reported to be around 22%.[108,147,153] For a given N/P ratio, the Nanostar transfection agent exhibited superior performance to l-PEI, achieving a maximum of approximately 65% transfected cells. Thereby, it also confirms published results in which a non-linear polycation structure led to higher TE outcomes. However, the amount of polymer required to attain a specific N/P ratio was three times higher than that needed for l-PEI, albeit with a lower molar ratio (8.4-fold). This increase in polymer quantity might contribute to the observed reduction in cell survival following nanostar-based transfection.

A limitation of adjusting the N/P ratio by increasing polycation amounts is the ever-increasing polymer concentration quantity per cell in the transfection process. This concern is more pronounced for high molecular weight transfection reagents, as demonstrated here for Nanostar (755 kDa) compared to l-PEI (25 kDa). Notably, these polymer concentrations remained below the LD_{50} values, as determined by MTT assay for free l-PEI (12 µg/mL) and Nanostar (500 µg/mL) in L929 cells, indicating no expected toxicity.[133,136] Previous studies have established that nanostar is less cytotoxic than l-PEI for various cell lines and primary cells.[133] However, in the case of Jurkat cells, an accumulation of nanostar-based polyplexes inside cells

resulted in cellular disturbances post-engulfment, and a similar process may contribute to the higher cytotoxicity of nanostar observed in ARPE-19 cells. In contrast, l-PEI led to relatively low TE, suggesting a lower tendency of l-PEI-based polyplexes to enter cells. Interestingly, nanostar-mediated transfection resulted in elevated levels of transgene expression compared to l-PEI. Notably, the population of "high producers," representing cells with very high EGFP fluorescence (MFI > 10^5 a.u.), was, on average, four times higher. It cannot be ruled out that the heightened EGFP expression levels might induce some degree of cytotoxicity, as proposed in the literature.[154]

As the augmentation of the N/P ratio by increasing polymer quantity appeared ineffective for transfecting ARPE-19 cells, we opted for a methodological shift. The N/P ratio was varied by the amount of pDNA while maintaining a constant polymer quantity. Prior investigations demonstrated that this approach could enhance cell viability without impacting TE.[136,144] In this series of experiments, the polymer concentration was set at 6 µg/mL, equivalent to 60 µg of polycation per 10^6 cells, a value chosen based on previously satisfactory TE outcomes (Figure 30). We included l-PEI in the experimental setup for comparative purposes, employing the same polymer concentration (Figure 31).
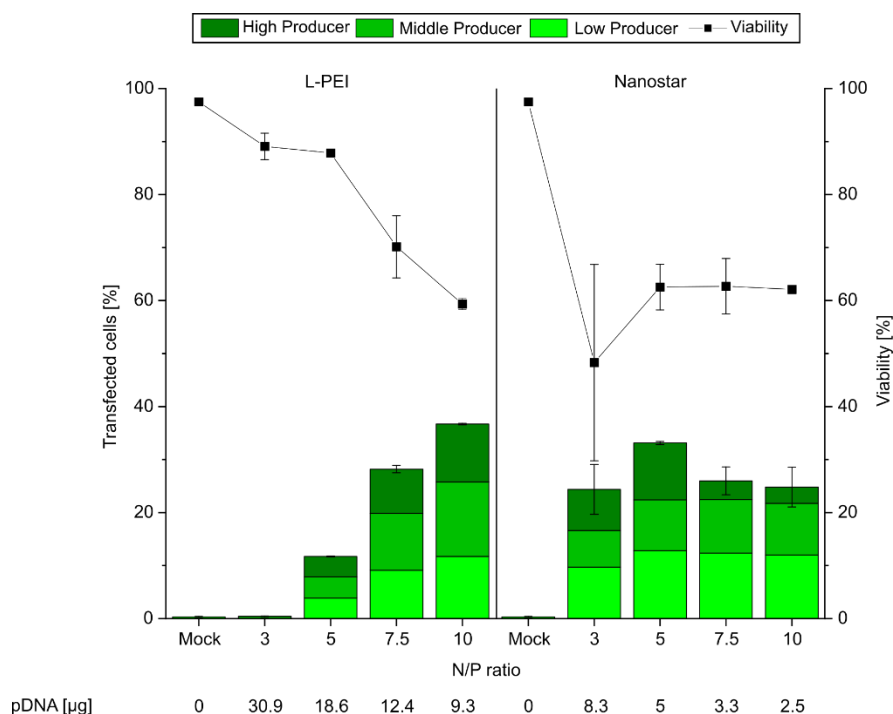

Figure 31: Influence of the N/P ratio on transfection efficiency and viability, keeping the amount of polycation constant at 60 µg polymer per 10^6 cells. Total cells: 2×10^5, transfection volume 2 mL (0.2 mL polyplex solution). Analysis was conducted after 24 h of recovery time post-transfection and 6 µg/mL polymer concentration. Bars represent percentages of transfected cells within the viable cell population. Lines are guides to the eye. Data represent mean values ± SD n ≥ 2.

In the context of nanostar-based transfection, TE was approximately 30%, exhibiting non-statistically significant fluctuations, notably lower than previous values, except for N/P 3 (Figure 30). However, cell viability stabilized around 60%, irrespective of the N/P ratio. These findings align with the overarching observation that nanostar concentration predominantly influences TE, provided total charge compensation for all genetic material is ensured. In l-PEI-based transfection, TE steadily increased with rising N/P ratios, reaching approximately 40% at N/P 10. Simultaneously, cell viability decreased, likely associated with a threefold greater concentration of polymers than N/P 7.5 and 10, as depicted in Figure 30. Collectively, these results underscore the distinct behavior of both polycations. While l-PEI shows an augmentation in TE with growing N/P ratios, accompanied by a decrease in viability, nanostar-based transfection outcomes remain relatively constant across the tested N/P ratios. This consistency may be linked to inherent mechanisms of polyplex formation, as alluded to by the ethidium bromide assay mentioned earlier.

3.2.2 Baseline parameter improvements

The primary goal was to build upon the preliminary results and improve TE and CV. The optimization process involved fine-tuning the reaction volume, the contact time during transfection, and the post-transfection recovery time to achieve ideal results characterized by high TE and robust cell survival. In addressing the impact of reaction volume and contact time during transfection, the rationale was guided by the following considerations: (I) minimizing the exposure time of cells to the transfection agent is advantageous for cell viability, and (II) a reduced space/volume enhances the likelihood of interactions between cells and polyplexes, thereby increasing TE. Transfections were conducted using nanostar and l-PEI polycations at a concentration of 80 µg per 10^6 cells and an N/P ratio of 5, with transfection volumes set at 0.5 mL and 1 mL and incubation times of 2h and 4h.

Purposefully elevating the polymer density aimed to emphasize potential changes in TE and cell survival. The plate format was also altered (6-well plate to 12-well plate) to decrease the number of cells per well from 2×10^5 to 8×10^4. The results, as presented in Table 3, unequivocally demonstrate that reducing the incubation time between nanostar polyplexes and cells improves cell viabilities for both 0.5 mL ($\Delta = 23.1\%$, $p < 0.001$) and 1 mL ($\Delta = 14.8\%$, $p < 0.01$) transfection volumes. A similar trend is observed for an increased volume during transfection, where, for contact times of 2h and 4h, 1 mL yields higher viability ($\Delta = 9\%$, $p < 0.05$) than 0.5 mL ($\Delta = 17.3\%$, $p < 0.01$), respectively.

Table 3: Analysis of the influence of incubation time and transfection volume on TE and cell viability using the nanostar polycation at 80 µg per 10^6 cells at an N/P ratio of 5. Data represent mean values ± SD, n = 2.

		TE [%]		Cell viability [%]	
		1 mL	**0.5 mL**	**1 mL**	**0.5 mL**
Nanostar	**2 h**	44.1 ± 2.8	55.2 ± 0.7	88.8 ± 1.8	79.8 ± 0.1[*]
	4 h	55.9 ± 4.9	69.5 ± 2.9	74 ± 1.6[**]	56.7 ± 1.6[***]
l-PEI	**2 h**	26 ± 0.6	31.8 ± 1.4	83.5 ± 0.5	73.2 ± 0.9
	4 h	23.9 ± 1.2	24.6 ± 6.9	89.2 ± 0.2	77.4 ± 12.6

Statistical significance between 2 h and 4 h is indicated as *($p < 0.05$), **($p < 0.01$), ***($p < 0.001$). TE: Transfection efficiency.

In l-PEI-based transfections, neither the incubation time nor the transfection volume significantly influences TE and cell viability. Still, a non-statistically significant trend towards improved TE could be identified in a reduced volume and incubation time. The results align well with the general thinking that decreasing exposure to polycation favors higher cell viability.[20] All further experiments were conducted with 8×10^4 cells in a total transfection volume of 0.5 mL, with a 2 h contact time between cells and polyplexes in a 12-well plate (Figure 32).
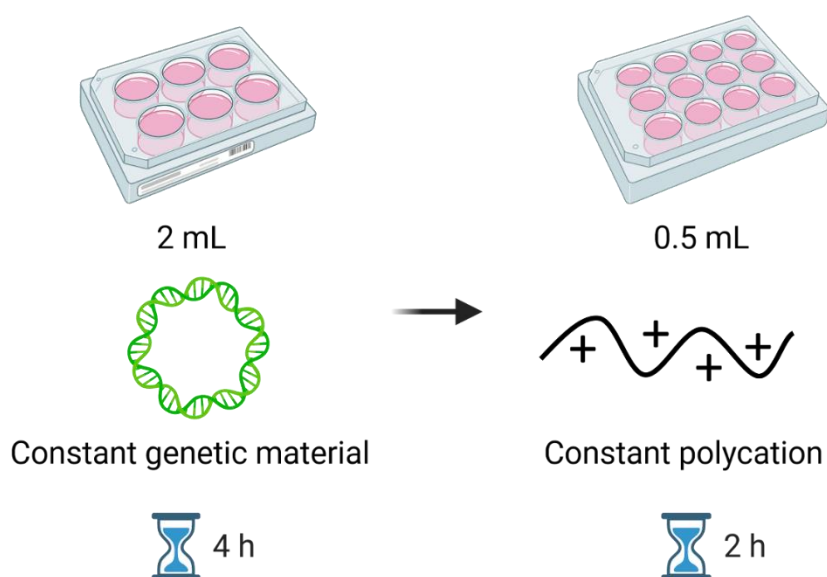
Figure 32: Adaption of baseline parameters to enhance TE and CV.

As previously documented, the transfection outcomes are significantly influenced by the quantity of polycation per 10^6 cells and the post-transfection recovery time. Initially, our investigation focused on assessing the impact of recovery time post-transfection while also screening for an optimal N/P ratio. Ratios ranging from 3 to 12.5 were employed for both polymers, maintaining a consistent polymer density of 60 µg per 10^6 cells (Figure 33). This specific polymer density was selected to balance transfection efficiency and cell viability, thereby elucidating the most pronounced differences across various N/P ratios. We evaluated TE at 24 hours and 48 hours after transfection. Notably, no transfected cells were detectable for l-PEI, as shown in Figure 33, regardless of the recovery time at an N/P ratio of 3. This observation aligns with the results obtained from the GRA depicted in Figure 24, where only partial binding of pDNA at this N/P was observed. Furthermore, there was no discernible impact on cell viability compared to the control sample. A plateau in TE was reached at an N/P ratio of ≥ 7.5, while at N/P 10, the cell viability also stagnated and consistently remained above 70%.
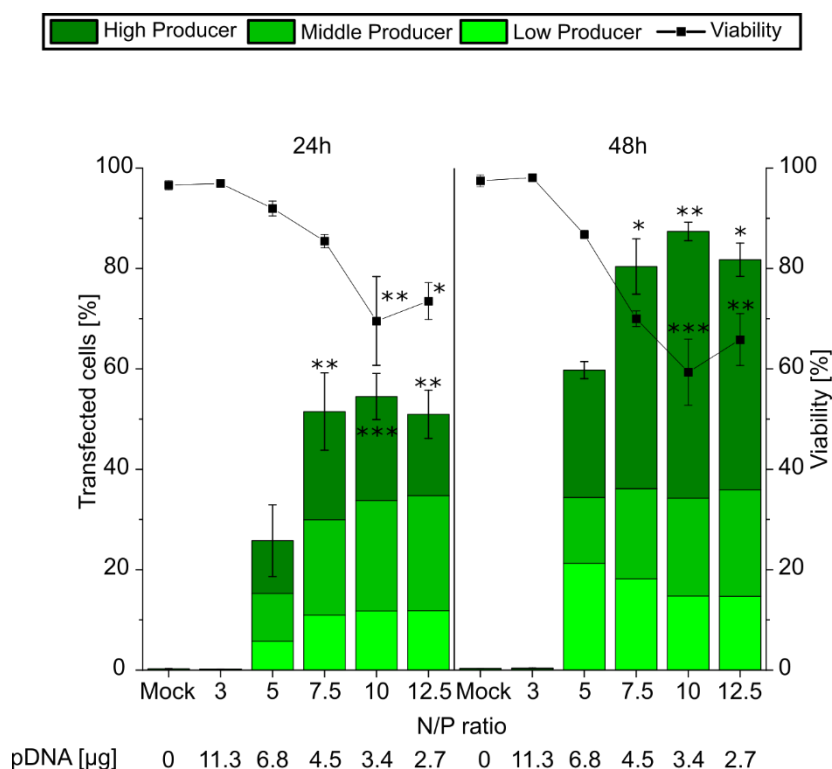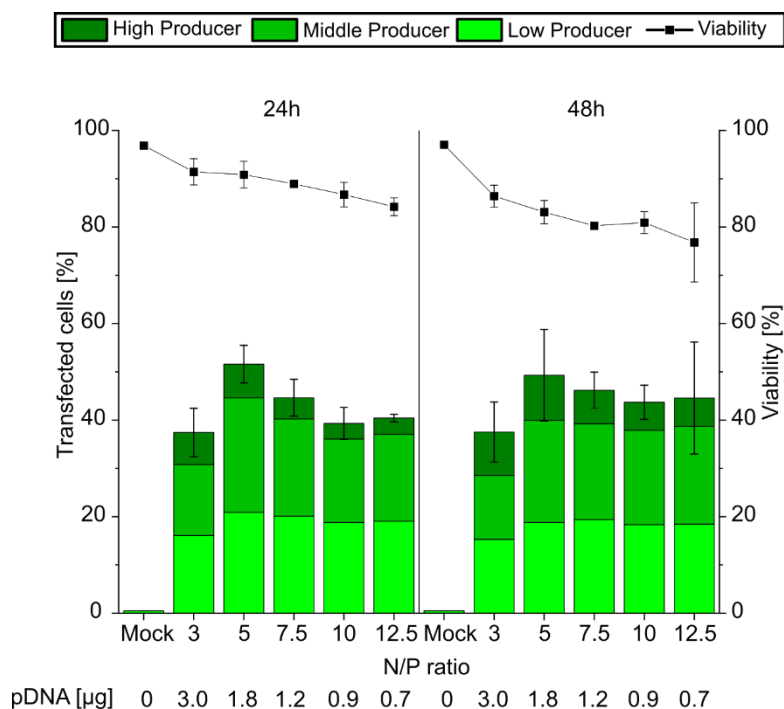

Figure 33: N/P ratio evaluation for l-PEI pDNA polyplexes. Polymer density and concentration were kept constant at 60 µg/10^6 cells and 9.6 µg/mL — total cells: 8×10^4, transfection volume 0.5 mL (0.05 mL polyplex solution). Analysis was conducted after 24 h and 48 h of recovery time post-transfection. Bars represent percentages of transfected cells within the viable cell population. Lines are guides to the eye. Data represent mean values $\pm$ SD $n \geq 2$. Statistical significance of cell viability and TE to N/P 5 is indicated as *($p < 0.05$) **($p < 0.01$) ***($p < 0.001$).

The analogous overarching pattern was observed after a recovery time of 48 hours post-transfection, which is recommended in the literature to achieve the highest TE.[155] In contrast

to the outcomes observed 24 hours post-transfection, the levels of transfection efficiency exhibited a notable increase, with a 2.3-fold rise for the N/P ratio of 5 and a 1.6-fold increase for other ratios. Concurrently, as TE elevated, cellular viability decreased to around 60%. Compared to the data illustrated in Figure 30, a twofold increase in TE was identified, accompanied by a slight reduction in cell viability (0.8-fold) for the corresponding N/P ratio.

In the case of the nanostar (Figure 34), alterations in the N/P ratio and variations in recovery time did not significantly impact transfection efficiency, which stabilized at approximately 45%. This occurred alongside a marginal reduction in cell viability (> 78%), consistently surpassing the corresponding values observed for l-PEI. Notably, N/P ratio 5 yielded the most favorable transfection outcomes, although the observed differences lacked statistical significance. This observation may be attributed to the complete condensation of pDNA at N/P ratio 3, as evidenced by GRA results (Figure 24) and ethidium bromide assay findings (Figure 27). Consistent with previous reports on nanostar systems, the transfection performance appears independent of the N/P ratio, provided that the polyplexes maintain a net positive charge.

Figure 34: N/P ratio evaluation for Nanostar pDNA polyplexes. Polymer density and concentration were kept constant at 60 µg/10^6 cells and 9.6 µg/mL — total cells: 8×10^4, transfection volume 0.5 mL (0.05 mL polyplex solution). Analysis was conducted after 24 h and 48 h of recovery time post-transfection. Bars represent percentages of transfected cells within the viable cell population. Lines are guides to the eye. Data represent mean values ± SD n ≥ 2.

Relative to the findings presented in Figure 30, consistent trends in transfection efficiency were observed for a given N/P ratio, such as N/P 5, where TE values were comparable (53% vs. 52%). At the same time, cell viability showed a slight improvement (N/P 5, 83% vs. 77%). The

polycation amount dominates TE and CV outcomes if the genetic material is fully bound. Notably, an increase in TE associated with extended incubation post-transfection was discernible only in the context of l-PEI-based transfection. It appears unlikely that the quantity of pDNA delivered plays a decisive role, as similar amounts of pDNA (l-PEI$_{N/P\ 12.5}$: 2.7 µg; Nanostar$_{N/P\ 3}$: 3 µg) yielded disparate results. A plausible hypothesis is that intracellular mechanisms governing pDNA release from polyplexes, and consequently the ability to access the cell's nucleus, may differ between l-PEI and nanostar. This speculation gains support from the distinct proportions of "high producers" observed at 24 and 48 hours for nanostar and l-PEI. The nanostar polymeric vector consistently induced less than 10% high producers, regardless of recovery time. In contrast, l-PEI transfection led to over 50% of the population being classified as "high producers" after 48 hours. This leads to a higher median fluorescence intensity (MFI), potentially allowing an assertion about protein production for therapeutic applications (Figure 35).
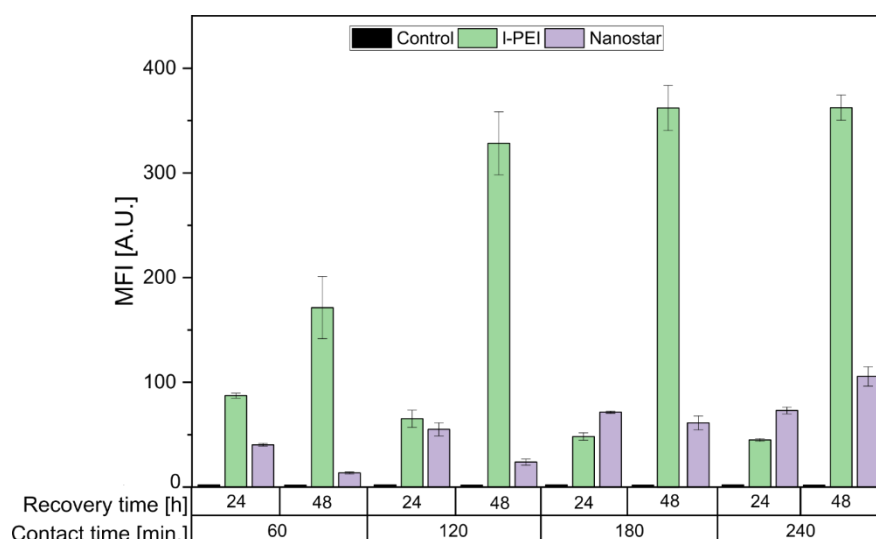
Figure 35:MFI comparison depending on polymer and contact time.

To enhance the aforementioned results, a range of 20-100 µg of polycation per 10^6 cells was employed to assess the impact of polymer density (Figure 36). A constant N/P ratio of 10 was selected to ensure the complete complexation of pDNA, as it had yielded optimal results previously (Figure 33). Once again, recovery times of 24 and 48 hours post-transfection were utilized in the analysis.
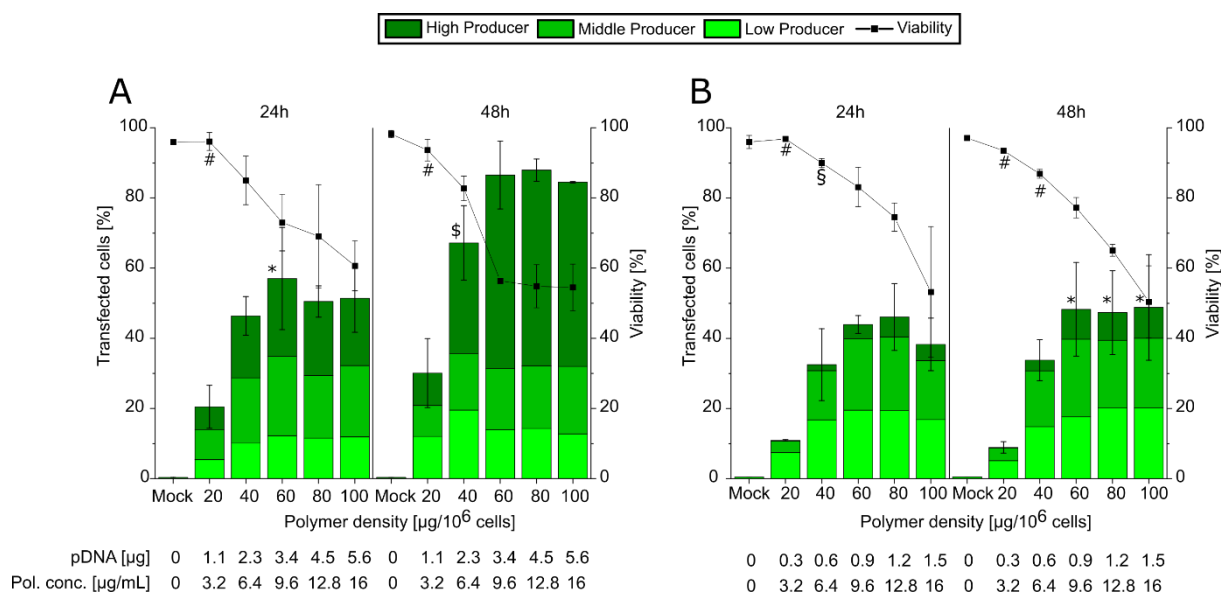
Figure 36: Polymer density evaluation for l-PEI (A) and nanostar (B) at an N/P ratio of 10. Total cells: 8×10^4, 12-well plate, transfection volume 0.5 mL (0.05 mL polyplex solution). Analysis was conducted after 24 h and 48 h of recovery time post-transfection. Bars represent percentages of transfected cells within the viable cell population. Data represent mean values ± SD n ≥ 2. Statistical significant differences in cell viability to 100 µg are indicated as §(p < 0.05), #(p < 0.01), and TE to 20 µg is marked as *(p < 0.05), $(p < 0.01).

For l-PEI, a gradual increase in transfection efficiency was observed with rising polymer quantities, reaching a plateau at approximately 40 µg polymer per 10^6 cells for a 24-hour recovery time and 60 µg polymer per 10^6 cells for a 48-hour recovery time. Nonetheless, this increase was not statistically significant compared to 40 µg of polymer per 10^6 cells after 48 hours of recovery. Cell viability decreased, reaching 45% at a polymer density of 100 µg per 10^6 cells. Extending the recovery time resulted in an additional improvement in TE by approximately 1.5-fold (90%). The expression level of EGFP followed a pattern similar to the values observed at N/P ratio 10 and remained unaffected by variations in polymer density. Notably, there was no significant difference in cell viability between 60 µg and 100 µg polymer per 10^6 cells after 24 and 48 hours of incubation. This unexpected result may be attributed to a potential saturation of the cell surface with polyplex/polymer above 60 µg per 10^6 cells, rendering additional polyplexes unable to interact with the cells and consequently having no further impact on cellular viability and transfection efficiency. For nanostar, irrespective of the post-transfection incubation time, TE remained in the same range as depicted in Figure 33, reaching a plateau at 60 µg polymer per 10^6 cells. Similar to l-PEI, the polymer density exhibited minimal influence on TE above a certain threshold. However, as previously observed in Figure 33, a slight, statistically non-significant change in expression level for the nanostar was noted after 48 hours of recovery. A consistent decline in cell viability was observed with increasing polymer density.

Both polycations demonstrated successful transfection of ARPE-19 cells with pDNA; however, after some optimization, l-PEI exhibited higher effectiveness. Optimal results were achieved with a polymer density of 40 µg per 10^6 cells for l-PEI and 60 µg per 10^6 cells for the nanostar polycation, at N/P ratios of 10 and 5, respectively. Adjusted parameters yielded a maximum TE of approximately 70%, with viability of roughly 80% for l-PEI, surpassing published results by other groups. Furthermore, an increase in recovery time led to a significant improvement in the expression level of the transgene.

3.2.3 mRNA transfection of ARPE-19

The encouraging outcomes achieved with pDNA prompted us to explore the efficacy of both polycations in delivering mRNA. Since intracellular stability is more crucial for mRNA than pDNA, the time points traditionally used for pDNA analysis (i.e., 24 and 48 h post-transfection) may not be appropriate. Additionally, considering that mRNA undergoes immediate translation upon delivery and release into the cytosol, it is conceivable that shorter post-transfection incubation times might suffice. To test this hypothesis, we initially examined the impact of the analysis time point post-transfection. Employing the nanostar at N/P 5 with 1.9 µg mRNA, 60 µg of polymer per 10^6 cells, a contact time of 2 h, and a transfection volume of 0.5 mL—parameters that yielded optimal results for pDNA—we compared transfection efficiency and cell viability after 16 h, 24 h, and 40 h of incubation post-transfection (Figure 37).
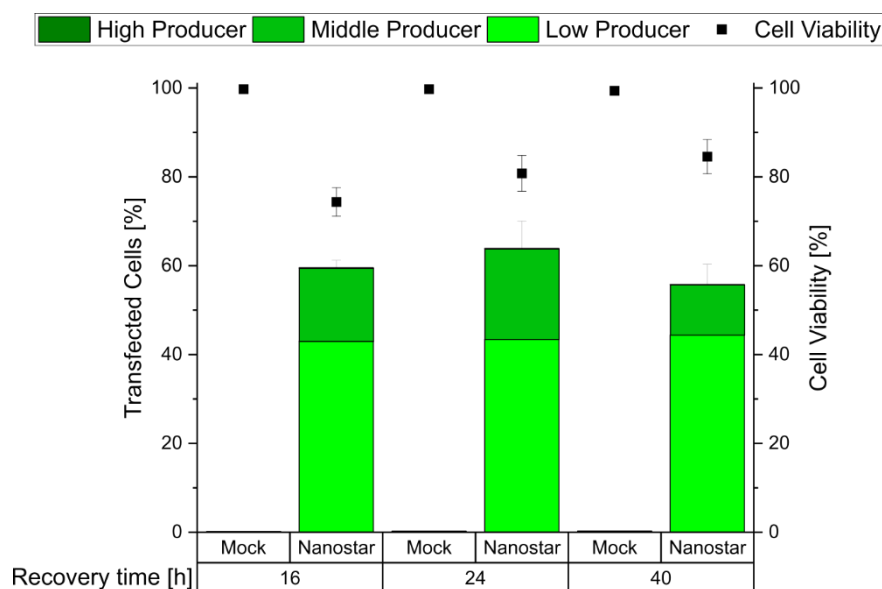

Figure 37: Influence of the incubation time post-transfection after mRNA transfection using the nanostar. Recovery times of 16 h, 24 h, and 40 h post-transfection were analyzed. Total cells: 8×10, 12-well plate, mRNA: 1.9 µg per well, polymer density: 60 µg polymer per 10^6 cells, contact time: 2 h, transfection volume 0.5 mL (0.05 mL polyplex solution), N/P ratio: 5. Data are represented as mean ± SD, n = 3.

An approximate transfection efficiency of 60% was observed, accompanied by approximately 80% cell viability, with no statistically significant differences noted among the varied recovery times. Although a marginal increase in cell viability was observed at longer recovery times, this increase did not reach statistical significance. Previous research from our laboratory has demonstrated that nanostars can enhance membrane permeability by destabilizing the plasma membrane, resulting in the formation of pores that render cells susceptible to transfection but also might increase mortality.[156] Over time, these pores are expected to close, contributing to an overall increase in cell viability.

This could be confirmed by kinetic analysis throughout 16 h (Figure 38), in which after 1 h, almost all cells are detected as dead. This might be because propidium iodide can enter through the generated pores and intercalate into the cell's DNA. Over time, a recovery of the cell viability is observable alongside an incremental increase of the transgene expression—the TE remains constant after around 6 h post-transfection. Regarding transgene expression levels, no high producers were identified; middle producers are recognizable after 7 h and continue to grow with time alongside a rising MFI and peaked at 24 hours post-transfection (Figure 37). Given that the tested recovery times did not significantly impact TE and cell viability, we have concluded that a recovery time of 16 hours is suitable for optimizing the transfection procedure for mRNA delivery using l-PEI and the nanostar polycations.
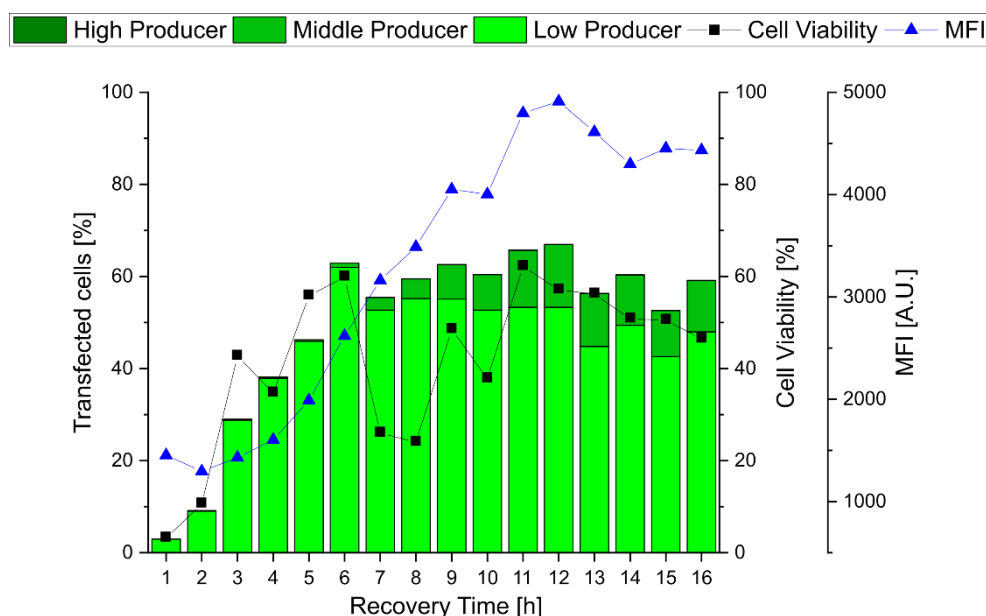

Figure 38: Expression kinetics of mRNA-Nanostar-based polyplexes. Total cells: 8×10, 12-well plate, mRNA: 1.9 µg per well, polymer density: 60 µg polymer per 10^6 cells, contact time: 2 h, transfection volume 0.5 mL (0.05 mL polyplex solution), N/P ratio: 5, n =1.

The initial challenge involved determining the optimal N/P ratio for both polycations. While it was feasible to adjust the mRNA quantity to achieve the desired N/P ratios for the nanostar-based polyplexes, a comparable strategy for l-PEI would have necessitated approximately 10-40 µg of mRNA per sample. Given the limited yield of the in vitro transcription process (with an overall production of ≤ 30 µg mRNA per experiment), such an extensive utilization of the expensive genetic material was not feasible. Consequently, for l-PEI-based transfection, we utilized 1.82 µg of mRNA and adjusted the N/P ratio by increasing the polycation quantity. N/P ratios ranging from 3 to 15 were tested with l-PEI (Figure 39 B) and 3 to 12.5 with the nanostar (Figure 39 A). Subsequently, N/P 15 was selected for l-PEI, as we did not observe the same trend towards lower transfection efficiency with increasing N/P ratios, as was noted with the nanostar.
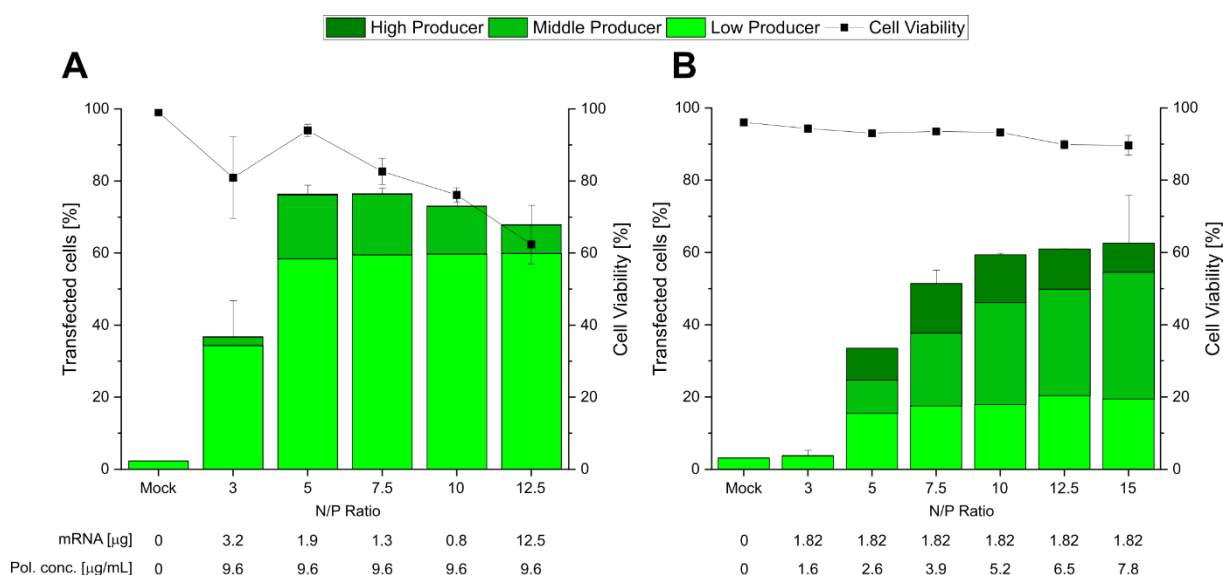
Figure 39: N/P ratio for nanostar (A) and l-PEI (B) mRNA polyplexes. For l-PEI, mRNA was kept constant at 1.82 µg, while for the nanostar, polymer density, and concentration were kept constant at 60 µg polymer per 10^6 cells and 9.6 µg/mL. Total cells: 8×10^4, 12-well plate, transfection volume 0.5 mL (0.05 mL polyplex solution). Bars represent percentages of transfected cells within the viable cell population. Data represent mean values ± SD, n ≥ 2. Data was generated by Elisabeth Ranze.

For l-PEI, the highest attainable TE was 65%, with a notable increase between N/P ratios of 3 and 5. Subsequently, a slight, though not statistically significant, increase was noted at N/P 7.5, reaching a plateau. Cell viability remained unaffected by escalating N/P ratios, consistently exceeding 80%. In contrast, the nanostar exhibited a TE exceeding 40% at N/P 3, which increased to 80% at N/P 5 and N/P 7.5. Interestingly, these two N/P ratios yielded the highest number of middle producers. At higher N/P ratios, TE experienced a slight decrease without reaching statistical significance. The correlation between increasing N/P ratio and lower overall mRNA quantity suggests that mRNA amounts exceeding 1 µg per sample may be necessary for supporting higher levels of transgene expression. Although a decreasing trend in cell viability

was observed, it consistently remained above 70%. Comparatively, the nanostar demonstrated greater efficiency than l-PEI, especially at N/P 3 regarding TE. The underlying reason can only be speculated upon and may be associated with the polyplex structure, potentially providing better protection against mRNA degradation in the case of the nanostar. A more detailed comparative analysis of the polyplexes' physicochemical properties will be necessary to address this point. Successful transfection with l-PEI-based mRNA delivery resulted in higher transgene expression, with approximately 10% high producers and 35% middle producers consistently achieved. The cell viability for both polycations consistently remained above 70%, within an acceptable range. In summary, these findings suggest that N/P ratios of 10 to 15 are optimal for mRNA transfection using l-PEI, while N/P 5 is optimal for the nanostar.

Subsequently, we explored the possibility of further enhancing TE and viability by varying polymer density. Polymer densities ranging from 20 to 100 µg per 10^6 cells were tested for both polycations, with N/P ratios set at 5 and 12.5 for the nanostar and l-PEI, respectively (Figure 40).
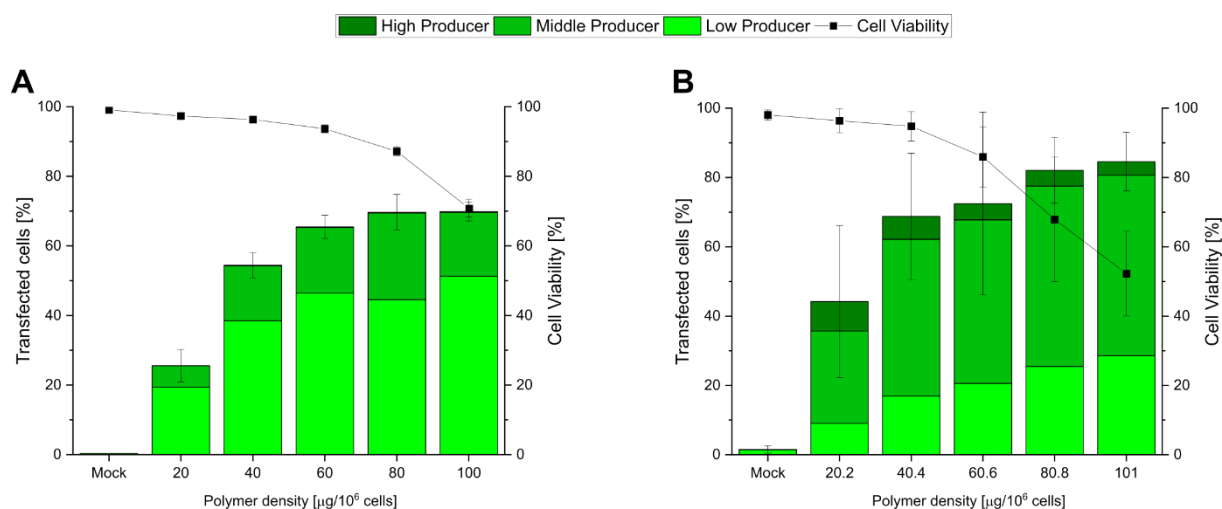
Figure 40: Polymer density evaluation for nanostar (A) and l-PEI (B) mRNA polyplexes. An N/P ratio of 12.5 for l-PEI and 5 for the nanostar was kept constant. Total cells: 8×10^4, 12-well plate, transfection volume 0.5 mL (0.05 mL polyplex solution). Bars represent percentages of transfected cells within the viable cell population. Lines are guides to the eye. Data represent mean values ± SD, n ≥ 4. Data was generated by Elisabeth Ranze.

For l-PEI, an incremental increase in polymer density resulted in a consistent rise in transfection efficiency, reaching 82%. However, this increase was accompanied by a decline in cell viability, observed from 40.4 µg of polymer per 10^6 cells onward (Figure 40, **B**). Similar trends were observed for nanostar-based transfections (Figure 40, **A**). Compared to the nanostar, l-PEI exhibited a higher level of transgene expression. Nevertheless, compared to pDNA-based transfection, mRNA supported only a limited production of "high producers," possibly linked to the reduced stability of the cargo in the intracellular compartment. The decrease in cell

viability observed for both polymers can be attributed to the rising polymer concentrations, as discussed earlier in the context of pDNA-based transfection. In summary, the optimal balance between TE and cell viability for transfection of mRNA at the tested N/P ratio was 60 µg of polymer per 10^6 cells for both l-PEI and nanostar.

3.2.4 Transition to post-mitotic cells

Since primary RPE cells in the human body are post-mitotic, transfecting non-dividing cells is crucial for *in vivo* applications.[157,158] The transfection of pDNA as genetic material relies on the ability to access the cell's nucleus. The entry of pDNA into the nucleus is thought to occur through nuclear pore complexes or the nuclear membrane disruption during mitosis.[18,110,159] The transfection efficiency may be influenced by the cell cycle and the proportion of cells in the S- and G_2M phases. Previous research from our group has demonstrated that the nanostar polycation can transfect post-mitotic C2C12 cells.[133] This could mean the nanostar can penetrate the cell's nucleus, thereby transfecting post-mitotic cells. Cell cycle analyses were conducted to investigate the transfection agent's capabilities to achieve this. The distribution of the cell cycle phases, G1, S, and G_2M, was established at the standard cell density of 8×10^4 cells per well. The analysis was performed on the day of transfection using a live staining technique with the Hoechst 33342 dye. The results showed that the proportion of cells in mitosis was approximately 50%, indicating suitable conditions for pDNA transfection (Figure 41). Transfection using l-PEI and the nanostar polycation resulted in efficiencies within the expected range, as reported earlier (~60 %, data not shown).
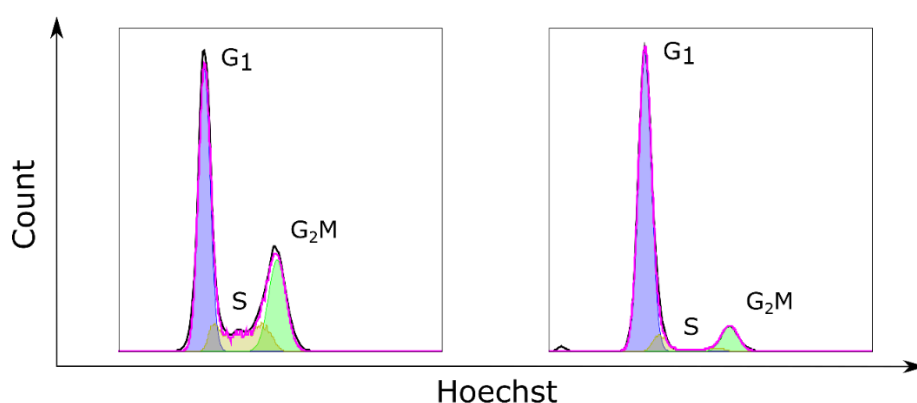

Figure 41: Cell cycle analysis of ARPE-19 cells after 24 hours (left) and 10 days (right) of seeding in a 12-well plate.

Subsequently, an attempt was made to synchronize the cell cycle by contact inhibition, culturing ARPE-19 cells for 10 days to restrict their growth space. The repeated light microscopical evaluation showed 100% confluency at around day 8. An additional two days of culturing time

were added to ensure the cell cycle was rested in the G1 phase, thereby preventing further cell division. The assumption was verified by measuring the cell cycle after 10 days, which revealed a significant reduction in the proportion of cells in the S (6 %) and G_2M (8 %) phases (Figure 41). However, not all cells seemed halted in the G1 phase. Transfection with these cells resulted in a greatly diminished TE for the nanostar (7 %) and l-PEI (17 %). While the TE was low, it surpassed the combined cells in the S and G2M phases, suggesting that transfection in postmitotic cells might still be feasible using the optimized procedure described in this study.

A stable transfection using the CRISPR/Cas9 system could negate the low TE in post-mitotic cells, as only a small percentage needs to be transfected for continuous protein production. Given the requirement for renewed protein production in malfunctioning RPE cells affected by age-related macular degeneration (AMD), developing a method for gene knock-in was considered essential. In this study, we employed a system featuring an HDR template equipped with the knock-in sequence flanked by both left and right homology arms and Cas9-mRNA to facilitate the intracellular synthesis of the Cas9 protein. Additionally, a sgRNA was utilized to target the specified locus precisely (Figure 41).
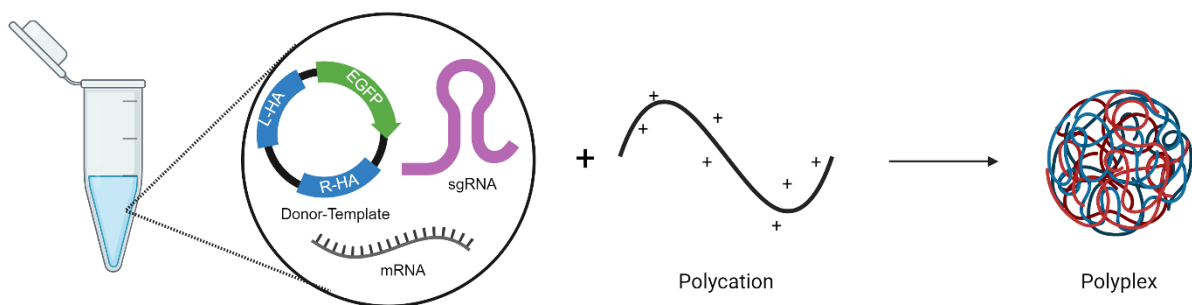

Figure 42: CRISPR/Cas9 system with mRNA(Cas9), sgRNA, and a plasmid donor template containing the knock-in sequence and the left- and right-homology arms.

As locus AAVS1 was selected, it is one of the recognized "safe harbors" that every human cell should contain in its genome. It allows gene knock-ins without disrupting essential parts of the cellular machinery.[160,161] For simple detection, EGFP as the knock-in sequence was selected; this way, cells in which the gene was successfully integrated were to maintain protein production over an extended period and would be identifiable via flow cytometry. EGFP production would regress with time in transiently transfected cells, and eventually, only non-fluorescent cells would remain. Because three separate polynucleotides were employed to fulfill their specialized task, the established procedure was a guideline for how much genetic material was used in polyplex formation. The optimized l-PEI transfection protocol for ARPE-19 will

deliver 3.4 µg of polynucleotides into the cell. Mass distribution among the HDR template (pDNA), Cas9-mRNA, and the sgRNA is a critical consideration. According to recommendations found in the literature, an initial experiment should adopt a sgRNA to mRNA ratio of 7.5, which implies that the molar quantities utilized were 7.5 pMol (242 ng) for the sgRNA and 1 pMol(1.45 µg) for the Cas9-mRNA. The remaining mass was filled with pDNA (1.7 µg) to reach the desired N/P ratio 10. Because of the different mass of pDNA utilized in this experimental setup, it was deemed necessary to evaluate additional N/P ratios (5 and 7.5), thereby increasing the mass of pDNA while keeping sgRNA and mRNA constant (Figure 43).
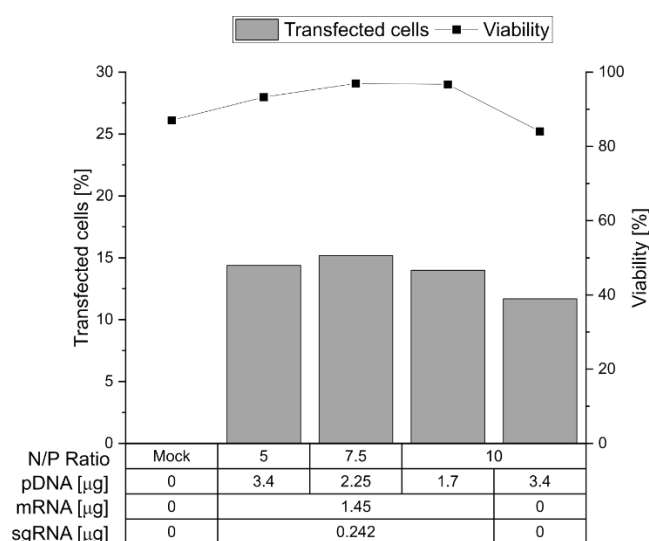
Figure 43: N/P ratio evaluation using the l-PEI and the CRISPR/Cas-9 system. Polymer density and concentration were kept constant at 60 µg/10^6 cells and 9.6 µg/mL — total cells: 8×10^4, transfection volume 0.5 mL (0.05 mL polyplex solution). Analysis was conducted via flow cytometry after 10 days of recovery time post-transfection.

After 10 days of cultivation post-transfection, around 15 % of EGFP-positive cells were detected regardless of the N/P ratio employed. At this time, transiently transfected cells should exhibit close to zero EGFP-positive cells. Interestingly, this observation does not apply to the control sample, which underwent a similar transfection process at an N/P ratio of 10 without sgRNA and mRNA. This condition should eliminate the possibility of deliberate double-strand breaks in genomic DNA for integration, allowing only random integration. Two EGFP pDNAs, pEGFPN-1 and pAAVS1 (containing homology-arms), were tested for further analysis. The variance in their sequences might result in a higher likelihood of random integration for pAAVS1.

Two biological replicates were tested to have an adequate dataset, and the optimized protocol developed above was utilized. It should ensure the highest TE and, thereby, the most significant likelihood of random integration for both pDNAs (Table 4). As expected, the highest TE was

observed 48 h after transfection. A slight difference between the two tested plasmids could be detected, but they are within the expected range of fluctuations.

Table 4: Results for the longtime cultivation experiments comparing the TE and CV for pEGFPN-1 and pAAVS1.

Recovery Time [d]	TE [%]		Cell viability [%]	
	pEGFPN-1	pAAVS1	pEGFPN-1	pAAVS1
2	89.2	78.7	83.6	88
7	16.2 $\pm$ 12.2	16.9 $\pm$ 7.42	91.3 $\pm$ 0.82	81.4 $\pm$ 0.62
12	6.92 $\pm$ 5.47	8.16 $\pm$ 3.41	89.4 $\pm$ 5.8	85.3 $\pm$ 1.63
14	3.68 $\pm$ 1.67	5.29 $\pm$ 0.88	81.7 $\pm$ 7.28	78.9 $\pm$ 11.7
19	2.17 $\pm$ 0.97	2.58 $\pm$ 0.26	77.9 $\pm$ 4.1	70.1 $\pm$ 7.14
21	1.9 $\pm$ 0.51	2.62 $\pm$ 0.57	56.5 $\pm$ 2.04	50.9 $\pm$ 1.27
28	1.29 $\pm$ 0.67	1.48 $\pm$ 0.1	55 $\pm$ 8.7	52.5 $\pm$ 4.6
34	0.55 $\pm$ 0.38	0.78 $\pm$ 0.15	60.4 $\pm$ 2.26	70.2 $\pm$ 0.78

As expected, a progressive decline in transfection efficiency correlating with an extended period of recovery time could be observed. Statistical evaluation concluded that the transfection efficiencies of the two plasmids under investigation did not significantly differ. Furthermore, at 34 days after the transfection process, comparative analysis revealed no statistically significant discrepancy in TE between the groups subjected to pDNA transfection and the control group, which did not receive any pDNA. Random integration can not be ruled out entirely and necessitates genomic DNA extraction and specific amplification of the potentially integrated pDNAs. Cell viability decreased with cultivation duration, regardless of pDNA usage or mock transfection (data not shown). The experiment, conducted in 12-well plates over an extended period, resulted in multiple cell divisions, eventually leading to spatial constraints for further cell growth. This lack of available growth space may have heightened the susceptibility of the cells to stress, potentially contributing to an increased rate of cell mortality. Future experiments should have an approximate recovery time of at least 34 days to confirm a

significant difference between potentially random integrated pDNA and deliberately inserted sequences.

3.2.5 Summary

Transfecting ARPE-19 cells with polycationic agents using commercially available vectors presents challenges. Notably, the utilization of l-PEI, a widely adopted polycation, lacked applicability. Diverging from conventional practices, which involve maintaining a constant quantity of genetic material, our approach maintains a consistent polycation quantity, significantly improving transfection efficiency while ensuring satisfactory cell viability. Additional modifications enhanced our results by reducing the transfection volume and decreasing the contact time between polyplexes and cells.
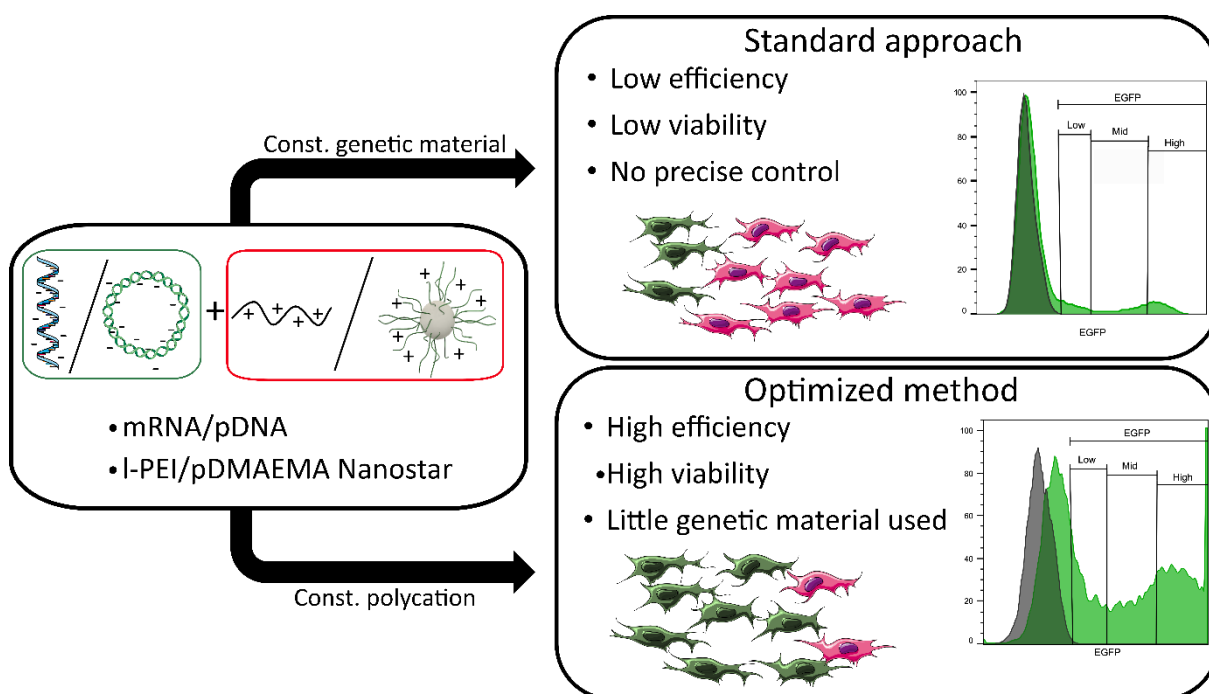
Figure 44:Summary of Procedure.

In contrast to the conventional methodology, our research advocates a novel strategy where the polycation amount remains fixed, and the genetic material quantity is adjusted to achieve the desired N/P ratio. Optimal outcomes with l-PEI were achieved at $60\ \mu g/10^6$ cells for mRNA transfection and $40\ \mu g/10^6$ cells for pDNA transfection, both at an N/P ratio of ≥ 10. The nanostar polycation achieved optimal results at an N/P ratio of 5 and a polymer density of $60\ \mu g/10^6$ cells, regardless of the polynucleotide used. Our findings affirm that efficient condensation of genetic material with nanostar transfection agents requires a lower N/P ratio, supported by various analyses, GRA, and ethidium bromide assay. Transfection efficiencies of approximately 70% were attainable for both polymers when using pDNA, maintaining cell

viability at around 80%. These results represent a substantial enhancement compared to previous studies using l-PEI, suggesting a promising advancement in transfection. Substituting proprietary, in-house-synthesized polymers with commercially available l-PEI in future ARPE-19 cell transfection studies may broaden the applicability and accessibility of this method. Further utilization of this methodology was tested for applying the CRISPR/Cas9 system. While it was confirmed that the general procedure could deliver transfected cells, a notable difference between the CRISPR system and the control group could not be validated and needs further optimization.

3.3 B cell transfection

Various methods are known to transfect human primary B cells successfully. So far, viral methods are being used to achieve high transfection efficiency, but this comes with a limited insert size and the danger of immunogenicity.[29] Non-viral vectors have been proposed as alternatives but seem limited by poor transfection efficiencies and high cell mortality in B lymphocytes.[162] Physical methods such as electroporation yielded up to 65% TE and a survival rate of 30%.[163] Optimizing conditions for this had moderate success and could improve TE to 80% with a CV of 55%.[164] Using a non-physical transfection method like lipofection yielded poor TE. Given the results of such reports, electroporation seems to be the go-to choice for non-viral gene delivery into B cells. However, electroporation requires many cells, which is not always guaranteed to be obtained from a single donor. Additionally, a high amount of genetic material is necessary, which drives up the procedure's cost. Other non-viral vectors, such as cationic polymers, were inefficient in transfecting primary murine B lymphoblasts.[165] Therefore, no suitable alternative for non-viral transfection of primary human B lymphocytes has been established yet. Primary cells often come with a higher demand for maintenance, lower TE compared to their cell-line counterpart, and a higher mortality rate when exposed to cell membrane-disrupting agents.[166,167] Additionally, their capacity for differentiation necessitates careful consideration when concluding the analysis of experimental data. The following section will explain which parameters may have hindered substantial progress in this field of research and offer an improvement for the non-viral transfection using polycationic vectors.

3.3.1. Transfection

Initially, a conventional approach was employed to formulate a transfection protocol for both l-PEI, which was recognized as the prevailing standard among polycationic transfection agents, and the nanostar. This methodology maintained a constant amount of pDNA at 3 µg, while the N/P ratio was adjusted by varying the quantity of polycation used in polyplex formation. Cell expansion in the growth medium was essential over several days to generate sufficient cells for the simultaneous assessment of multiple transfection conditions (e.g., N/P ratios). For this purpose, cells were cultured with mitogenic factors, namely CD40L, IL-4, and IL-21, requiring four to six days to attain the necessary cell quantity. Additionally, the induction of active cell division, characterized by a temporary disassembly of the nuclear membrane, is generally acknowledged to enhance transfection efficiency.[168]

In the specified experiments, transfections were conducted on the fourth day of culture, and the cells were subsequently incubated with the polyplexes for four hours in 6-well plates (transfection volume: 2 mL). Transfection outcomes, including TE and cell survival, were evaluated 24 and 48 hours post-transfection using flow cytometry. The gating strategy employed in this analysis is illustrated in Figure 45.
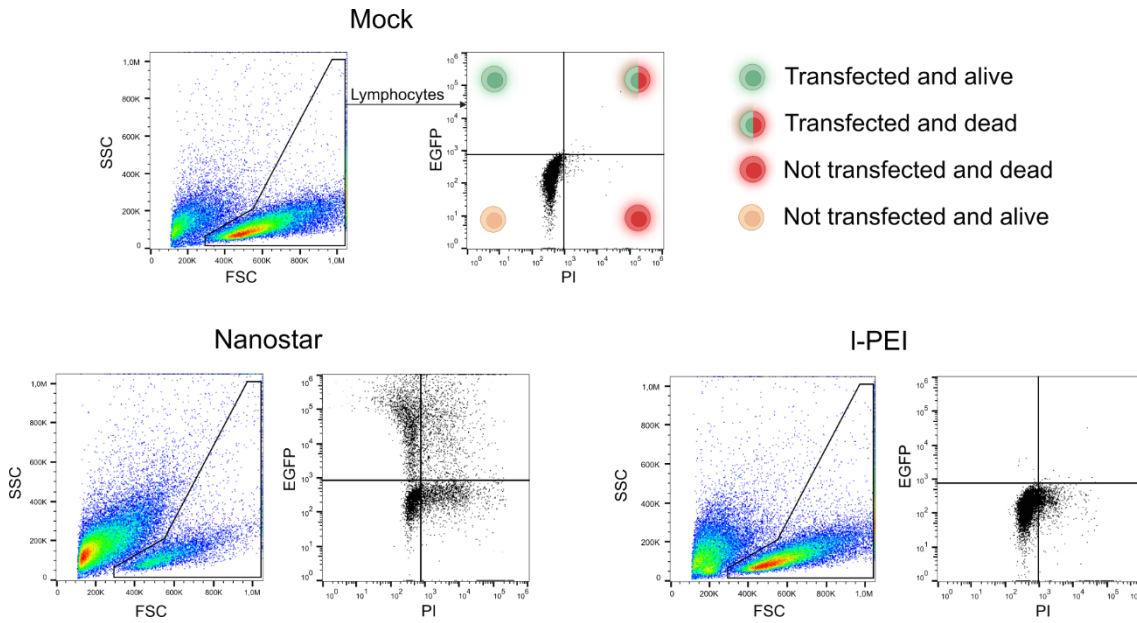

Figure 45: Gating strategy for flow cytometry analysis. Top: mock transfection, bottom: Cells transfected with Nanostar (left) and l-PEI (right).

Replicates were not performed due to limited primary cell availability from individual donors and expected variability in responses between donors.[122] To avoid possible cytotoxic effects, we limited our testing to N/P ratios corresponding to polymer concentrations ≤40 µg/mL for nanostar and ≤4 µg/mL for l-PEI.
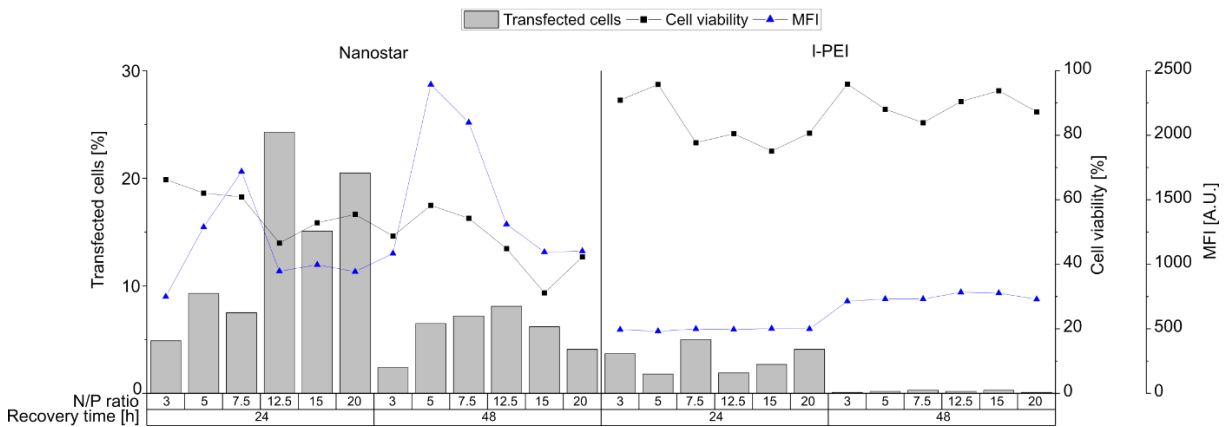
Figure 46: Initial transfection of primary human B cells using the Nanostar and l-PEI polycations in a 6-well plate format, 4 days post-thawing, pDNA: 3 µg, N/P ratio adjusted by varying the amount of polycation. Cell number for transfection: 2×10^5 cells. Contact time: 4 h. Transfection volume: 2.0 mL, $n = 1$. Cell viability on the day of transfection: >80%.

Increasing the N/P ratio for nanostar transfection agents led to higher transfection efficiency but lower cell viability. Specifically, an N/P ratio of 20 achieved a TE of approximately 20% at 24 hours post-transfection, but only 50% of the cells survived. The highest GFP expression was observed at an N/P ratio of 7.5, as indicated by the median fluorescence intensity (MFI). On the contrary, l-PEI consistently produced TE in the single-digit percentage range with about 80% cell survival. This aligns with the common observation that higher TE often correlates with increased cytotoxicity.[169] Notably, TE declined sharply for both transfection agents over time post-transfection, dropping to less than 1% for l-PEI and less than 10% for nanostar by 48 hours. However, the MFI increased in all scenarios, suggesting that the surviving transfected cells remained transcriptionally active.

In our study, the transfection was designed to be transient, without permanent genomic integration. Unexpectedly, we observed a rapid decline in transfection efficiency that deviated from typical outcomes in similarly transfected cell lines, where GFP expression usually persists for at least 72 hours.[170] The cause of this phenomenon is speculative. SEIFFERT et al. previously noted that pDNA can trigger apoptosis in nucleofected primary B cells, which might be relevant here. [171] Additionally, exposure to apoptotic stimuli is known to cause a swift reduction in cell volume, termed apoptotic volume decrease. Given that our analysis was confined to lymphocytes, identified by their scattering characteristics, a significant decrease in cell volume post-transfection could reclassify these cells beyond the "Lymphocytes" gate due to decreased forward scatter, thus artificially lowering the apparent TE.

The comparatively higher survival rate of cells transfected with l-PEI could be attributed to its lower required polymer densities (6.0 to 39.0 $\mu g/10^6$ cells for l-PEI, compared to 22.0 to 144.0 $\mu g/10^6$ cells for the nanostar) and concentrations (0.6 to 4.0 $\mu g/mL$ for l-PEI, versus 2.0 to 14.0 $\mu g/mL$ for the nanostar) to achieve the same N/P ratios. Despite this, the polymer concentrations used, even at the highest N/P ratios, were below the LD_{50} values determined for free l-PEI (12 $\mu g/mL$) and nanostar (39 $\mu g/mL$) in L929 cells, as established by our group through MTT assays.[136] Our previous research indicated that human primary T-cells are twice as sensitive to these polycations compared to L929 cells, suggesting a possible similar sensitivity in primary B cells.[133] Nevertheless, toxicity was not anticipated within the tested concentration ranges of the polymers. The observed harmful effects on cell viability post-transfection with nanostar might be linked to cellular dysfunctions following the internalization of the polyplexes, a phenomenon observed during the post-transfection period. This is supported by recent findings in Jurkat cells.[156] In contrast, l-PEI, which has a lower cellular uptake rate (resulting in lower

TE), is likely removed during the washing process; thus, it is not expected to induce a similar effect.

3.3.2 Influence of cell density on transfection efficiency

Previously, research of this group demonstrated that altering the geometry of the transfection vessel from a plate to a tube enables a decrease in the reaction volume. This reduction enhances the interactions between cells and polyplexes, thereby expediting transfection kinetics, as evidenced in experiments with ARPE-19 cells. Consequently, this tube-based transfection protocol significantly improved both the transfection efficiency (TE) and post-transfection viability of certain "hard-to-transfect" cell types.[144] Building on this, we hypothesized that primary B cells might similarly benefit from this approach. To optimize conditions specifically for primary B cells, we examined the impact of varying the cell count and polymer density ($\mu g/10^6$ cells), starting with the quantities previously identified as most effective for gene delivery into human T cells.[144]

In the consideration of optimal cell numbers for transfection, quantities of 2, 3, or 5×10^5 cells were incubated with polyplexes for 90 min., at an N/P ratio of 10. Initial screening indicated that polymer densities of $\leq 10\,\mu g$ per 10^6 cells (or $\leq 4\,\mu g/mL$) resulted in transfection efficiencies below 15%. Therefore, subsequent experiments were conducted with polymer densities ranging from 15 to $25\,\mu g/10^6$ cells (6 to $25\,\mu g/mL$) and maintaining the N/P at 10. The transfection efficiencies and cell viabilities assessments were conducted 48 hours post-transfection using flow cytometry, following the methodology recommended by RIEDL et al. for primary T-cells.[144] It's worth noting that evaluating outcomes at 48 hours post-transfection (Figure 47) likely represents a conservative or "worst case scenario" assessment, given the observed trend of decreasing TE over time post-transfection in earlier experiments.
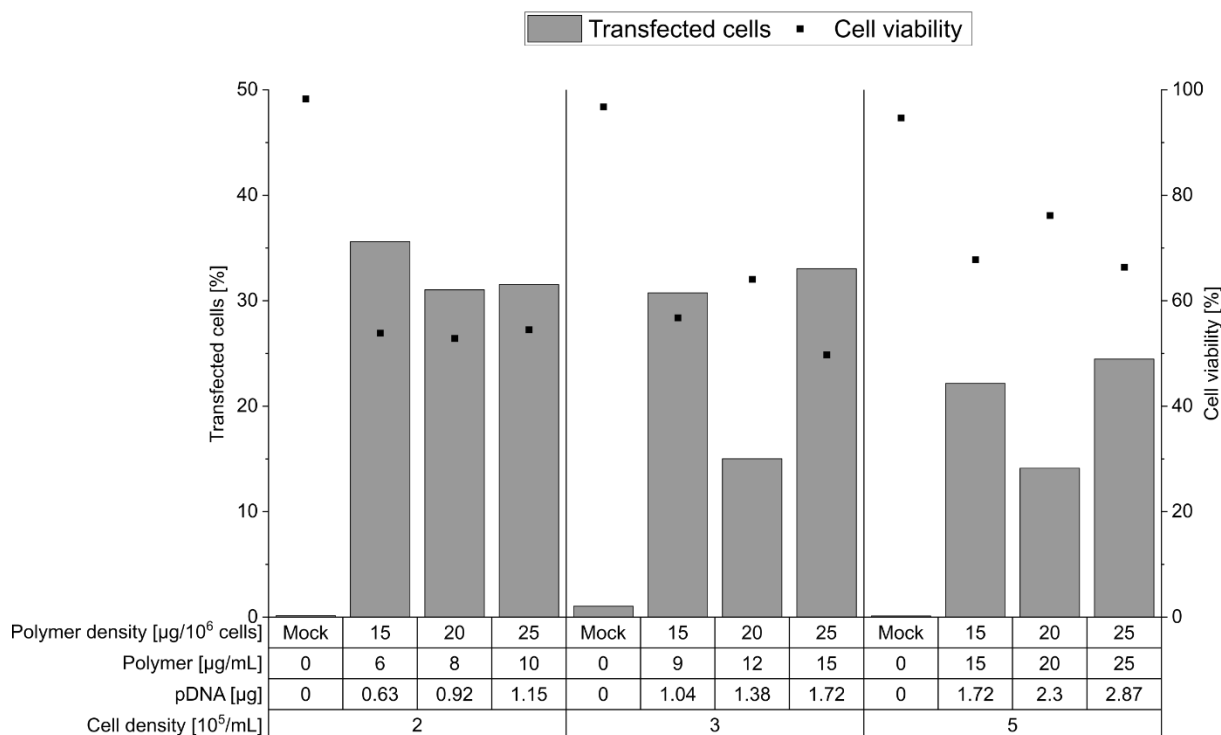
Polymer density [µg/10⁶ cells]	Mock	15	20	25	Mock	15	20	25	Mock	15	20	25
Polymer [µg/mL]	0	6	8	10	0	9	12	15	0	15	20	25
pDNA [µg]	0	0.63	0.92	1.15	0	1.04	1.38	1.72	0	1.72	2.3	2.87
Cell density [10⁵/mL]	2				3				5			

Figure 47: Cell number and polymer density influence transfection efficiency and viability. Transfection in tubes at day 6 post-thawing. Contact time: 90 min. N/P: 10, transfection volume: 0.5 mL. TE and viability were measured 48 h post-transfection. "Mock": cells subjected to mock transfection. n = 1. Cell viability on the day of transfection: 81%.

Achieving a maximum TE of 36% was possible with either 2 or 3×10^5 cells per tube, significantly surpassing the results from the plate protocol, where TEs were typically below 10% after 48 hours. Increasing the cell count to 5×10^5 cells per tube led to a 1.8-fold reduction in TE, potentially due to inadequate mixing of cells and polyplexes due to increased mixture viscosity. Notably, at the same polymer concentration (15 µg/mL) and pDNA quantity (1.7 µg), both 3 and 5×10^5 cells exhibited a significant TE increase and viability decrease, associated with higher polymer density during transfection. This suggests a higher polyplex dose per cell enhances TE but adversely affects cell survival.

Attributing the unexpectedly low TEs observed with 20 µg of polymer per 10^6 cells for 3 and 5×10^5 cells per tube to experimental error suggests that polymer density may not significantly impact transfection outcomes for a fixed cell number. This observation mirrors trends previously noted in Jurkat cells.[144] The lack of effect from increasing polymer density (and consequently, the polyplex and pDNA doses) on overall TE might indicate a saturation point for one or more critical steps in the transfection process, such as cellular or nuclear uptake, and polyplex decomplexation, among others. Beyond a certain polymer density threshold, further increases do not enhance transfection efficacy but rather diminish cell viability. Additionally, the possibility of transcriptional machinery overload due to excessive pDNA within the nucleus,

potentially saturating transcription factors, cannot be dismissed. Conversely, diluting the relative polyplex dose by increasing the cell count while maintaining polyplex quantity appears to lower TE. This effect likely results from a decreased average number of polyplexes per cell, aligning with the observed trend towards higher cell viability and suggesting a lower GFP expression level. While flow cytometry can detect cells expressing GFP, distinguishing cells with low expression from the background autofluorescence of non-transfected cells remains challenging due to overlapping distributions. Therefore, the actual TE might be underreported in these conditions.

The cell viabilities in the experiments displayed variability, ranging from 50% to 70%, yet they generally improved compared to results when using the plate protocol, even alongside enhanced TEs. Viabilities of mock-transfected cells exceeded 90%, suggesting that the transfection procedure itself did not adversely affect B cell viability within the observed 48-hour period. Notably, within the tested range, the adjusted polymer concentration during transfection did not have a significant impact on cell viability. This initial dataset suggests that using 2×10^5 cells per tube with polymer densities ranging from 15 to 25 µg/mL creates beneficial conditions for further optimization efforts.

3.3.3 Impact of polyplex exposure and recovery on B cell transfection

Given the observation that the nanostar facilitates transient poration of the plasma membrane, the extended 90-minute exposure to polyplexes, as recommended by the standard protocol, could negatively affect sensitive primary cells, which possess a less efficient plasma membrane repair mechanism than, e.g., cancer cells.[156,172] To explore the possibility that shorter contact times might be advantageous, we conducted experiments where 2×10^5 cells per tube were exposed to nanostar polyplexes (N/P 10, equivalent to 15 to 30 µg polymer per 10^6 cells or 6 to 12 µg polymer/mL) for durations ranging from 10 to 90 minutes (Figure 48). Constraints on cell numbers available from individual batches post-freezing/thawing necessitated conducting tests across two batches of thawed cells from the same donor to span the desired exposure timeframe (group A: 10 to 30 min, group B: 30 to 90 min). The experiments commenced once enough cells were secured from the combined batches, specifically on day 4 post-thawing.
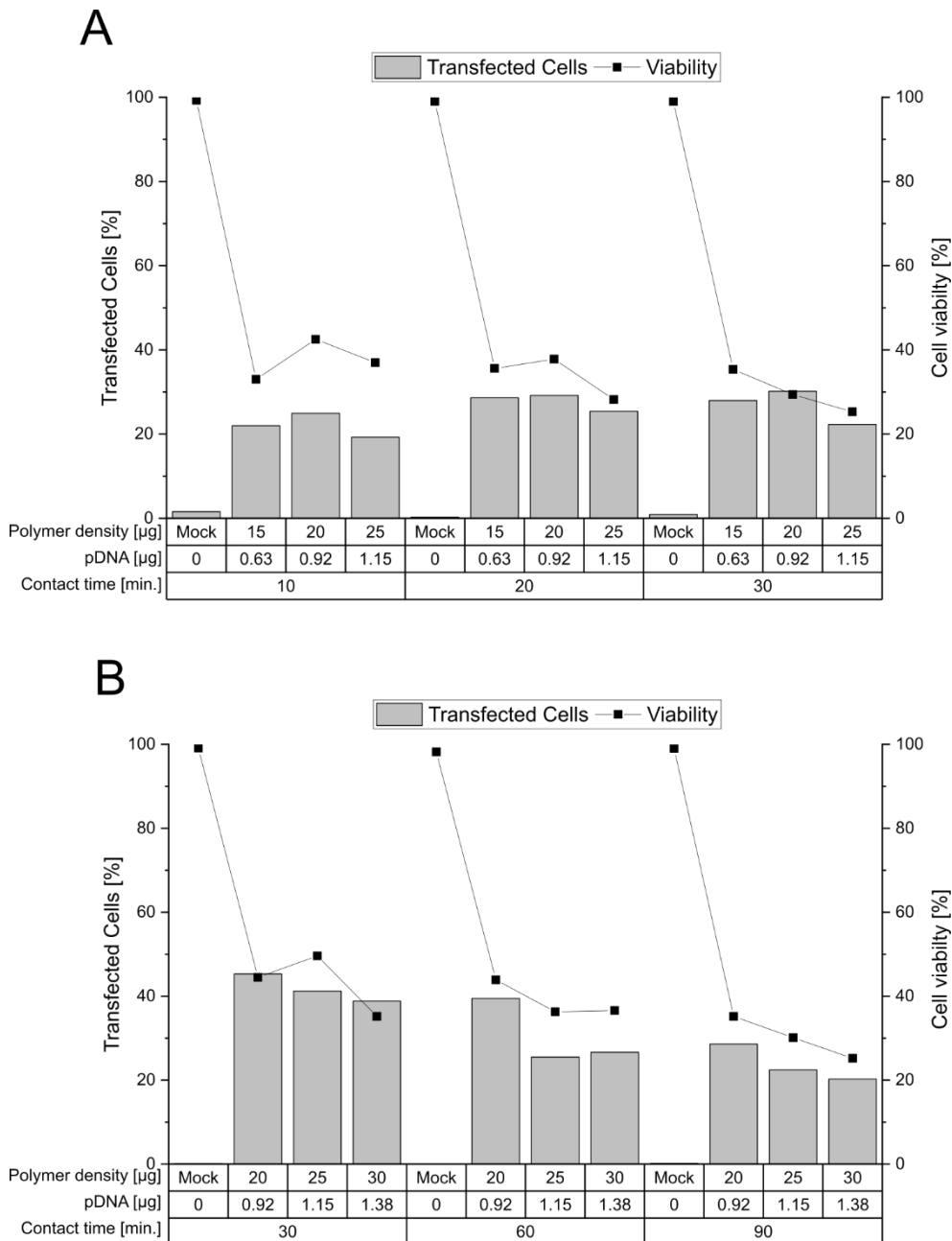
Figure 48: Effect of polyplex exposure duration on the efficiency of transfection and cell survival. Cell number during transfection: 2×10^5 cells (day 4 post-thawing), tube transfection protocol. pDNA corresponds to the amount of plasmid per tube. N/P: 10, transfection volume: 0.5 mL. TE and viability were measured 48 h post-transfection. Mock: cells subjected to mock transfection. n = 1. Cell viability on the day of transfection: 80%, group A (A) and 93%, group B (B).

Despite originating from the same donor tissue, the B cell pools prepared for transfection demonstrated variability in viability on the day of transfection — 80% for group A and 93% for group B. This variation in cell viability could be attributed to the sensitivity of B cells to freezing damage, impacting their recovery post-thawing.[173] Efforts were made to standardize the experimental procedures as much as possible, though with varying degrees of success. The transfection efficiencies observed for the 90-minute incubation were consistent with previous findings for cells transfected 6 days post-thawing, indicating that reducing the pre-transfection

cultivation time does not significantly alter the transfection outcomes in terms of TE. Shortening the polyplex exposure time from 90 to 60 and then to 30 minutes positively influenced both the TE and cell viability, with no further benefits observed for even shorter exposure times (Figure 48).

Therefore, a 30-minute exposure period is identified as the optimal contact time for transfecting primary B cells using the tube protocol. However, despite similar experimental conditions, group A exhibited lower TEs and viabilities than group B at a 30-minute exposure for a given polymer density, likely due to the lower initial viability of group A's cells. In standard protocols for cell lines, a viability of over 90% is recommended for non-viral transfection, a benchmark that is challenging to achieve with primary cells. Further assessment of potential intra- and inter-experimental variability involved transfecting cells recovered from five cryovials (same donor) after 4 days of cultivation with mitogens. Here, 2×10^5 cells were incubated for 30 minutes with nanostar polyplexes at a density of 15 µg polymer per 10^6 cells (6 µg polymer/mL, N/P ratio: 10). The measured transfection efficiencies and cell viabilities 48 hours post-transfection indicated low intra-experimental variation (3.6% for TE; 1.4% for viability) but more significant inter-experimental variability (9.2% for TE; 11.6% for viability). These results also suggest a correlation between higher cell viability at the time of transfection and improved transfection outcomes (Table 5).

Table 5:Influence of the batch variation on transfection efficiency and viability.

Cryovial	Viability before TF [%]	TE [%]	Viability after TF [%]
		22	33
I [*]	79.9	28.6	35.6
		28	35.4
II	90.4	41.3	54.1
III	84.4	16	46.2
IV	86.9	31.8	52.9
V	82.6	40.8	63.6
Mean ± SD [%]	83.4 ± 4.1	29.8 ± 9.2	45.8 ± 11.6

Transfection in tubes. Cell number during transfection: 2×10^5 cells (day 4 post-thawing). Polymer density: 15 µg per 10^6 cells, polymer concentration: 6 µg mL^{-1}, pDNA: 0.6 µg per tube. Contact time: 30 min. N/P: 10, transfection volume: 0.5 mL. TE and viability were measured 48 h post-transfection. $n = 1$. [*]: Technical replicates, mean$_{TE}$: 26.2 ± 3.6 % and mean$_{Viability}$: 34.7 ± 1.4 %.

Lastly, the transfection efficacy of l-PEI using the tube protocol was evaluated under conditions similar to those applied for the nanostar, albeit with a broader range of N/P ratios. The results, obtained 48 hours post-transfection, indicated that transfection efficiency was consistently below 0.5% across all conditions, while cell viability remained above 73%. These findings underscore the lack of improvement in B cell transfection outcomes when transitioning to the tube protocol with l-PEI (Table S 1).

To further assess the potential impact of recovery time post-thawing on transfection performance, cells derived from various cryovials of the same donor were transfected between three to five days post-thawing, a period during which cells were in exponential growth (growth rate: 0.071 h^{-1} (Figure S 3)). Notably, even when originating from the same donor, variability was evident among batches, with cell viability ranging from 65% to over 90% after three to five days of post-thawing cultivation. To mitigate the influence of cell viability on transfection outcomes, only cells with viability exceeding 80% on the day of transfection were utilized.

Compiled data suggested optimal tolerance to transfection conditions on day 4 post-thawing, as evidenced by the highest viabilities observed (Figure 49). TE values on day 4 were comparable to those on day 3, yet both TE and viability decreased for cells transfected on day 5. Although a trend towards increased GFP expression was noted for cells transfected on day

4, this was not statistically significant. As with previous observations, both TE and cell viability generally declined 48 hours post-transfection relative to the 24-hour mark, with statistically significant differences for cells transfected on day 3 of cultivation. This pattern suggests a broader issue with B cell transfection, highlighting the complex interplay between transfection conditions, post-thaw recovery, and temporal aspects of cell viability and gene expression.
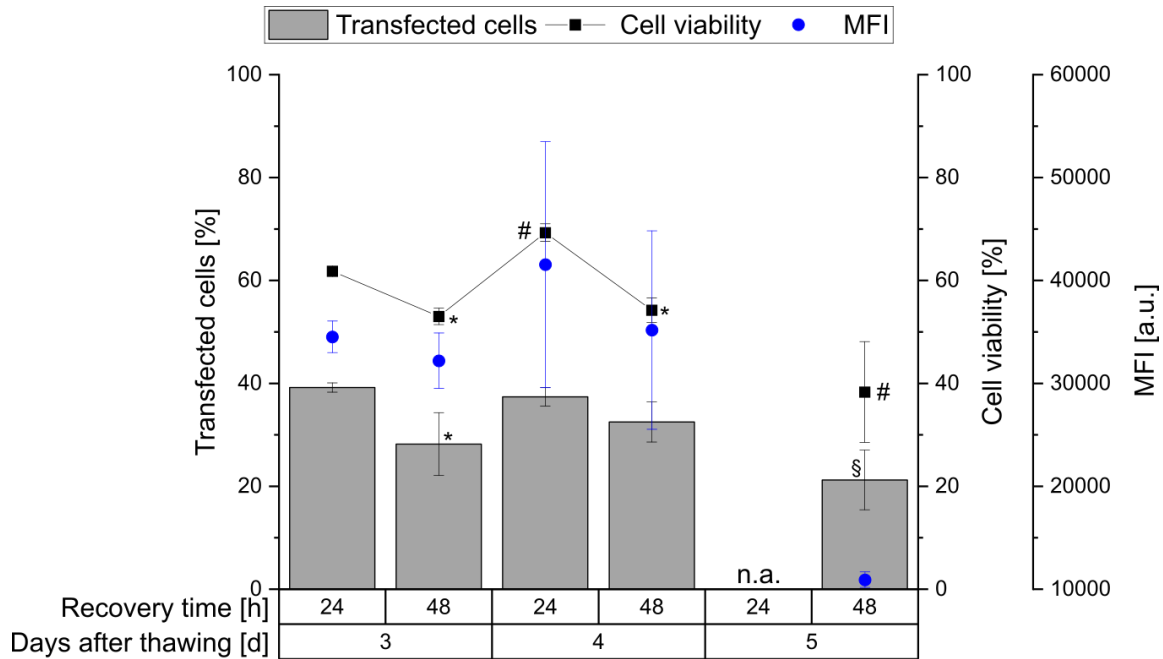

Figure 49: Overview of refined baseline parameters for transfecting primary human B cells using the Nanostar transfection reagent. 2×10^5 cells per sample; N/P 10; 15 µg polymer per 10^6 cells; 6 µg polymer per mL. Contact time: 30 min. Transfection in tubes, transfection volume: 0.5 mL. Cell viability on the day of transfection: >80%. Data represent mean values ± SD. n.a.: not available. Statistical significance between "day of cultivation pre-transfection" groups is indicated as [#] ($p < 0.05$). Statistical significance between day 5 and day 3 or day 4 is indicated as [§] ($p < 0.05$). Statistical significance between "24 h" and "48 h" groups is indicated as * ($p < 0.05$).

3.3.4 B cell subclasses

As mentioned above, primary human B cells develop a heterogeneous subset and are distinguishable by their respective CD-markers.[126,174] In preparation for transfection, B cells were activated using a set of mitogenic factors, notably including recombinant human CD40 ligand (rhCD40L), which not only induced B cell proliferation but also promoted differentiation into various B cell subtypes.[175,176] Following transfection, the cells continued to be cultivated in an activation medium containing rhCD40L. The cytomegalovirus (CMV) regulated this study's transgene expression promoter, primarily controlled by transcription factors of nuclear factor κB (NFκB), which are essential in transcriptional regulation across different cellular processes.[177,178] CD40L stimulation is recognized for enhancing NFκB expression, which varies among B cell subsets as indicated by recent findings from HUSE et al., showing differential NFκB expression levels with generally lower activity in germinal center (GC) cells

compared to naïve and memory B cells.[179–181] NFκB is also a critical regulator in plasma cells, suggesting that the distribution of B cell subsets at the time of transfection could influence not only their susceptibility to the transfection agent but also the resulting transfection efficiency, or transgene expression, under otherwise identical conditions.[182] This variability could lead to significant differences in polyplex uptake and transgene expression among the B cell subpopulations, thereby impacting the overall transfection outcomes. This aspect has been previously overlooked in studies of primary B cell transfection, which typically utilized heterogeneous pools of B cells without considering the variability and specific characteristics of different B cell subtypes. The herein-used gating strategy to adequately distinguish between the subsets is displayed in Figure 50.
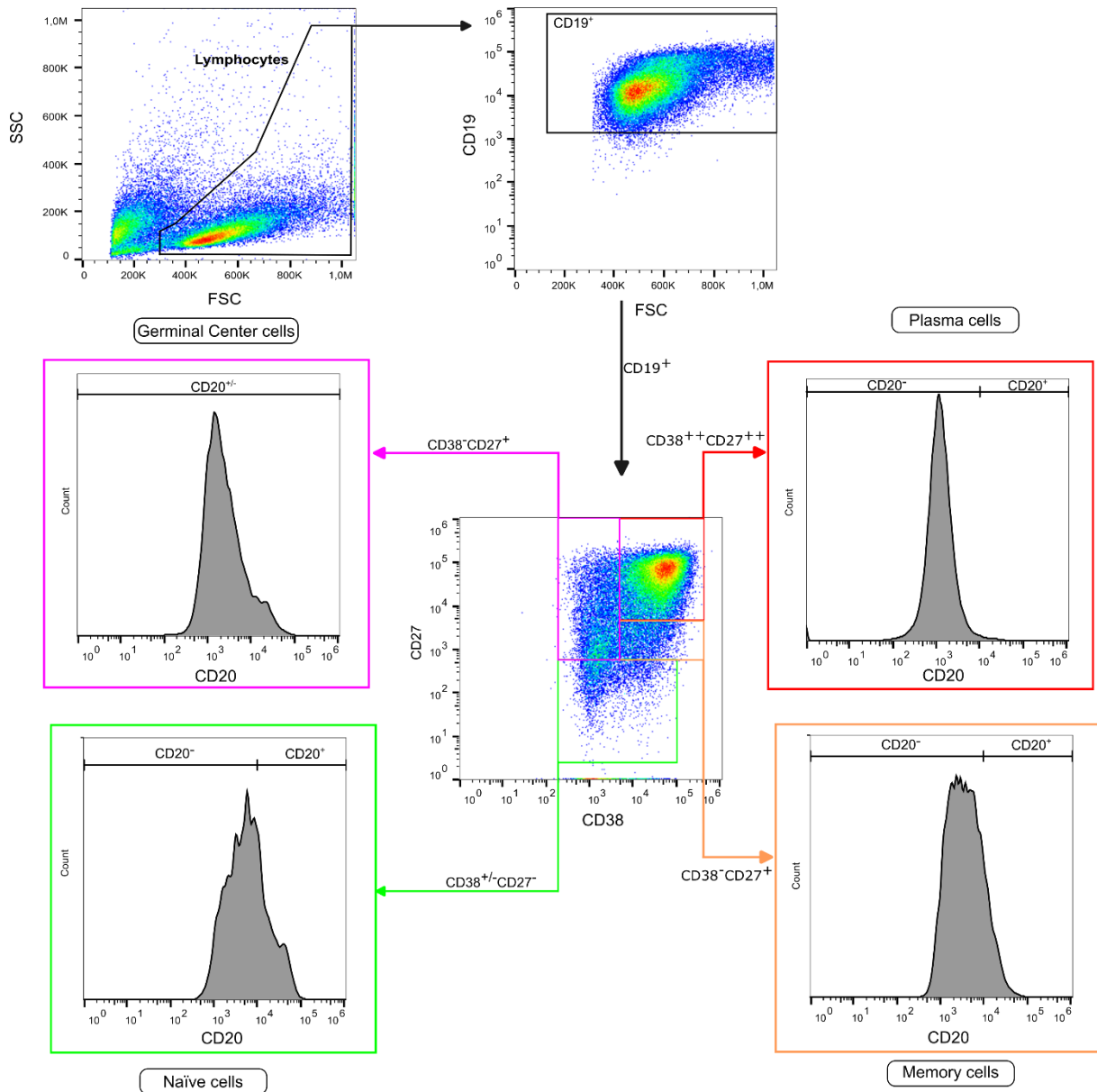
Figure 50: Gating strategy for the analysis of the B cell subclasses.

Flow cytometry analysis revealed significant shifts in the distribution of B cell subpopulations between days 3 and 5 post-thawing, particularly notable in the plasma cells (highlighted in red in Figure 51), whose proportion increased until day 5 of cultivation.
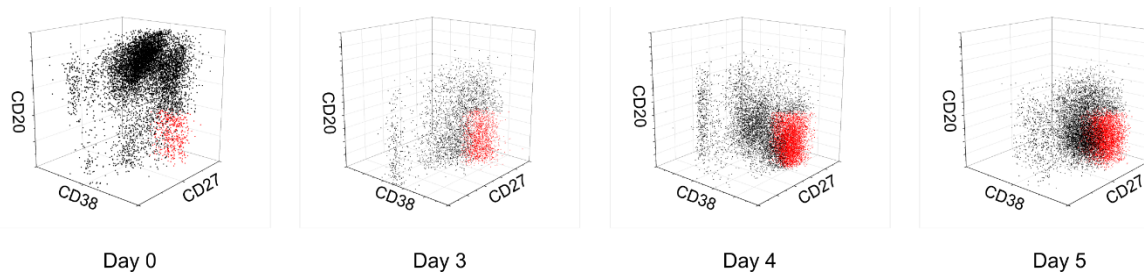
Figure 51: Three-parameter analysis of B cell subpopulations on the day of thawing (day 0) and following 3 to 5 days of cultivation.

Simultaneously, the populations of naïve and memory cells declined during cultivation in the growth medium. In contrast, cells with germinal center (GC) signatures initially decreased in the first 3 days and then saw an increase. Notably, the plasma cell population surged to over 60% during this period (Table 6).

Table 6: Variation in the percentages of B cell subclasses as related to cultivation time following thawing.

		Total Cultivation Time (Days)			
Subclasses	**Classification[1]**	**0**	**3**	**4**	**5**
CD20$^+$CD27$^-$CD38$^{-/+}$	Naive	21.0 ± 0.1	7.7	7.9 ± 3.7	2.7 ± 0.7
CD20$^+$CD27$^+$CD38$^-$	Memory	24.6 ± 5.8	7.4	4.1 ± 2.6	0.6 ± 0.04
CD20$^{-/+}$CD27$^+$CD38$^+$	GC	12.8 ± 1.0	3.9	6.1 ± 2.5	7.0 ± 4.4
CD20$^-$CD27^{++}CD38^{++}	Plasma	2.8 ± 0.6	43.1	55.2 ± 6.1	69.0 ± 10.6

[1] Classification according to JACKSON et al.[125,126]

The variation in transfection outcomes observed may be related to the distinct responses of different B cell subsets to the transfection agent. Plasma cell blasts, characterized by their larger size in forward and side scatter (FSC/SSC) profiles, may play a crucial role due to their increased membrane area, facilitating greater interaction with polyplexes. Recent studies have shown that diluting the electro-transfection buffer with water can significantly enhance the transfection rate across various B cells (including lymphoblastoid lines, B cell lines, and peripheral blood mononuclear cells), though this is often accompanied by reduced cell viability.[183] This effect may be attributed to a hypoosmotic environment induced by the reduced salt concentration, leading to cell swelling and an expanded cell membrane surface area due to altered osmotic pressure. Such a relationship between the cellular membrane area and transfection efficiency, previously suggested for CHO cells during electroporation, could be instrumental in understanding the dynamics of B cell transfection.[184] Furthermore, the

prominence of the plasma cell fraction, reaching up to 50% during expansion, is noteworthy, especially considering that most studies on B cell transfection report maximum transfection efficiencies not exceeding 50%.[163,171,185,186] This observation underscores the potential influence of B cell subset distribution on transfection efficiency. It highlights the complexity of optimizing transfection protocols for primary B cells, considering their heterogeneous and dynamic nature.

3.3.5   B cell subset dependency on transfection

Since the established cultivation protocol used for B cells activates the cells and promotes differentiation, it is interesting to find out which cell type is transfected. Since B cell differentiation occurs before transfection is done, their transfection capability can also be different. As mentioned above, it is possible to distinguish these sub-classes by their expressed CD markers on the cell membrane surface. The so-called antibody-producing cells (APC) or plasma cells (PC) are particularly interesting. Since their whole internal machinery is designed to produce antibodies, it is reasonable to assume that if transfected, these cells should be capable of synthesizing various proteins coded on the inserted genetic material.[187]

As established earlier, with a progressively higher PC ratio, the transfection efficiency also improves.[78] Since PC is easily recognizable with a very high expression of CD-27 and CD-38, an experiment was conducted to examine TE and determine if any cells other than PC were transfected. Before examining the transfected cells, a baseline must be established for the number of species present. Therefore, mock-transfected B cells were stained with CD-38 and CD-27 and evaluated. For simplicity, only the "Lymphocytes-gate"-population was observed. To gain an even deeper understanding of which cells are transfected, this approach might need to be reconsidered and changed to evaluate all cells, such as memory- and germinal center cells. CD-20 and propidium iodide could not be employed in this experiment since there would be a more significant non-compensatable overlap between the chosen fluorochromes.

Going forward, the cells in the gate were investigated for their expression of CD-27 and CD-38. As shown (Figure 52 A), only two relevant populations can be observed. Since no CD-20 marker was used in this experiment, no assertion of their expression in the different subclasses, such as Memory- or Germinal-center- cells, can be made.
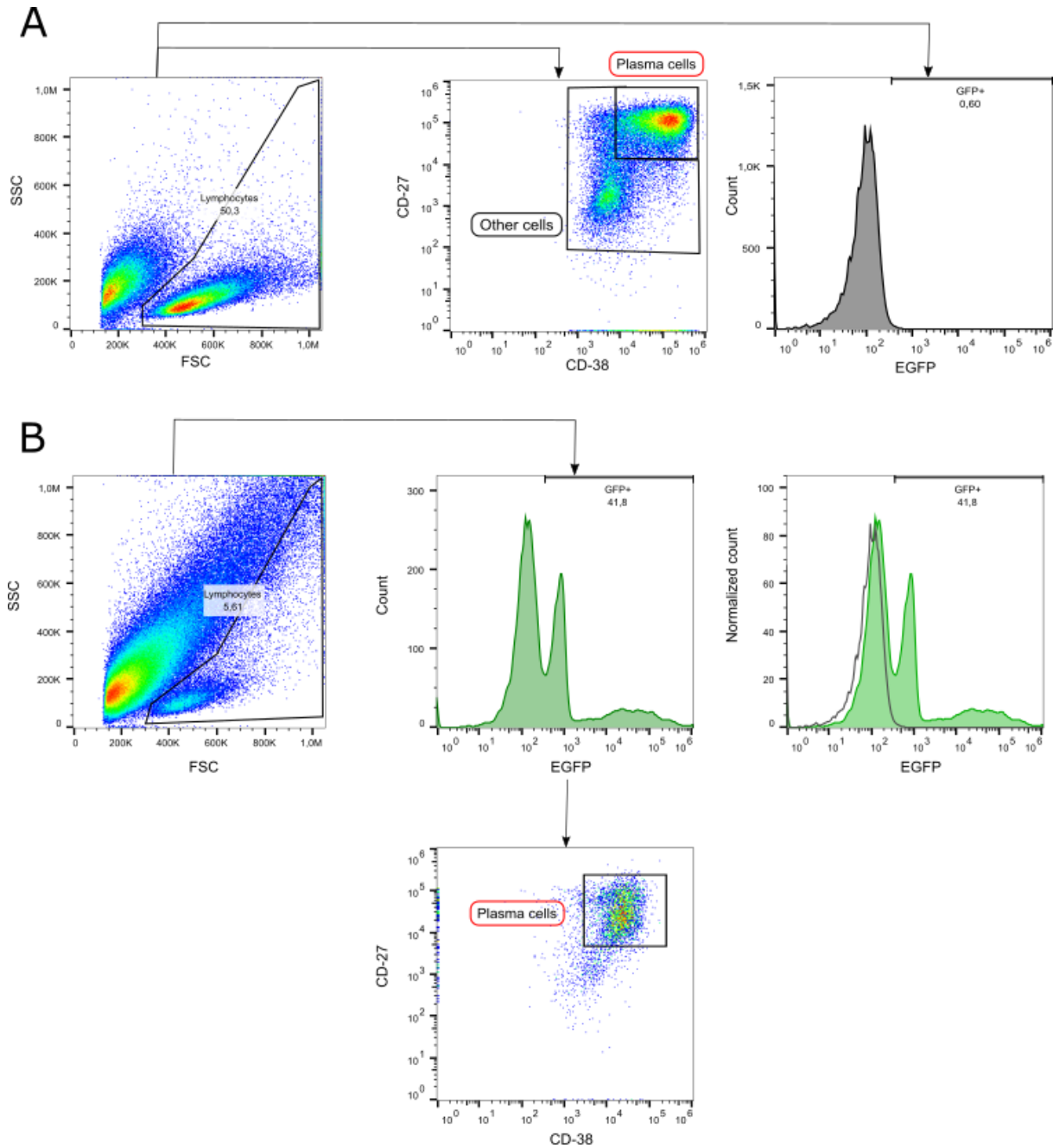
Figure 52: Analysis of transfected cells and categorization of sub-classes. (A) Mock transfection (B) transfected cells. Cell number during transfection: 2×10^5 cells (day 4 post-thawing), tube transfection protocol N/P: 10, transfection volume: 0.5 mL. TE and subclasses were measured 24 h post-transfection. Mock: cells subjected to mock transfection. n = 1. Cell viability on the day of transfection: 92%.

Upon investigation of the transfected cells (Figure 52 B), it can be seen that a significant portion lays outside the "Lymphocyte-gate" and is therefore not being examined. Continuing, it is of particular interest only to consider transfected cells. Gating for GFP-positive cells and examining their expression of CD-27 and CD-38 can show that only one distinct population remains. Considering the unique expression set of PC, it can be determined that only these cells were transfected.

Because of the expression of various CD-markers on the cell's surface, it is hypothesized that CD-138 (Syndecan-1, SDC-1) might play into why some B cell sub-classes are transfectable and some are not. It is theorized that proteoglycans are responsible for the first contact point between the polyplex and cell membrane.[13] Furthermore, some groups have specifically investigated the role of Syndecan-1 and -2 in transfection.[188–190] Multiple experiments concluded two main hypotheses: firstly, SDC-2 hinders transfection because it immobilizes polyplexes too far away from the cell membrane to interact with it; secondly, SDC-1 does the same but also can bind polyplexes much more closely to the cell surface so that internalization can take place and therefore allow transfection (Figure 53).
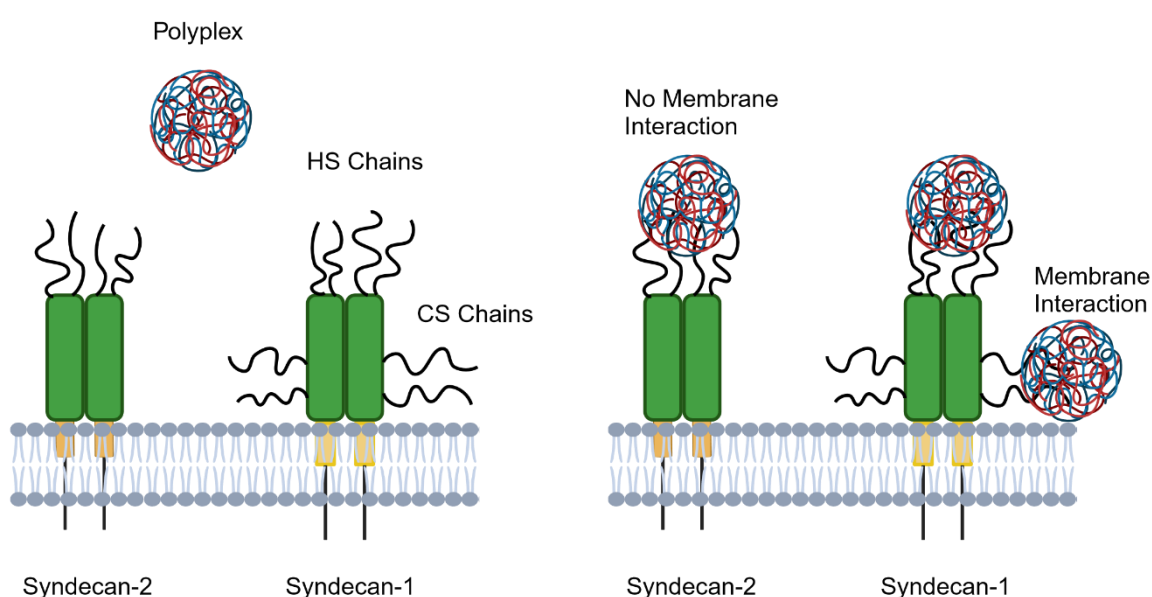
Figure 53: Proposed influence of SDC-1 and SDC-2.[16,191] HS: Heparan-sulfate; CS: chondroitin sulfate

Furthermore, it was discovered that not all B cell subclasses show CD-138 expression. Only Plasmablast, short-lived-Plasma- and long-lived-Plasma-cells express this marker.[192] Since a correlation between PC development and TE was observed, an involvement of CD-138 is probable and needs to be investigated in more detail. In conclusion, the heterogeneity of primary human B cells plays a vital role in transfection these cells. Preliminary experiments could show that the plasma cell type is mainly transfected, and other subclasses such as memory- or the germinal center cells are either dying or not taking up the polyplex. Future experiments should consider whether the hypothesized influence of CD-138 is a driving factor in B cell transfectability.

3.3.6 Drawbacks

The findings represent a noteworthy advancement in non-viral gene delivery to primary human B cells utilizing a polycationic vector. However, a significant limitation identified in this study is the observable decrease in the number of viable transfected cells compared to the non-transfected control group. This reduction in cell viability post-transfection underscores a critical challenge that must be addressed to enhance the efficiency and applicability of this gene delivery method (Figure 54).
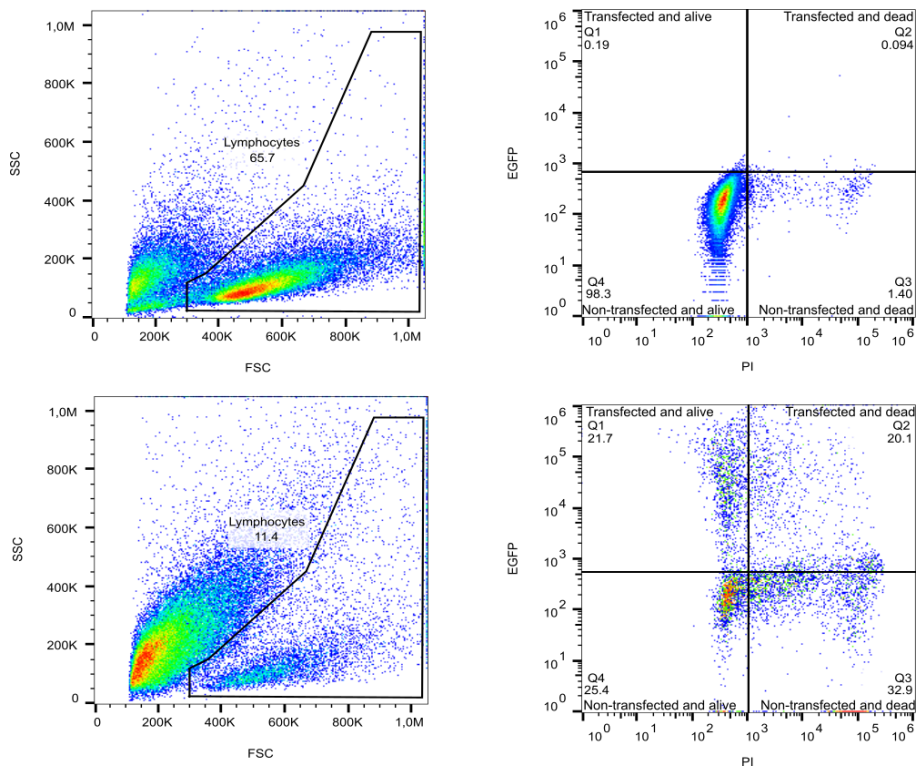
Figure 54: Comparison between mock-transfected cells and transfected cells.

As shown in Figure 54, the analysis covers merely 11.4% of cells, a stark contrast to the control group, which exhibits a significantly larger "Lymphocytes gate" population. This disparity raises concerns about the potential misrepresentation of transfection efficiency (TE) and cell viability (CV) metrics, suggesting that the actual outcomes might be more favorable than reported. To address this discrepancy and provide a more accurate and comprehensive evaluation of transfection outcomes, an additional metric, the Effective Transfection Index (ETI), is proposed. The ETI is calculated by multiplying the percentage of cells within the "Lymphocyte gate" (CG) by the transfection efficiency (TE) (Equation 5), offering a refined measure that accounts for both the proportion of analyzed cells and the efficiency of transfection. This new parameter aims to deliver a more nuanced understanding of the

transfection process, ensuring that the assessment reflects the actual performance of the polycationic vector in primary human B cell transfection.

$$ETI = CG \times TE$$

Equation 5: Calculation of ETI.

Using this approach, it seems clear that improving CG directly influences ETI and, therefore, the total number of transfected and viable cells. The upcoming experiments were designed to increase CV and CG.

3.3.7 Enhancing the quantity of lymphocyte population

As mentioned above, it seems critical to drastically improve the cell population size in the "Lymphocytes"-gate after transfection (Figure 54). Various approaches were tried to accomplish this, summarized in the following section.

First, it was assumed that due to the transfection methodology, a significant portion of the polyplex solution might be left with the cells and could drastically affect CV and CG. To check this, after transfection, the cells were washed with OPTI-MEM to remove excess polyplex. Screening for significant differences with a non-washed control transfection yielded no significant differences in CV, TE, or CG, indicating that no substantial amounts of polyplex solution were left behind (see appendix, Figure S 4).

To investigate the dynamics of gene expression following transfection with a nanostar polycation vector, we employed EGFP-mRNA instead of the plasmid pEGFP-N1 to enable immediate observation of EGFP expression in transfected cells. This methodological choice aimed to uncover the potentially lethal effects associated with the transfection process. According to research by JÉRÔME et al., the nanostar polycation can perforate the cellular membrane, thereby facilitating its entry into the cell.[156] It is hypothesized that the subsequent repair of these membrane disruptions is crucial for cell survival; failure in this repair mechanism could result in increased cell mortality. Our observations, as illustrated in Figure 55, reveal that cell viability post-transfection drops to around 20%. This suggests that the transfection process, potentially leading to pore formation in the cell membrane, allows propidium iodide, a dye used to identify dead cells, to penetrate the membrane, thereby marking the cells as "dead." However, excluding the third and fourth hours post-transfection, we noted a progressive increase in cell viability and an enhancement in transfection efficiency. This improvement is likely due to the

healing of the cell membrane pores, highlighting the cell's intrinsic repair capabilities post-transfection.
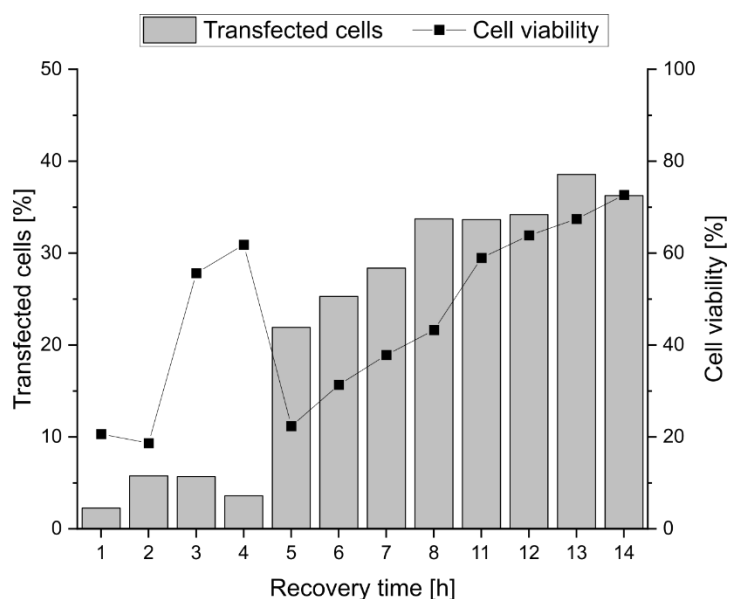
Figure 55: Transfection of primary human B cells using the nanostar polycation and EGFP-mRNA. Cell number during transfection: 2×10^5 cells (day 4 post-thawing), tube transfection protocol N/P: 7.5, transfection volume: 0.5 mL. TE CV were measured according to the depicted recovery time.. n = 1 — cell viability on the day of transfection: 91%.

Given the observed capability of the nanostar polycation to induce pore formation in cell membranes, it was considered relevant to investigate the effects of temperature on transfection efficiency through a temperature-dependent transfection study. This approach altered the temperature during the interaction between the polyplex and the cell membrane. Transfection was performed at 37°C, 25°C, and 4°C at the established contact time of 30 min. (see Figure 56).
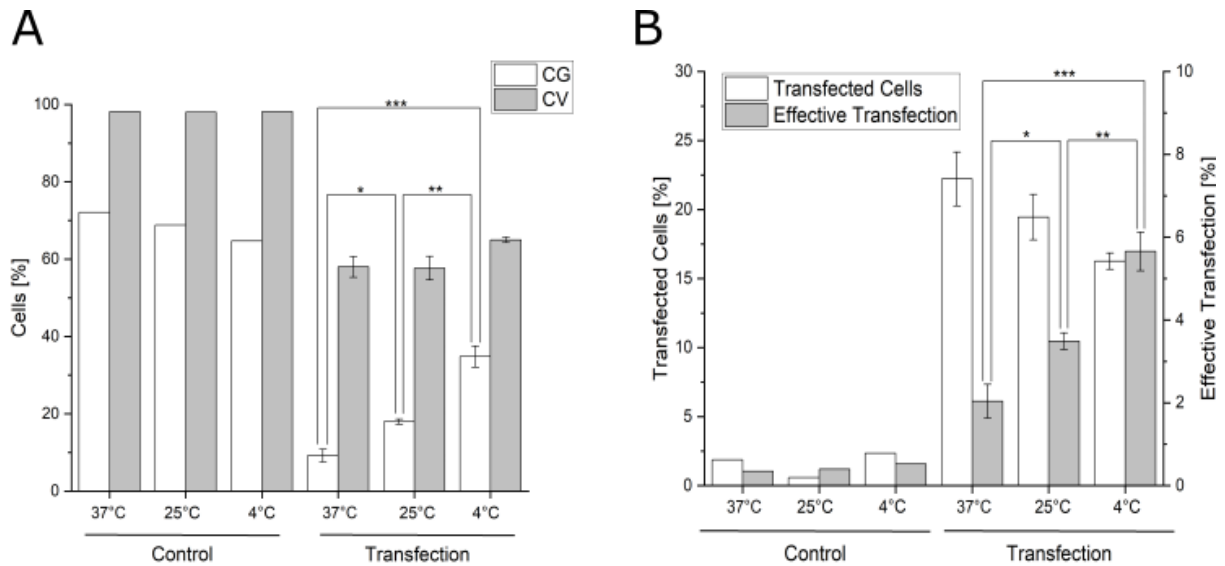
Figure 56: Results of transfection conducted at 37°C, 25°C, and 4°C. (A) Comparison of cell viability (CV) and cell population in the "Lymphocytes gate" (CG), (B) Analysis of TE and ETI. Polymer-density = 15µg/10^6 cells, N/P = 10, $t_{contact}$ = 30 min., n = 3, cell viability on the day of transfection: 88%. Statistical significance was defined as *p < 0.05, **p < 0.01, *** p < 0.001.

While the TE at reduced temperatures was lower than that achieved at the standard 37°C, both the percentage of cells within the "Lymphocyte gate" (CG) and the effective transfection index (ETI) were significantly enhanced. For CG, an increase from around 10% to approximately 30% could be observed, while TE was reduced from ~ 25% to 17%; ETI also increased accordingly. This indicates a higher success rate in transfecting cells under these conditions. The data suggest a notable trend where the incubation temperature of the polyplex-cell mixture plays a critical role in the transfection process. The rigidity of cell membranes is significantly influenced by temperature, a phenomenon extensively documented in biophysics. At lower temperatures, cell membranes tend to become more rigid and less fluid, a state that can impact membrane-associated processes such as cell signaling, fusion, and transport mechanisms.[193] The observation of a higher CV at 4°C, compared to standard transfection protocols, may be ascribed to the enhanced rigidity of the cell membrane at this lower temperature. Similarly, a heightened CV is likely advantageous for achieving a larger population within the "Lymphocytes gate," resulting in an improved Effective Transfection Index (ETI).

Because of the lower TE at temperatures below 37°C, additional factors influencing TE were explored, including the duration of contact between the polyplex and the cells, as shown in Figure 57.
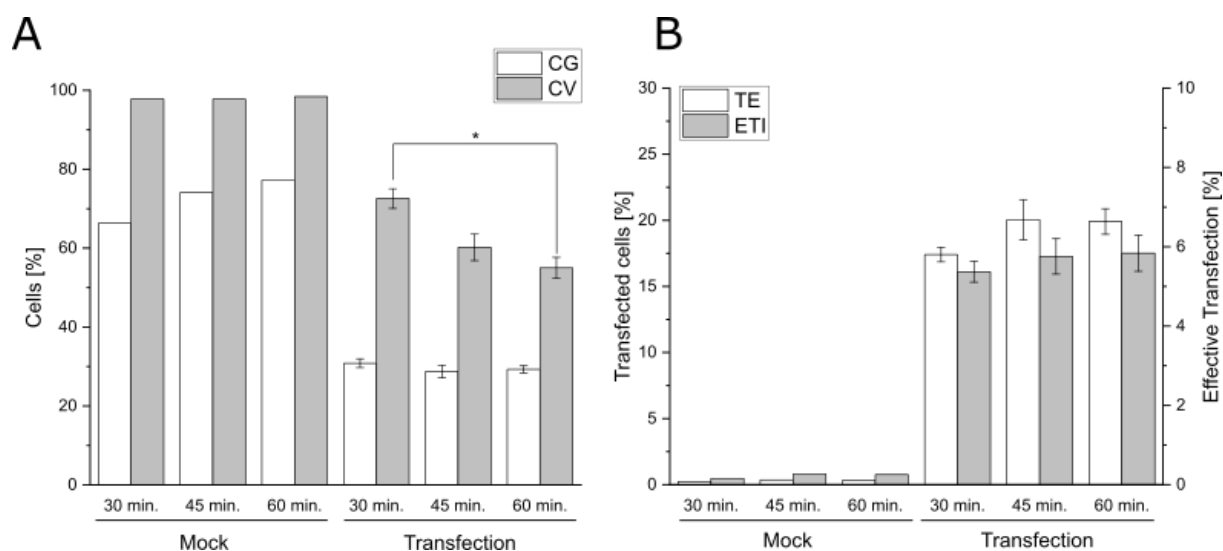
Figure 57: Results of transfection by different contact times at 4°C.
Polymer-density = 15µg/10^6 cells, N/P = 10, t$_{contact}$ = 30 min., T = 4°C, n = 3, cell viability on the day of transfection: 88%. Statistical significance was defined as *p < 0.05.

Since transfection conducted at 4°C had the most significant impact on CG and ETI, it was tested to improve TE by adapting the contact time between polyplex and cells. As evident in Figure 57, this was not the case. No significant difference in TE could be observed for varying contact times, although CV significantly reduced when comparing 30 min. of contact time to 60 min. which is in accordance with experiments that were conducted earlier.[78]

Next to external factors disrupting CV and CG could be that the internal machinery of the cells is being put under too much pressure after transfection, and the cell dies while producing EGFP. A hint for this is the distribution of transfected but dead cells to transfected and alive cells (Figure 54). Because cells producing EGFP first had to survive the initial transfection procedure and produce protein before death, it was assumed that something afterward would be the deciding factor for cell death. GFP is known to have cytotoxic effects above specific concentrations in the cell cytosol and, therefore, may be responsible to an extent for the high mortality in B cells.[154,194] Modifying genetic payloads presents an opportunity to explore the metabolic stress experienced by cells during protein synthesis. Various plasmids, such as pEAK8-EGFP, pZs-Yellow, pEAK8-ScFv49M-His, and pEGFP-N1, were transfected under the same standardized conditions and evaluated for TE and CV (Figure 58).
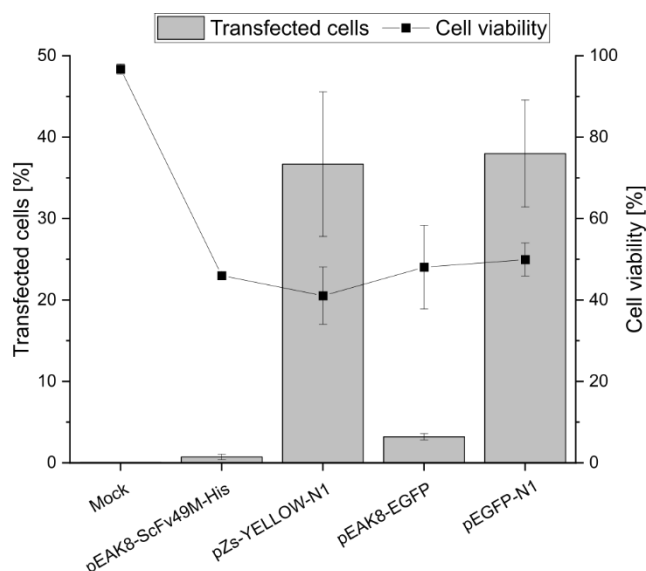
Figure 58: Evaluation of transfection efficiency and cell viability when transfected with different genetic cargos. Polymer-density = $15\mu g/10^6$ cells, N/P = 10, $t_{contact}$ = 30 min., T = 4°C, n = 3

While pEGFP-N1 and pZs-Yellow use the CMV-promoter, a strong expression promotor, pEAK8-EGFP, and pEAK8-ScFv49M-His are using the weaker TK-promoter.[195] Thus, a difference in CV should be detectable if metabolic stress while producing protein would be the cause of death. However, evaluating the results, no significant difference could be observed between the different transgenes and promotors, indicating that protein production is not a deciding factor for cell mortality.

Up to this point, all transfection experiments have been carried out using a single human donor (Table 7; entry 1). For the herein-developed method, it was deemed necessary to test more than one donor with the established transfection conditions(Table 7).

Table 7: Results of transfection using a set of different donors.

Entry	Donor-code	Age	Sex	Mean TE [%][a]	Mean CV [%][a]
1	300919_WE_TK	Adult	Female	37.4 ± 1.80	69.3 ± 0.3
2	090320_WE_TK	Adult	Female	27.5 ± 4.31	44.9 ± 0.57
3	090919_WE_TK	Adult	Female	34.0 ± 1.13	68.5 ± 8.56

[a] derived from experiments with N/P=10, polymer density of 15 µg/10^6 cells, and 4 days in culture before transfection.

Comparable results for CV and TE suggest the potential for a standardized protocol that reliably yields consistent outcomes. Given the inherent variability associated with primary human cells, results are expected to fluctuate. Efforts to minimize these variations through standardizing the overall procedure warrant continued investigation.

3.3.8 Summary

Amidst the substantial advancements in the research and development of non-viral cell transfection methods, efficiently delivering nucleic acids into primary cells, especially immune cells, remains a difficult challenge. In this study, we introduce a novel nanostructure-based approach utilizing a star-shaped cationic DMAEMA-polymer for transfection, showing particular efficacy in the transfection of human primary B cells. By optimizing the interaction between the polyplexes and the cells, adjusting the quantities of polymer and plasmid, as well as fine-tuning the culture conditions pre- and post-transfection, we achieved a transfection efficiency of 40% in human tonsillar B cells while maintaining reasonable cell viability of approximately 70% (Figure 59). This performance marks a considerable enhancement over existing non-viral chemical transfection methods. Furthermore, compared to Nucleofection, currently the preferred non-viral method for gene delivery into B cells, our nanostructure-based technique requires 500 times fewer cells and approximately 370 times less pDNA to achieve similar levels of transfection efficiency. This reduction in resource requirements could enable more experiments to be conducted using cells from a single biopsy and reduce the demand for large quantities of high-quality pDNA.
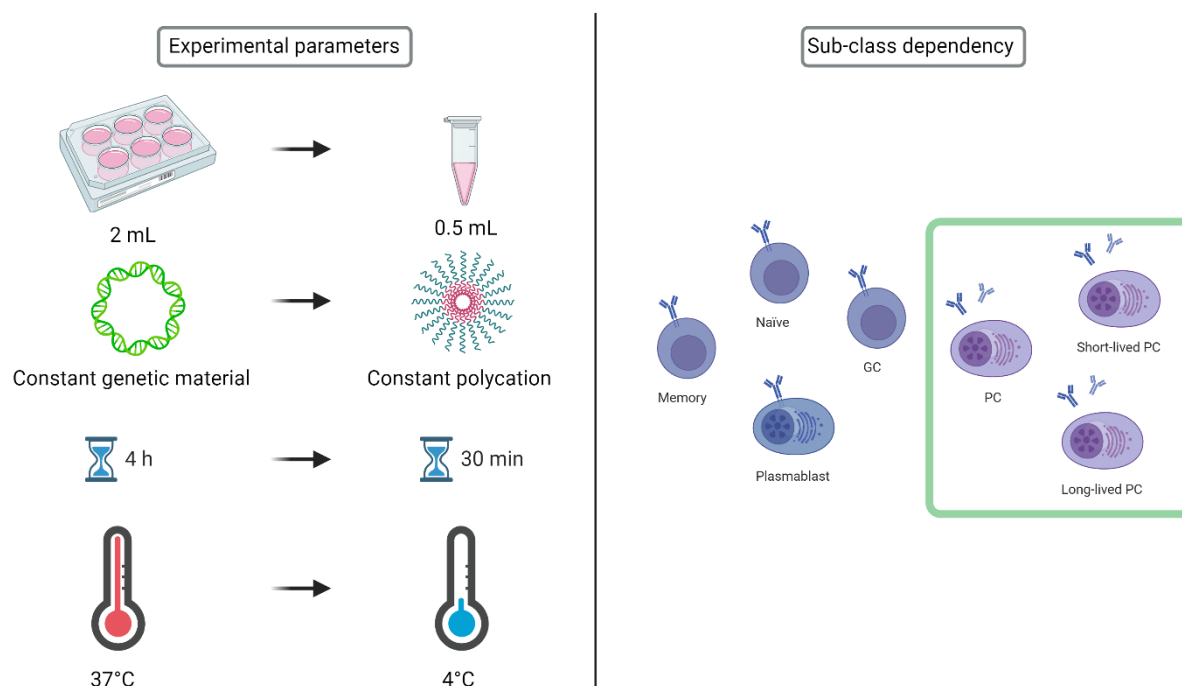
Figure 59: Experimental parameter evaluation for the transfection of primary human B cells.

Most crucially, our findings indicate that the complexity and distribution of B cell subpopulations before and after transfection may play a significant role in the process.

Subsequent research focused on the influence of B cell subset dynamics before and after transfection, uncovering TE dependency on the plasma cell population.

Additionally, an overall improvement in cell survival was explored, with the most significant effects observed when reducing the temperature during transfection. This enhancement is likely due to changes in the cell membrane's fluidity and increased rigidity. This work has developed a novel approach for the non-viral transfection of primary human B cells. Several critical parameters were identified to address the need for high TE and cell viability. Future studies should concentrate more on the transfection of specific subsets, including the role and influence of CD-138 on TE, and try to improve the population in CG.

4   Summary and outlook

In summary, this work showed substantial improvements in the transfection outcomes of the retinal cell line ARPE-19 and primary human B cells. Analysis of resulting polyplexes from two distinct polycations, namely l-PEI and the nanostar, revealed that slightly different N/P ratios are needed for the complete complexation of the genetic material. For l-PEI, an N/P ratio of 3 was necessary when using pDNA and mRNA polyplexes. The nanostar polycation demonstrated sufficient complexation at an N/P ratio of around 1, regardless of the polynucleotide used.

Adopting a multifactorial approach led to an improvement in the transfection efficiency of ARPE-19 cells. Specifically, reducing the transfection volume from the standard 2 mL to 0.5 mL significantly enhanced transfection efficiency, achieving a 1.6-fold increase with l-PEI and a 1.7-fold for the nanostar. Further optimization efforts included a deviation from the literature-recommended transfection protocol, maintaining a constant polycation concentration, and varying the polynucleotide, which increased transfection efficiency and cell viability. Moreover, limiting the duration of exposure between the cells and polyplexes improved cell viability substantially while retaining adequate transfection efficiency. Overall, the herein-developed method could show a substantial enhancement compared to previously published results, especially the most widely used l-PEI performed up to 4 times better.

Furthermore, an effort was made to adopt the optimized transfection parameters to enable a stable transfection using the CRISPR/Cas9 system. Here, the transfection capability of the designed pDNA for stable integration could be verified, albeit with a non-statistical difference over an extended time compared to the standard plasmid used in previous transfection experiments. Therefore, a refined method must be developed to ensure stable integration of the donor-template pDNA.

Future research in ARPE-19 transfection should include studies in which post-mitotic cells are being investigated for their transfection capability. Furthermore, additional attention is required to validate and refine the CRISPR/Cas9 procedure. Successful genomic integration should be verified via genomic DNA isolation and PCR amplification of the inserted genetic sequence. Lastly, the integration of therapeutic significant gene sequences should be explored further.

In the context of B cell transfection, it has been demonstrated that polymeric transfection approaches may serve as a viable alternative to the traditionally employed nucleofection method. Similar to the ARPE-19 transfection procedure, a wide range of parameters was

optimized for primary B cell transfection. The optimization of the polymer density per 10^6 cells, adjustments in the N/P ratio, and augmentation of the contact time have surpassed outcomes documented in the existing literature. Nonetheless, the intrinsic characteristics of primary human B cells, which can differentiate into various subtypes, including memory, germinal center, and plasma cells, introduce variability in transfection efficiency across these subclasses. Preliminary findings indicate a significant correlation between the proportion of plasma cell populations and transfection efficacy, suggesting the critical role of plasma cells in transfection success. Further investigation revealed that plasma cells predominantly account for the transfected cell population, highlighting their importance. Combined with the optimized transfection procedure and a lowered temperature during the contact of polyplexes and cells, even better results could be obtained.

For B cell transfection, the role of the plasma cell population has to be further analyzed and validated in more detail. Fluoresence-activated cell sorting (FACS) could be utilized to isolate B cell subclasses before and after transfection transfection. Additionally, our group's recent results have shown that modified culturing parameters can influence the distribution of the B cell subset.[196] Utilizing this knowledge could lead to further improvements in B cell transfection. Since primary cells exhibit a broader variation of transfection efficiency, multiple additional donor cells should be investigated for their transfection behavior.

Finally, the non-viral polycationic transfection method for primary human B cells has the potential for various therapeutic applications. When efficient and viable transfection, tailored to specific B cell subsets, is achieved, it becomes possible to transfect long-lived plasma cells stably. These cells can then be reimplanted into a patient, offering significant therapeutic benefits.

5   Appendix
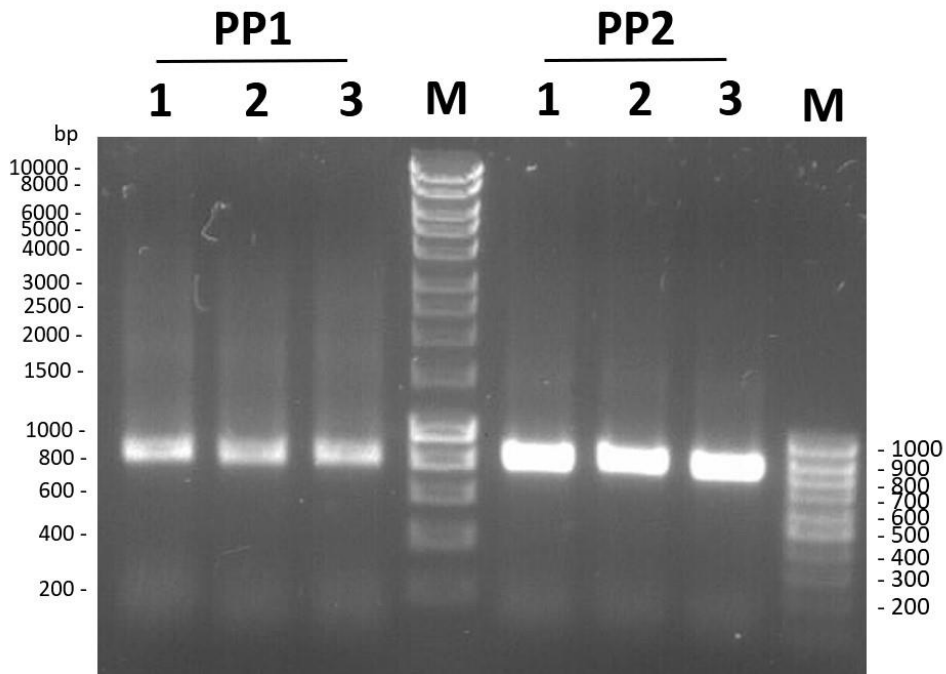
Figure S 1: Gelectrophoresis of synthesized cDNA from pEGFPN-1.
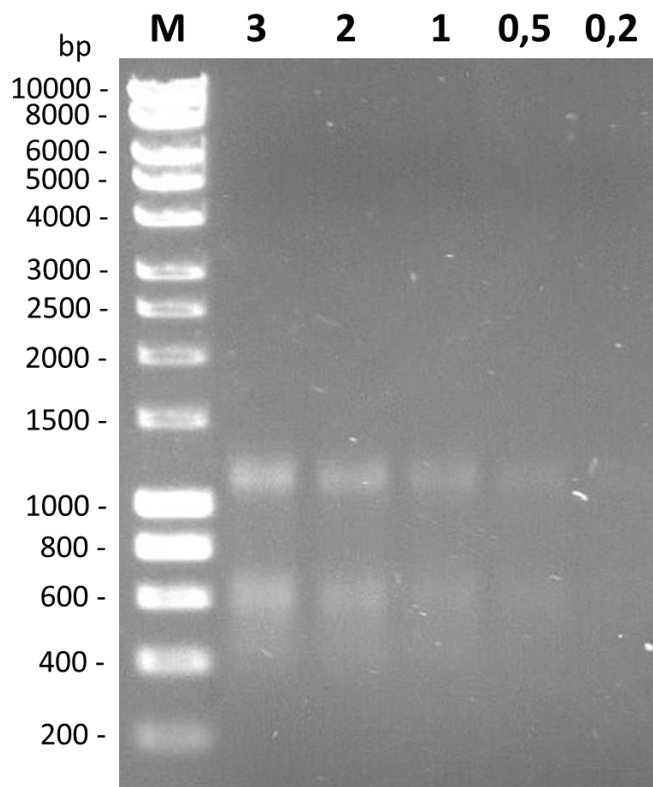
Figure S 2: Geleltrophoresis of EGFP-mRNA.
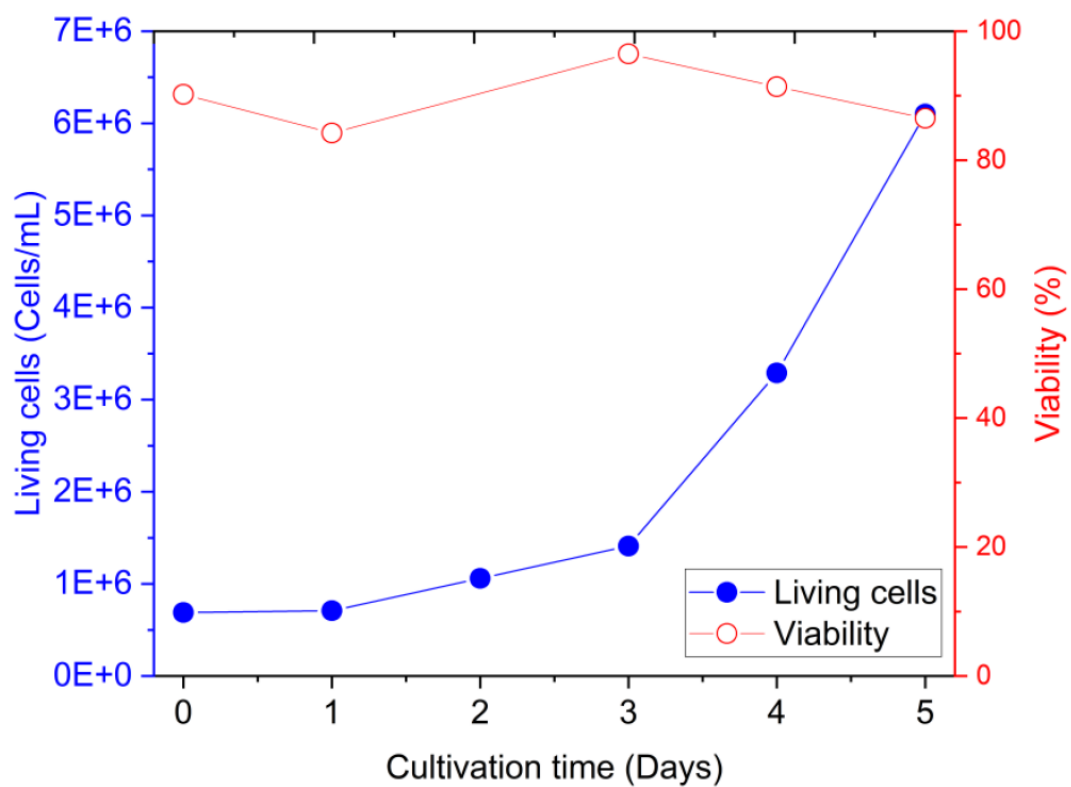
Figure S 3: Proliferation curve of primary human B cell.
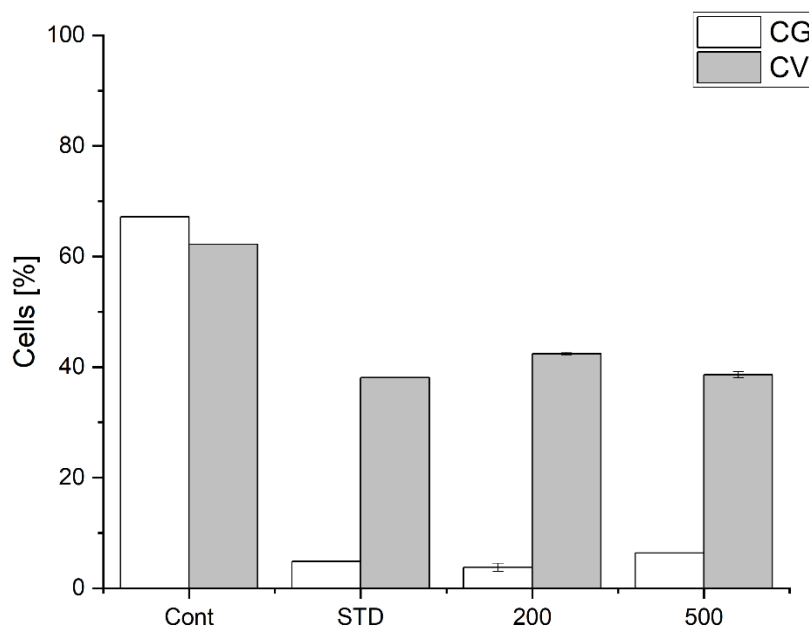
Figure S 4: Comparison of washing after TF.
Polymer-density = 15µg/10^6 cells, N/P = 10, $t_{contact}$ = 30 min., n = 2

Table S 1: Transfection of B cells using l-PEI in a tube setup transfection.

N/P ratio	Amount of pDNA/tube [ug]	TE [%]	Viability [%]
Mock	0	0	96.9
3	4.6	0	91.9
5	3.1	0	85.9
7.5	2.3	0.1	85.9
10	1.9	0.1	82.1
12.5	1.6	0.1	93.2
15	1.2	0.2	84.5
20	0.9	0.2	78.1
35	0.7	0.2	85
40	0.6	0.2	73

Polymer density: 15 µg per 10^6 cells, polymer concentration: 6 µg/mL, N/P ratio adjusted by varying pDNA amounts. Transfection day 4 post-thawing. Cell number during transfection: 2 x 10^5 cells. Contact time: 30 min. Transfection volume: 0.5 mL. n = 1. Cell viability on the day of transfection: > 80%. TE and viability were measured 48h post-transfection. "Mock": cells solely incubated with the complexation buffer.

6 Lists

6.1 List of Figures

6.2 List of Tables

6.3 List of Equations

6.4   List of Publications

Keim, D.; Gollner, K.; Gollner, U.; Jérôme, V.; Freitag, R. **(2021)**, "Generation of Recombinant Primary Human B Lymphocytes Using Non-Viral Vectors", *International journal of molecular sciences*, 22, DOI: 10.3390/ijms22158239.

Keim, D.; Dehne, M.; Miller, P.; Jérôme, V.; Bahnemann, J; Freitag, R. **(2024)**, "Non-viral transfection of ARPE-19 cells using an open access microfluidic system", *Finished manuscript*.

7 References

[1] Papanikolaou, E.; Bosio, A. **(2021)**, "The Promise and the Hope of Gene Therapy", *Frontiers in genome editing*, 3, p. 618346, DOI: 10.3389/fgeed.2021.618346.

[2] Zuris, J. A.; Thompson, D. B.; Shu, Y.; Guilinger, J. P.; Bessen, J. L.; Hu, J. H.; Maeder, M. L.; Joung, J. K.; Chen, Z.-Y.; Liu, D. R. **(2015)**, "Cationic lipid-mediated delivery of proteins enables efficient protein-based genome editing in vitro and in vivo", *Nature biotechnology*, 33, pp. 73–80, DOI: 10.1038/nbt.3081.

[3] Tay, A. **(2020)**, "The Benefits of Going Small: Nanostructures for Mammalian Cell Transfection", *ACS nano*, 14, pp. 7714–7721, DOI: 10.1021/acsnano.0c04624.

[4] Bulcha, J. T.; Wang, Y.; Ma, H.; Tai, P. W. L.; Gao, G. **(2021)**, "Viral vector platforms within the gene therapy landscape", *Signal transduction and targeted therapy*, 6, p. 53, DOI: 10.1038/s41392-021-00487-6.

[5] Rouse, B. T.; Sehrawat, S. **(2010)**, "Immunity and immunopathology to viruses: what decides the outcome?", *Nature reviews. Immunology*, 10, pp. 514–526, DOI: 10.1038/nri2802.

[6] Nayak, S.; Herzog, R. W. **(2010)**, "Progress and prospects: immune responses to viral vectors", *Gene therapy*, 17, pp. 295–304, DOI: 10.1038/gt.2009.148.

[7] Manno, C. S.; Pierce, G. F.; Arruda, V. R.; Glader, B.; Ragni, M.; Rasko, J. J.; Ozelo, M. C.; Hoots, K.; Blatt, P.; Konkle, B.; Dake, M.; Kaye, R.; Razavi, M.; Zajko, A.; Zehnder, J.; Rustagi, P. K.; Nakai, H.; Chew, A.; Leonard, D.; Wright, J. F.; Lessard, R. R.; Sommer, J. M.; Tigges, M.; Sabatino, D.; Luk, A.; Jiang, H.; Mingozzi, F.; Couto, L.; Ertl, H. C.; High, K. A.; Kay, M. A. **(2006)**, "Successful transduction of liver in hemophilia by AAV-Factor IX and limitations imposed by the host immune response", *Nature medicine*, 12, pp. 342–347, DOI: 10.1038/nm1358.

[8] Howe, S. J.; Mansour, M. R.; Schwarzwaelder, K.; Bartholomae, C.; Hubank, M.; Kempski, H.; Brugman, M. H.; Pike-Overzet, K.; Chatters, S. J.; Ridder, D. de; Gilmour, K. C.; Adams, S.; Thornhill, S. I.; Parsley, K. L.; Staal, F. J. T.; Gale, R. E.; Linch, D. C.; Bayford, J.; Brown, L.; Quaye, M.; Kinnon, C.; Ancliff, P.; Webb, D. K.; Schmidt, M.; Kalle, C. von; Gaspar, H. B.; Thrasher, A. J. **(2008)**, "Insertional mutagenesis combined with acquired somatic mutations causes leukemogenesis following gene therapy of SCID-X1 patients", *The Journal of clinical investigation*, 118, pp. 3143–3150, DOI: 10.1172/JCI35798.

[9]   Raper, S. E.; Chirmule, N.; Lee, F. S.; Wivel, N. A.; Bagg, A.; Gao, G.; Wilson, J. M.; Batshaw, M. L. **(2003)**, "Fatal systemic inflammatory response syndrome in a ornithine transcarbamylase deficient patient following adenoviral gene transfer", *Molecular genetics and metabolism*, 80, pp. 148–158, DOI: 10.1016/j.ymgme.2003.08.016.

[10]   Szybalska, E. H.; Szybalski, W. **(1962)**, "Genetics of human cell line. IV. DNA-mediated heritable transformation of a biochemical trait", *Proceedings of the National Academy of Sciences of the United States of America*, 48, pp. 2026–2034, DOI: 10.1073/pnas.48.12.2026.

[11]   Gigante, A.; Li, M.; Junghänel, S.; Hirschhäuser, C.; Knauer, S.; Schmuck, C. **(2019)**, "Non-viral transfection vectors: are hybrid materials the way forward?", *MedChemComm*, 10, pp. 1692–1718, DOI: 10.1039/c9md00275h.

[12]   Pandey, A. P.; Sawant, K. K. **(2016)**, "Polyethylenimine: A versatile, multifunctional non-viral vector for nucleic acid delivery", *Materials science & engineering. C, Materials for biological applications*, 68, pp. 904–918, DOI: 10.1016/j.msec.2016.07.066.

[13]   Gupta, A.; Andresen, J. L.; Manan, R. S.; Langer, R. **(2021)**, "Nucleic acid delivery for therapeutic applications", *Advanced drug delivery reviews*, 178, p. 113834, DOI: 10.1016/j.addr.2021.113834.

[14]   Andresen, J. L.; Fenton, O. S. **(2021)**, "Nucleic acid delivery and nanoparticle design for COVID vaccines", *MRS bulletin*, 46, pp. 832–839, DOI: 10.1557/s43577-021-00169-2.

[15]   Ni, R.; Feng, R.; Chau, Y. **(2019)**, "Synthetic Approaches for Nucleic Acid Delivery: Choosing the Right Carriers", *Life (Basel, Switzerland)*, 9, DOI: 10.3390/life9030059.

[16]   Created with Biorender.com.

[17]   Kopatz, I.; Remy, J.-S.; Behr, J.-P. **(2004)**, "A model for non-viral gene delivery: through syndecan adhesion molecules and powered by actin", *The journal of gene medicine*, 6, pp. 769–776, DOI: 10.1002/jgm.558.

[18]   Durymanov, M.; Reineke, J. **(2018)**, "Non-viral Delivery of Nucleic Acids: Insight Into Mechanisms of Overcoming Intracellular Barriers", *Frontiers in pharmacology*, 9, p. 971, DOI: 10.3389/fphar.2018.00971.

[19]   Wang, P.; Ke, Y. **(2018)**, "Attack on the Cell Membrane: The Pointy Ends of DNA Nanostructures Lead the Way", *ACS central science*, 4, pp. 1298–1299, DOI: 10.1021/acscentsci.8b00600.

[20] Fus-Kujawa, A.; Prus, P.; Bajdak-Rusinek, K.; Teper, P.; Gawron, K.; Kowalczuk, A.; Sieron, A. L. **(2021)**, "An Overview of Methods and Tools for Transfection of Eukaryotic Cells in vitro", *Frontiers in bioengineering and biotechnology*, 9, p. 701031, DOI: 10.3389/fbioe.2021.701031.

[21] Lechardeur, D.; Sohn, K. J.; Haardt, M.; Joshi, P. B.; Monck, M.; Graham, R. W.; Beatty, B.; Squire, J.; O'Brodovich, H.; Lukacs, G. L. **(1999)**, "Metabolic instability of plasmid DNA in the cytosol: a potential barrier to gene transfer", *Gene therapy*, 6, pp. 482–497, DOI: 10.1038/sj.gt.3300867.

[22] Byrne, M.; Victory, D.; Hibbitts, A.; Lanigan, M.; Heise, A.; Cryan, S.-A. **(2013)**, "Molecular weight and architectural dependence of well-defined star-shaped poly(lysine) as a gene delivery vector", *Biomaterials science*, 1, pp. 1223–1234, DOI: 10.1039/c3bm60123d.

[23] Cohen, S.; Au, S.; Panté, N. **(2011)**, "How viruses access the nucleus", *Biochimica et biophysica acta*, 1813, pp. 1634–1645, DOI: 10.1016/j.bbamcr.2010.12.009.

[24] Weaver, J. C.; Chizmadzhev, Y. **(1996)**, "Theory of electroporation: A review", *Bioelectrochemistry and Bioenergetics*, 41, pp. 135–160, DOI: 10.1016/S0302-4598(96)05062-3.

[25] Broderick, K. E.; Humeau, L. M. **(2015)**, "Electroporation-enhanced delivery of nucleic acid vaccines", *Expert review of vaccines*, 14, pp. 195–204, DOI: 10.1586/14760584.2015.990890.

[26] Rols, M.-P. **(2008)**, "Mechanism by which electroporation mediates DNA migration and entry into cells and targeted tissues", *Methods in molecular biology (Clifton, N.J.)*, 423, pp. 19–33, DOI: 10.1007/978-1-59745-194-9_2.

[27] Paliwal, S. R.; Paliwal, R.; Vyas, S. P. **(2015)**, "A review of mechanistic insight and application of pH-sensitive liposomes in drug delivery", *Drug delivery*, 22, pp. 231–242, DOI: 10.3109/10717544.2014.882469.

[28] Mali, S. **(2013)**, "Delivery systems for gene therapy", *Indian journal of human genetics*, 19, pp. 3–8, DOI: 10.4103/0971-6866.112870.

[29] Lundstrom, K. **(2018)**, "Viral Vectors in Gene Therapy", *Diseases (Basel, Switzerland)*, 6, DOI: 10.3390/diseases6020042.

[30] Kim, T. K.; Eberwine, J. H. **(2010)**, "Mammalian cell transfection: the present and the future", *Analytical and bioanalytical chemistry*, 397, pp. 3173–3178, DOI: 10.1007/s00216-010-3821-6.

[31] Tanemura, H.; Masuda, K.; Okumura, T.; Takagi, E.; Kajihara, D.; Kakihara, H.; Nonaka, K.; Ushioda, R. **(2022)**, "Development of a stable antibody production system utilizing an Hspa5 promoter in CHO cells", *Scientific reports*, 12, p. 7239, DOI: 10.1038/s41598-022-11342-1.

[32] Miura, M.; Yuan, J. **(2000)**, "Transient transfection assay of cell death genes", *Methods in enzymology*, 322, pp. 480–492, DOI: 10.1016/S0076-6879(00)22044-2.

[33] Howarth, J. L.; Lee, Y. B.; Uney, J. B. **(2010)**, "Using viral vectors as gene transfer tools (Cell Biology and Toxicology Special Issue: ETCS-UK 1 day meeting on genetic manipulation of cells)", *Cell biology and toxicology*, 26, pp. 1–20, DOI: 10.1007/s10565-009-9139-5.

[34] Chen, Y. H.; Keiser, M. S.; Davidson, B. L. **(2018)**, "Viral Vectors for Gene Transfer", *Current protocols in mouse biology*, 8, e58, DOI: 10.1002/cpmo.58.

[35] Wang, F.; Wang, Z.; Tian, H.; Qi, M.; Zhai, Z.; Li, S.; Li, R.; Zhang, H.; Wang, W.; Fu, S.; Lu, J.; Rodriguez, R.; Guo, Y.; Zhou, L. **(2012)**, "Biodistribution and safety assessment of bladder cancer specific recombinant oncolytic adenovirus in subcutaneous xenografts tumor model in nude mice", *Current gene therapy*, 12, pp. 67–76, DOI: 10.2174/156652312800099599.

[36] McCormack, M. P.; Rabbitts, T. H. **(2004)**, "Activation of the T-cell oncogene LMO2 after gene therapy for X-linked severe combined immunodeficiency", *The New England journal of medicine*, 350, pp. 913–922, DOI: 10.1056/NEJMra032207.

[37] Hacein-Bey-Abina, S.; Garrigue, A.; Wang, G. P.; Soulier, J.; Lim, A.; Morillon, E.; Clappier, E.; Caccavelli, L.; Delabesse, E.; Beldjord, K.; Asnafi, V.; MacIntyre, E.; Dal Cortivo, L.; Radford, I.; Brousse, N.; Sigaux, F.; Moshous, D.; Hauer, J.; Borkhardt, A.; Belohradsky, B. H.; Wintergerst, U.; Velez, M. C.; Leiva, L.; Sorensen, R.; Wulffraat, N.; Blanche, S.; Bushman, F. D.; Fischer, A.; Cavazzana-Calvo, M. **(2008)**, "Insertional oncogenesis in 4 patients after retrovirus-mediated gene therapy of SCID-X1", *The Journal of clinical investigation*, 118, pp. 3132–3142, DOI: 10.1172/JCI35700.

[38] Wei, Q.; Fan, J.; Liao, J.; Zou, Y.; Song, D.; Liu, J.; Cui, J.; Liu, F.; Ma, C.; Hu, X.; Li, L.; Yu, Y.; Qu, X.; Chen, L.; Yu, X.; Zhang, Z.; Zhao, C.; Zeng, Z.; Zhang, R.; Yan, S.; Wu, X.; Shu, Y.; Reid, R. R.; Lee, M. J.; Wolf, J. M.; He, T.-C. **(2017)**, "Engineering the Rapid Adenovirus Production and Amplification (RAPA) Cell Line to Expedite the Generation of Recombinant Adenoviruses", *Cellular physiology and biochemistry : international journal of experimental cellular physiology, biochemistry, and pharmacology*, 41, pp. 2383–2398, DOI: 10.1159/000475909.

[39] Kay, M. A.; Glorioso, J. C.; Naldini, L. **(2001)**, "Viral vectors for gene therapy: the art of turning infectious agents into vehicles of therapeutics", *Nature medicine*, 7, pp. 33–40, DOI: 10.1038/83324.

[40] Costa-Verdera, H.; Unzu, C.; Valeri, E.; Adriouch, S.; González Aseguinolaza, G.; Mingozzi, F.; Kajaste-Rudnitski, A. **(2023)**, "Understanding and Tackling Immune Responses to Adeno-Associated Viral Vectors", *Human gene therapy*, 34, pp. 836–852, DOI: 10.1089/hum.2023.119.

[41] Wang, Y.; Shao, W. **(2023)**, "Innate Immune Response to Viral Vectors in Gene Therapy", *Viruses*, 15, DOI: 10.3390/v15091801.

[42] Waehler, R.; Russell, S. J.; Curiel, D. T. **(2007)**, "Engineering targeted viral vectors for gene therapy", *Nature reviews. Genetics*, 8, pp. 573–587, DOI: 10.1038/nrg2141.

[43] Puzzo, F.; Zhang, C.; Powell Gray, B.; Zhang, F.; Sullenger, B. A.; Kay, M. A. **(2023)**, "Aptamer-programmable adeno-associated viral vectors as a novel platform for cell-specific gene transfer", *Molecular therapy. Nucleic acids*, 31, pp. 383–397, DOI: 10.1016/j.omtn.2023.01.007.

[44] Bull, J. J. **(2015)**, "Evolutionary reversion of live viral vaccines: Can genetic engineering subdue it?", *Virus evolution*, 1, DOI: 10.1093/ve/vev005.

[45] Sterner, R. C.; Sterner, R. M. **(2021)**, "CAR-T cell therapy: current limitations and potential strategies", *Blood cancer journal*, 11, p. 69, DOI: 10.1038/s41408-021-00459-7.

[46] Crees, Z. D.; Ghobadi, A. **(2021)**, "Cellular Therapy Updates in B-Cell Lymphoma: The State of the CAR-T", *Cancers*, 13, DOI: 10.3390/cancers13205181.

[47] Wang, A. X.; Ong, X. J.; D'Souza, C.; Neeson, P. J.; Zhu, J. J. **(2023)**, "Combining chemotherapy with CAR-T cell therapy in treating solid tumors", *Frontiers in immunology*, 14, p. 1140541, DOI: 10.3389/fimmu.2023.1140541.

[48] Mahase, E. **(2021)**, "How the Oxford-AstraZeneca covid-19 vaccine was made", *BMJ (Clinical research ed.)*, 372, n86, DOI: 10.1136/bmj.n86.

[49] Fathizadeh, H.; Afshar, S.; Masoudi, M. R.; Gholizadeh, P.; Asgharzadeh, M.; Ganbarov, K.; Köse, Ş.; Yousefi, M.; Kafil, H. S. **(2021)**, "SARS-CoV-2 (Covid-19) vaccines structure, mechanisms and effectiveness: A review", *International journal of biological macromolecules*, 188, pp. 740–750, DOI: 10.1016/j.ijbiomac.2021.08.076.

[50] Heinz, F. X.; Stiasny, K. **(2021)**, "Distinguishing features of current COVID-19 vaccines: knowns and unknowns of antigen presentation and modes of action", *npj Vaccines*, 6, DOI: 10.1038/s41541-021-00369-6.

[51] Sayed, N.; Allawadhi, P.; Khurana, A.; Singh, V.; Navik, U.; Pasumarthi, S. K.; Khurana, I.; Banothu, A. K.; Weiskirchen, R.; Bharani, K. K. **(2022)**, "Gene therapy: Comprehensive overview and therapeutic applications", *Life sciences*, 294, p. 120375, DOI: 10.1016/j.lfs.2022.120375.

[52] Hamm, A.; Krott, N.; Breibach, I.; Blindt, R.; Bosserhoff, A. K. **(2002)**, "Efficient transfection method for primary cells", *Tissue engineering*, 8, pp. 235–245, DOI: 10.1089/107632702753725003.

[53] Søndergaard, J. N.; Geng, K.; Sommerauer, C.; Atanasoai, I.; Yin, X.; Kutter, C. **(2020)**, "Successful delivery of large-size CRISPR/Cas9 vectors in hard-to-transfect human cells using small plasmids", *Communications biology*, 3, p. 319, DOI: 10.1038/s42003-020-1045-7.

[54] *Electroporation-mediated gene delivery***2015**.

[55] Cervia, L. D.; Yuan, F. **(2018)**, "Current Progress in Electrotransfection as a Nonviral Method for Gene Delivery", *Molecular pharmaceutics*, 15, pp. 3617–3624, DOI: 10.1021/acs.molpharmaceut.8b00207.

[56] Scuderi, M.; Dermol-Černe, J.; Da Amaral Silva, C.; Muralidharan, A.; Boukany, P. E.; Rems, L. **(2022)**, "Models of electroporation and the associated transmembrane molecular transport should be revisited", *Bioelectrochemistry (Amsterdam, Netherlands)*, 147, p. 108216, DOI: 10.1016/j.bioelechem.2022.108216.

[57] Mendes, B. B.; Conniot, J.; Avital, A.; Yao, D.; Jiang, X.; Zhou, X.; Sharf-Pauker, N.; Xiao, Y.; Adir, O.; Liang, H.; Shi, J.; Schroeder, A.; Conde, J. **(2022)**, "Nanodelivery of nucleic acids", *Nature reviews. Methods primers*, 2, DOI: 10.1038/ s43586-022-00104-y.

[58] Shtykalova, S.; Deviatkin, D.; Freund, S.; Egorova, A.; Kiselev, A. **(2023)**, "Non-Viral Carriers for Nucleic Acids Delivery: Fundamentals and Current Applications", *Life (Basel, Switzerland)*, 13, DOI: 10.3390/life13040903.

[59] Wasungu, L.; Hoekstra, D. **(2006)**, "Cationic lipids, lipoplexes and intracellular delivery of genes", *Journal of controlled release : official journal of the Controlled Release Society*, 116, pp. 255–264, DOI: 10.1016/j.jconrel.2006.06.024.

[60] Wittrup, A.; Ai, A.; Liu, X.; Hamar, P.; Trifonova, R.; Charisse, K.; Manoharan, M.; Kirchhausen, T.; Lieberman, J. **(2015)**, "Visualizing lipid-formulated siRNA release from endosomes and target gene knockdown", *Nature biotechnology*, 33, pp. 870–876, DOI: 10.1038/nbt.3298.

[61] Clarke, D.; Idris, A.; McMillan, N. A. J. **(2019)**, "Development of novel lipidic particles for siRNA delivery that are highly effective after 12 months storage", *PloS one*, 14, e0211954, DOI: 10.1371/journal.pone.0211954.

[62] Clement, J.; Kiefer, K.; Kimpfler, A.; Garidel, P.; Peschka-Süss, R. **(2005)**, "Large-scale production of lipoplexes with long shelf-life", *European journal of pharmaceutics and biopharmaceutics : official journal of Arbeitsgemeinschaft fur Pharmazeutische Verfahrenstechnik e.V*, 59, pp. 35–43, DOI: 10.1016/j.ejpb.2004.06.001.

[63] Zou, S.; Scarfo, K.; Nantz, M. H.; Hecker, J. G. **(2010)**, "Lipid-mediated delivery of RNA is more efficient than delivery of DNA in non-dividing cells", *International journal of pharmaceutics*, 389, pp. 232–243, DOI: 10.1016/j.ijpharm.2010.01.019.

[64] Alshehri, A.; Grabowska, A.; Stolnik, S. **(2018)**, "Pathways of cellular internalisation of liposomes delivered siRNA and effects on siRNA engagement with target mRNA and silencing in cancer cells", *Scientific reports*, 8, p. 3748, DOI: 10.1038/s41598-018-22166-3.

[65] Elouahabi, A.; Ruysschaert, J.-M. **(2005)**, "Formation and intracellular trafficking of lipoplexes and polyplexes", *Molecular therapy : the journal of the American Society of Gene Therapy*, 11, pp. 336–347, DOI: 10.1016/j.ymthe.2004.12.006.

[66] ur Rehman, Z.; Hoekstra, D.; Zuhorn, I. S. **(2013)**, "Mechanism of polyplex- and lipoplex-mediated delivery of nucleic acids: real-time visualization of transient membrane destabilization without endosomal lysis", *ACS nano*, 7, pp. 3767–3777, DOI: 10.1021/nn3049494.

[67] Bus, T.; Traeger, A.; Schubert, U. S. **(2018)**, "The great escape: how cationic polyplexes overcome the endosomal barrier", *Journal of materials chemistry. B*, 6, pp. 6904–6918, DOI: 10.1039/c8tb00967h.

[68] Vermeulen, L. M. P.; Smedt, S. C. de; Remaut, K.; Braeckmans, K. **(2018)**, "The proton sponge hypothesis: Fable or fact?", *European journal of pharmaceutics and biopharmaceutics : official journal of Arbeitsgemeinschaft fur Pharmazeutische Verfahrenstechnik e.V*, 129, pp. 184–190, DOI: 10.1016/j.ejpb.2018.05.034.

[69] Benjaminsen, R. V.; Mattebjerg, M. A.; Henriksen, J. R.; Moghimi, S. M.; Andresen, T. L. **(2013)**, "The possible "proton sponge " effect of polyethylenimine (PEI) does not include change in lysosomal pH", *Molecular therapy : the journal of the American Society of Gene Therapy*, 21, pp. 149–157, DOI: 10.1038/mt.2012.185.

[70] Freeman, E. C.; Weiland, L. M.; Meng, W. S. (**2012**), "Modeling the Proton Sponge Hypothesis: Examining Proton Sponge Effectiveness for Enhancing Intracellular Gene Delivery through Multiscale Modeling", *Journal of biomaterials science. Polymer edition*, 24, pp. 398–416, DOI: 10.1080/09205063.2012.690282.

[71] Rattan, R.; Vaidyanathan, S.; Wu, G. S.-H.; Shakya, A.; Orr, B. G.; Banaszak Holl, M. M. (**2013**), "Polyplex-induced cytosolic nuclease activation leads to differential transgene expression", *Molecular pharmaceutics*, 10, pp. 3013–3022, DOI: 10.1021/mp400103f.

[72] Ponti, F.; Campolungo, M.; Melchiori, C.; Bono, N.; Candiani, G. (**2021**), "Cationic lipids for gene delivery: many players, one goal", *Chemistry and physics of lipids*, 235, p. 105032, DOI: 10.1016/j.chemphyslip.2020.105032.

[73] Rinkenauer, A. C.; Schubert, S.; Traeger, A.; Schubert, U. S. (**2015**), "The influence of polymer architecture on in vitro pDNA transfection", *Journal of materials chemistry. B*, 3, pp. 7477–7493, DOI: 10.1039/c5tb00782h.

[74] Taranejoo, S.; Liu, J.; Verma, P.; Hourigan, K. (**2015**), "A review of the developments of characteristics of PEI derivatives for gene delivery applications", *J. Appl. Polym. Sci.*, 132, DOI: 10.1002/APP.42096.

[75] Stahlschmidt, U.; Jérôme, V.; Majewski, A. P.; Müller, A. H. E.; Freitag, R. (**2017**), "Systematic Study of a Library of PDMAEMA-Based, Superparamagnetic Nano-Stars for the Transfection of CHO-K1 Cells", *Polymers*, 9, DOI: 10.3390/polym9050156.

[76] Majewski, A. P.; Stahlschmidt, U.; Jérôme, V.; Freitag, R.; Müller, A. H. E.; Schmalz, H. (**2013**), "PDMAEMA-grafted core-shell-corona particles for nonviral gene delivery and magnetic cell separation", *Biomacromolecules*, 14, pp. 3081–3090, DOI: 10.1021/bm400703d.

[77] Diaz, I. L.; Sierra, C. A.; Jérôme, V.; Freitag, R.; Perez, L. D. (**2020**), "Target grafting of poly(2-(dimethylamino)ethyl methacrylate) to biodegradable block copolymers", *Journal of Polymer Science*, 58, pp. 2168–2180, DOI: 10.1002/pol.20200204.

[78] Keim, D.; Gollner, K.; Gollner, U.; Jérôme, V.; Freitag, R. (**2021**), "Generation of Recombinant Primary Human B Lymphocytes Using Non-Viral Vectors", *International journal of molecular sciences*, 22, DOI: 10.3390/ijms22158239.

[79] Kim, K.; Ryu, K.; Cho, H.; Shim, M. S.; Cho, Y.-Y.; Lee, J. Y.; Lee, H. S.; Kang, H. C. **(2020)**, "Effects of Decomplexation Rates on Ternary Gene Complex Transfection with α-Poly(l-Lysine) or ε-Poly(l-Lysine) as a Decomplexation Controller in An Easy-To-Transfect Cell or A Hard-To-Transfect Cell", *Pharmaceutics*, 12, DOI: 10.3390/pharmaceutics12060490.

[80] Synatschke, C. V.; Schallon, A.; Jérôme, V.; Freitag, R.; Müller, A. H. E. **(2011)**, "Influence of polymer architecture and molecular weight of poly(2-(dimethylamino)ethyl methacrylate) polycations on transfection efficiency and cell viability in gene delivery", *Biomacromolecules*, 12, pp. 4247–4255, DOI: 10.1021/bm201111d.

[81] Liao, X.; Walden, G.; Falcon, N. D.; Donell, S.; Raxworthy, M. J.; Wormstone, M.; Riley, G. P.; Saeed, A. **(2017)**, "A direct comparison of linear and star-shaped poly(dimethylaminoethyl acrylate) polymers for polyplexation with DNA and cytotoxicity in cultured cell lines", *European Polymer Journal*, 87, pp. 458–467, DOI: 10.1016/j.eurpolymj.2016.08.021.

[82] Grimme, C. J.; Hanson, M. G.; Corcoran, L. G.; Reineke, T. M. **(2022)**, "Polycation Architecture Affects Complexation and Delivery of Short Antisense Oligonucleotides: Micelleplexes Outperform Polyplexes", *Biomacromolecules*, 23, pp. 3257–3271, DOI: 10.1021/acs.biomac.2c00338.

[83] Leiske, M. N. **(2023)**, "Poly(2-oxazoline)-derived star-shaped polymers as potential materials for biomedical applications: A review", *European Polymer Journal*, 185, p. 111832, DOI: 10.1016/j.eurpolymj.2023.111832.

[84] Nemati Mahand, S.; Aliakbarzadeh, S.; Moghaddam, A.; Salehi Moghaddam, A.; Kruppke, B.; Nasrollahzadeh, M.; Khonakdar, H. A. **(2022)**, "Polyoxazoline: A review article from polymerization to smart behaviors and biomedical applications", *European Polymer Journal*, 178, p. 111484, DOI: 10.1016/j.eurpolymj.2022.111484.

[85] Knop, K.; Hoogenboom, R.; Fischer, D.; Schubert, U. S. **(2010)**, "Poly(ethylene glycol) in drug delivery: pros and cons as well as potential alternatives", *Angewandte Chemie (International ed. in English)*, 49, pp. 6288–6308, DOI: 10.1002/anie.200902672.

[86] Dogan, N. O.; Bozuyuk, U.; Erkoc, P.; Karacakol, A. C.; Cingoz, A.; Seker-Polat, F.; Nazeer, M. A.; Sitti, M.; Bagci-Onder, T.; Kizilel, S. **(2022)**, "Parameters Influencing Gene Delivery Efficiency of PEGylated Chitosan Nanoparticles: Experimental and Modeling Approach", *Advanced NanoBiomed Research*, 2, p. 2100033, DOI: 10.1002/anbr.202100033.

[87] Stepto, R. F. T. **(2009)**, "Dispersity in polymer science (IUPAC Recommendations 2009)", *Pure and Applied Chemistry*, 81, pp. 351–353, DOI: 10.1351/PAC-REC-08-05-02.

[88] Truong, N. P.; Jones, G. R.; Bradford, K. G. E.; Konkolewicz, D.; Anastasaki, A. **(2021)**, "A comparison of RAFT and ATRP methods for controlled radical polymerization", *Nat Rev Chem*, 5, pp. 859–869, DOI: 10.1038/s41570-021-00328-8.

[89] Perrier, S. **(2017)**, "50th Anniversary Perspective : RAFT Polymerization—A User Guide", *Macromolecules*, 50, pp. 7433–7447, DOI: 10.1021/acs.macromol.7b00767.

[90] Matyjaszewski, K. **(2012)**, "Atom Transfer Radical Polymerization (ATRP): Current Status and Future Perspectives", *Macromolecules*, 45, pp. 4015–4039, DOI: 10.1021/ma3001719.

[91] Tang, W.; Kwak, Y.; Braunecker, W.; Tsarevsky, N. V.; Coote, M. L.; Matyjaszewski, K. **(2008)**, "Understanding atom transfer radical polymerization: effect of ligand and initiator structures on the equilibrium constants", *Journal of the American Chemical Society*, 130, pp. 10702–10713, DOI: 10.1021/ja802290a.

[92] Tang, W.; Matyjaszewski, K. **(2007)**, "Effects of Initiator Structure on Activation Rate Constants in ATRP", *Macromolecules*, 40, pp. 1858–1863, DOI: 10.1021/ma062897b.

[93] Braunecker, W. A.; Tsarevsky, N. V.; Gennaro, A.; Matyjaszewski, K. **(2009)**, "Thermodynamic Components of the Atom Transfer Radical Polymerization Equilibrium: Quantifying Solvent Effects", *Macromolecules*, 42, pp. 6348–6360, DOI: 10.1021/ma901094s.

[94] Su, G.; Zhou, H.; Mu, Q.; Zhang, Y.; Li, L.; Jiao, P.; Jiang, G.; Yan, B. **(2012)**, "Effective Surface Charge Density Determines the Electrostatic Attraction between Nanoparticles and Cells", *J. Phys. Chem. C*, 116, pp. 4993–4998, DOI: 10.1021/jp211041m.

[95] Kaksonen, M.; Roux, A. **(2018)**, "Mechanisms of clathrin-mediated endocytosis", *Nature reviews. Molecular cell biology*, 19, pp. 313–326, DOI: 10.1038/nrm.2017.132.

[96] Kumar, R.; Santa Chalarca, C. F.; Bockman, M. R.; van Bruggen, C.; Grimme, C. J.; Dalal, R. J.; Hanson, M. G.; Hexum, J. K.; Reineke, T. M. **(2021)**, "Polymeric Delivery of Therapeutic Nucleic Acids", *Chemical reviews*, 121, pp. 11527–11652, DOI: 10.1021/acs.chemrev.0c00997.

[97] Li, T.; Senesi, A. J.; Lee, B. **(2016)**, "Small Angle X-ray Scattering for Nanoparticle Research", *Chemical reviews*, 116, pp. 11128–11180, DOI: 10.1021/acs.chemrev.5b00690.

[98] Andersen, H.; Parhamifar, L.; Hunter, A. C.; Shahin, V.; Moghimi, S. M. **(2016)**, "AFM visualization of sub-50nm polyplex disposition to the nuclear pore complex without compromising the integrity of the nuclear envelope", *Journal of controlled release : official journal of the Controlled Release Society*, 244, pp. 24–29, DOI: 10.1016/j.jconrel.2016.11.008.

[99] Farkas, N.; Scaria, P. V.; Woodle, M. C.; Dagata, J. A. **(2019)**, "Physical-chemical measurement method development for self-assembled, core-shell nanoparticles", *Scientific reports*, 9, p. 1655, DOI: 10.1038/s41598-018-38194-y.

[100] Di Cola, E.; Grillo, I.; Ristori, S. **(2016)**, "Small Angle X-ray and Neutron Scattering: Powerful Tools for Studying the Structure of Drug-Loaded Liposomes", *Pharmaceutics*, 8, DOI: 10.3390/pharmaceutics8020010.

[101] Dunn, K. C.; Aotaki-Keen, A. E.; Putkey, F. R.; Hjelmeland, L. M. **(1996)**, "ARPE-19, a human retinal pigment epithelial cell line with differentiated properties", *Experimental eye research*, 62, pp. 155–169, DOI: 10.1006/exer.1996.0020.

[102] Lim, L. S.; Mitchell, P.; Seddon, J. M.; Holz, F. G.; Wong, T. Y. **(2012)**, "Age-related macular degeneration", *Lancet (London, England)*, 379, pp. 1728–1738, DOI: 10.1016/S0140-6736(12)60282-7.

[103] Catanzaro, M.; Lanni, C.; Basagni, F.; Rosini, M.; Govoni, S.; Amadio, M. **(2020)**, "Eye-Light on Age-Related Macular Degeneration: Targeting Nrf2-Pathway as a Novel Therapeutic Strategy for Retinal Pigment Epithelium", *Frontiers in pharmacology*, 11, p. 844, DOI: 10.3389/fphar.2020.00844.

[104] Stahl, A. **(2020)**, "The Diagnosis and Treatment of Age-Related Macular Degeneration", *Deutsches Arzteblatt international*, 117, pp. 513–520, DOI: 10.3238/arztebl.2020.0513.

[105] Amadio, M.; Govoni, S.; Pascale, A. **(2016)**, "Targeting VEGF in eye neovascularization: What's new?: A comprehensive review on current therapies and oligonucleotide-based interventions under development", *Pharmacological research*, 103, pp. 253–269, DOI: 10.1016/j.phrs.2015.11.027.

[106] Kozlowski, M. R. **(2015)**, "The ARPE-19 cell line: mortality status and utility in macular degeneration research", *Current eye research*, 40, pp. 501–509, DOI: 10.3109/02713683.2014.935440.

[107] Lund, R. D.; Adamson, P.; Sauvé, Y.; Keegan, D. J.; Girman, S. V.; Wang, S.; Winton, H.; Kanuga, N.; Kwan, A. S.; Beauchène, L.; Zerbib, A.; Hetherington, L.; Couraud, P. O.; Coffey, P.; Greenwood, J. **(2001)**, "Subretinal transplantation of genetically modified human cell lines attenuates loss of visual function in dystrophic rats", *Proceedings of the National Academy of Sciences of the United States of America*, 98, pp. 9942–9947, DOI: 10.1073/pnas.171266298.

[108] Sunshine, J. C.; Sunshine, S. B.; Bhutto, I.; Handa, J. T.; Green, J. J. **(2012)**, "Poly(β-amino ester)-nanoparticle mediated transfection of retinal pigment epithelial cells in vitro and in vivo", *PloS one*, 7, e37543, DOI: 10.1371/journal.pone.0037543.

[109] Shmueli, R. B.; Sunshine, J. C.; Xu, Z.; Duh, E. J.; Green, J. J. **(2012)**, "Gene delivery nanoparticles specific for human microvasculature and macrovasculature", *Nanomedicine : nanotechnology, biology, and medicine*, 8, pp. 1200–1207, DOI: 10.1016/j.nano.2012.01.006.

[110] Del Pozo-Rodríguez, A.; Delgado, D.; Solinís, M. A.; Gascón, A. R.; Pedraz, J. L. **(2008)**, "Solid lipid nanoparticles for retinal gene therapy: transfection and intracellular trafficking in RPE cells", *International journal of pharmaceutics*, 360, pp. 177–183, DOI: 10.1016/j.ijpharm.2008.04.023.

[111] Puras, G.; Mashal, M.; Zárate, J.; Agirre, M.; Ojeda, E.; Grijalvo, S.; Eritja, R.; Diaz-Tahoces, A.; Martínez Navarrete, G.; Avilés-Trigueros, M.; Fernández, E.; Pedraz, J. L. **(2014)**, "A novel cationic niosome formulation for gene delivery to the retina", *Journal of controlled release : official journal of the Controlled Release Society*, 174, pp. 27–36, DOI: 10.1016/j.jconrel.2013.11.004.

[112] Ojeda, E.; Puras, G.; Agirre, M.; Zárate, J.; Grijalvo, S.; Pons, R.; Eritja, R.; Martinez-Navarrete, G.; Soto-Sanchez, C.; Fernández, E.; Pedraz, J. L. **(2015)**, "Niosomes based on synthetic cationic lipids for gene delivery: the influence of polar head-groups on the transfection efficiency in HEK-293, ARPE-19 and MSC-D1 cells", *Organic & biomolecular chemistry*, 13, pp. 1068–1081, DOI: 10.1039/c4ob02087a.

[113] Thumann, G.; Stöcker, M.; Maltusch, C.; Salz, A. K.; Barth, S.; Walter, P.; Johnen, S. **(2010)**, "High efficiency non-viral transfection of retinal and iris pigment epithelial cells with pigment epithelium-derived factor", *Gene therapy*, 17, pp. 181–189, DOI: 10.1038/gt.2009.124.

[114] Da Sun; Maeno, H.; Gujrati, M.; Schur, R.; Maeda, A.; Maeda, T.; Palczewski, K.; Lu, Z.-R. **(2015)**, "Self-Assembly of a Multifunctional Lipid With Core-Shell Dendrimer DNA Nanoparticles Enhanced Efficient Gene Delivery at Low Charge Ratios into RPE Cells", *Macromolecular bioscience*, 15, pp. 1663–1672, DOI: 10.1002/mabi.201500192.

[115] Kaneshiro, T. L.; Wang, X.; Lu, Z.-R. **(2007)**, "Synthesis, characterization, and gene delivery of poly-L-lysine octa(3-aminopropyl)silsesquioxane dendrimers: nanoglobular drug carriers with precisely defined molecular architectures", *Molecular pharmaceutics*, 4, pp. 759–768, DOI: 10.1021/mp070036z.

[116] Rajewsky, K. **(1996)**, "Clonal selection and learning in the antibody system", *Nature*, 381, pp. 751–758, DOI: 10.1038/381751a0.

[117] LeBien, T. W.; Tedder, T. F. **(2008)**, "B lymphocytes: how they develop and function", *Blood*, 112, pp. 1570–1580, DOI: 10.1182/blood-2008-02-078071.

[118] Adamo, L.; Rocha-Resende, C.; Mann, D. L. **(2020)**, "The Emerging Role of B Lymphocytes in Cardiovascular Disease", *Annual review of immunology*, 38, pp. 99–121, DOI: 10.1146/annurev-immunol-042617-053104.

[119] Sabatino, J. J.; Pröbstel, A.-K.; Zamvil, S. S. **(2019)**, "B cells in autoimmune and neurodegenerative central nervous system diseases", *Nature reviews. Neuroscience*, 20, pp. 728–745, DOI: 10.1038/s41583-019-0233-2.

[120] Mauri, C.; Bosma, A. **(2012)**, "Immune regulatory function of B cells", *Annual review of immunology*, 30, pp. 221–241, DOI: 10.1146/annurev-immunol-020711-074934.

[121] Cho, S.-F.; Anderson, K. C.; Tai, Y.-T. **(2018)**, "Targeting B Cell Maturation Antigen (BCMA) in Multiple Myeloma: Potential Uses of BCMA-Based Immunotherapy", *Frontiers in immunology*, 9, p. 1821, DOI: 10.3389/fimmu.2018.01821.

[122] Helm, M.; A B Riedl, S.; Gollner, K.; Gollner, U.; Jérôme, V.; Freitag, R. **(2021)**, "Isolation of primary human B lymphocytes from tonsils compared to blood as alternative source for ex vivo application", *Journal of chromatography. B, Analytical technologies in the biomedical and life sciences*, 1179, p. 122853, DOI: 10.1016/j.jchromb.2021.122853.

[123] Glass, D. R.; Tsai, A. G.; Oliveria, J. P.; Hartmann, F. J.; Kimmey, S. C.; Calderon, A. A.; Borges, L.; Glass, M. C.; Wagar, L. E.; Davis, M. M.; Bendall, S. C. **(2020)**, "An Integrated Multi-omic Single-Cell Atlas of Human B Cell Identity", *Immunity*, 53, 217-232.e5, DOI: 10.1016/j.immuni.2020.06.013.

[124] Pesando, J. M.; Bouchard, L. S.; McMaster, B. E. **(1989)**, "CD19 is functionally and physically associated with surface immunoglobulin", *The Journal of experimental medicine*, 170, pp. 2159–2164, DOI: 10.1084/jem.170.6.2159.

[125] Jellusova, J. **(2020)**, "Metabolic control of B cell immune responses", *Current opinion in immunology*, 63, pp. 21–28, DOI: 10.1016/j.coi.2019.11.002.

[126] Jackson, S. M.; Wilson, P. C.; James, J. A.; Capra, J. D. **(2008)**, "Human B cell subsets", *Advances in immunology*, 98, pp. 151–224, DOI: 10.1016/S0065-2776(08)00405-7.

[127] Ishino, Y.; Shinagawa, H.; Makino, K.; Amemura, M.; Nakata, A. **(1987)**, "Nucleotide sequence of the iap gene, responsible for alkaline phosphatase isozyme conversion in Escherichia coli, and identification of the gene product", *Journal of bacteriology*, 169, pp. 5429–5433, DOI: 10.1128/jb.169.12.5429-5433.1987.

[128] Hsu, P. D.; Lander, E. S.; Zhang, F. **(2014)**, "Development and applications of CRISPR-Cas9 for genome engineering", *Cell*, 157, pp. 1262–1278, DOI: 10.1016/j.cell.2014.05.010.

[129] Adli, M. **(2018)**, "The CRISPR tool kit for genome editing and beyond", *Nature communications*, 9, p. 1911, DOI: 10.1038/s41467-018-04252-2.

[130] Pickar-Oliver, A.; Gersbach, C. A. **(2019)**, "The next generation of CRISPR-Cas technologies and applications", *Nature reviews. Molecular cell biology*, 20, pp. 490–507, DOI: 10.1038/s41580-019-0131-5.

[131] Zhao, B.; Rothenberg, E.; Ramsden, D. A.; Lieber, M. R. **(2020)**, "The molecular basis and disease relevance of non-homologous DNA end joining", *Nature reviews. Molecular cell biology*, 21, pp. 765–781, DOI: 10.1038/s41580-020-00297-8.

[132] Chapman, J. R.; Taylor, M. R. G.; Boulton, S. J. **(2012)**, "Playing the end game: DNA double-strand break repair pathway choice", *Molecular cell*, 47, pp. 497–510, DOI: 10.1016/j.molcel.2012.07.029.

[133] Schallon, A.; Synatschke, C. V.; Jérôme, V.; Müller, A. H. E.; Freitag, R. **(2012)**, "Nanoparticulate nonviral agent for the effective delivery of pDNA and siRNA to differentiated cells and primary human T lymphocytes", *Biomacromolecules*, 13, pp. 3463–3474, DOI: 10.1021/bm3012055.

[134] Herb, M.; Farid, A.; Gluschko, A.; Krönke, M.; Schramm, M. **(2019)**, "Highly Efficient Transfection of Primary Macrophages with In Vitro Transcribed mRNA", *Journal of visualized experiments : JoVE,* DOI: 10.3791/60143.

[135] Plamper, F. A.; Schmalz, A.; Penott-Chang, E.; Drechsler, M.; Jusufi, A.; Ballauff, M.; Müller, A. H. E. **(2007)**, "Synthesis and Characterization of Star-Shaped Poly(N,N - dimethylaminoethyl methacrylate) and Its Quaternized Ammonium Salts", *Macromolecules*, 40, pp. 5689–5697, DOI: 10.1021/ma070452x.

[136] Diaz Ariza, I. L.; Jérôme, V.; Pérez Pérez, L. D.; Freitag, R. **(2021)**, "Amphiphilic Graft Copolymers Capable of Mixed-Mode Interaction as Alternative Nonviral Transfection Agents", *ACS applied bio materials*, 4, pp. 1268–1282, DOI: 10.1021/acsabm.0c01123.

[137] Karra, D.; Dahm, R. **(2010)**, "Transfection techniques for neuronal cells", *The Journal of neuroscience : the official journal of the Society for Neuroscience*, 30, pp. 6171–6177, DOI: 10.1523/JNEUROSCI.0183-10.2010.

[138] Müller, M., *Polyelectrolyte Complexes in the Dispersed and Solid State II*, Springer Berlin Heidelberg, Berlin, Heidelberg**2014**.

[139] Tan, J. F.; Too, H. P.; Hatton, T. A.; Tam, K. C. **(2006)**, "Aggregation behavior and thermodynamics of binding between poly(ethylene oxide)-block-poly(2-(diethylamino)ethyl methacrylate) and plasmid DNA", *Langmuir : the ACS journal of surfaces and colloids*, 22, pp. 3744–3750, DOI: 10.1021/la052591i.

[140] Yen, A.; Cheng, Y.; Sylvestre, M.; Gustafson, H. H.; Puri, S.; Pun, S. H. **(2018)**, "Serum Nuclease Susceptibility of mRNA Cargo in Condensed Polyplexes", *Molecular pharmaceutics*, 15, pp. 2268–2276, DOI: 10.1021/acs.molpharmaceut.8b00134.

[141] Avci-Adali, M.; Behring, A.; Steinle, H.; Keller, T.; Krajeweski, S.; Schlensak, C.; Wendel, H. P. **(2014)**, "In vitro synthesis of modified mRNA for induction of protein expression in human cells", *Journal of visualized experiments : JoVE*, e51943, DOI: 10.3791/51943.

[142] Vardevanyan, P. O.; Antonyan, A. P.; Parsadanyan, M. A.; Davtyan, H. G.; Karapetyan, A. T. **(2003)**, "The binding of ethidium bromide with DNA: interaction with single- and double-stranded structures", *Experimental & molecular medicine*, 35, pp. 527–533, DOI: 10.1038/emm.2003.68.

[143] dos Santos, T.; Varela, J.; Lynch, I.; Salvati, A.; Dawson, K. A. **(2011)**, "Effects of transport inhibitors on the cellular uptake of carboxylated polystyrene nanoparticles in different cell lines", *PloS one*, 6, e24438, DOI: 10.1371/journal.pone.0024438.

[144] Riedl, S.; Kaiser, P.; Raup, A.; Synatschke, C.; Jérôme, V.; Freitag, R. **(2018)**, "Non-Viral Transfection of Human T Lymphocytes", *Processes*, 6, p. 188, DOI: 10.3390/pr6100188.

[145] Hazim, R. A.; Volland, S.; Yen, A.; Burgess, B. L.; Williams, D. S. **(2019)**, "Rapid differentiation of the human RPE cell line, ARPE-19, induced by nicotinamide", *Experimental eye research*, 179, pp. 18–24, DOI: 10.1016/j.exer.2018.10.009.

[146] Ponnalagu, M.; Subramani, M.; Jayadev, C.; Shetty, R.; Das, D. **(2017)**, "Retinal pigment epithelium-secretome: A diabetic retinopathy perspective", *Cytokine*, 95, pp. 126–135, DOI: 10.1016/j.cyto.2017.02.013.

[147] Li, H.; Wan, C.; Li, F. **(2015)**, "Recombinant adeno-associated virus-, polyethylenimine/plasmid- and lipofectamine/carboxyfluorescein-labeled small interfering RNA-based transfection in retinal pigment epithelial cells with ultrasound and/or SonoVue", *Molecular medicine reports*, 11, pp. 3609–3614, DOI: 10.3892/mmr.2015.3219.

[148] Hyvönen, Z.; Hämäläinen, V.; Ruponen, M.; Lucas, B.; Rejman, J.; Vercauteren, D.; Demeester, J.; Smedt, S. de; Braeckmans, K. **(2012)**, "Elucidating the pre- and post-nuclear intracellular processing of 1,4-dihydropyridine based gene delivery carriers", *Journal of controlled release : official journal of the Controlled Release Society*, 162, pp. 167–175, DOI: 10.1016/j.jconrel.2012.06.013.

[149] Oliveira, A. V.; Silva, A. P.; Bitoque, D. B.; Silva, G. A.; Da Rosa Costa, A. M. **(2013)**, "Transfection efficiency of chitosan and thiolated chitosan in retinal pigment epithelium cells: A comparative study", *Journal of pharmacy & bioallied sciences*, 5, pp. 111–118, DOI: 10.4103/0975-7406.111823.

[150] Mashal, M.; Attia, N.; Martínez-Navarrete, G.; Soto-Sánchez, C.; Fernández, E.; Grijalvo, S.; Eritja, R.; Puras, G.; Pedraz, J. L. **(2019)**, "Gene delivery to the rat retina by non-viral vectors based on chloroquine-containing cationic niosomes", *Journal of controlled release : official journal of the Controlled Release Society*, 304, pp. 181–190, DOI: 10.1016/j.jconrel.2019.05.010.

[151] Liu, M. A. **(2019)**, "A Comparison of Plasmid DNA and mRNA as Vaccine Technologies", *Vaccines*, 7, DOI: 10.3390/vaccines7020037.

[152] Raup, A.; Jérôme, V.; Freitag, R.; Synatschke, C. V.; Müller, A. H. E. **(2016)**, "Promoter, transgene, and cell line effects in the transfection of mammalian cells using PDMAEMA-based nano-stars", *Biotechnology reports (Amsterdam, Netherlands)*, 11, pp. 53–61, DOI: 10.1016/j.btre.2016.05.003.

[153] Kumar, R.; Le, N.; Oviedo, F.; Brown, M. E.; Reineke, T. M. **(2022)**, "Combinatorial Polycation Synthesis and Causal Machine Learning Reveal Divergent Polymer Design Rules for Effective pDNA and Ribonucleoprotein Delivery", *JACS Au*, 2, pp. 428–442, DOI: 10.1021/jacsau.1c00467.

[154] Ansari, A. M.; Ahmed, A. K.; Matsangos, A. E.; Lay, F.; Born, L. J.; Marti, G.; Harmon, J. W.; Sun, Z. **(2016)**, "Cellular GFP Toxicity and Immunogenicity: Potential Confounders in in Vivo Cell Tracking Experiments", *Stem cell reviews and reports*, 12, pp. 553–559, DOI: 10.1007/s12015-016-9670-8.

[155] Subrizi, A.; Yliperttula, M.; Tibaldi, L.; Schacht, E.; Dubruel, P.; Joliot, A.; Urtti, A. **(2009)**, "Optimized transfection protocol for efficient in vitro non-viral polymeric gene delivery to human retinal pigment epithelial cells (ARPE-19)", *Protocol Exchange,* DOI: 10.1038/nprot.2009.78.

[156] Jérôme, V.; Synatschke, C. V.; Freitag, R. **(2020)**, "Transient Destabilization of Biological Membranes Contributes to the Superior Performance of Star-Shaped PDMAEMA in Delivering pDNA", *ACS omega*, 5, pp. 26640–26654, DOI: 10.1021/acsomega.0c03367.

[157] Yang, S.; Zhou, J.; Li, D. **(2021)**, "Functions and Diseases of the Retinal Pigment Epithelium", *Frontiers in pharmacology*, 12, p. 727870, DOI: 10.3389/fphar.2021.727870.

[158] Chen, M.; Rajapakse, D.; Fraczek, M.; Luo, C.; Forrester, J. V.; Xu, H. **(2016)**, "Retinal pigment epithelial cell multinucleation in the aging eye - a mechanism to repair damage and maintain homoeostasis", *Aging cell*, 15, pp. 436–445, DOI: 10.1111/acel.12447.

[159] Olden, B. R.; Cheng, Y.; Yu, J. L.; Pun, S. H. **(2018)**, "Cationic polymers for non-viral gene delivery to human T cells", *Journal of controlled release : official journal of the Controlled Release Society*, 282, pp. 140–147, DOI: 10.1016/j.jconrel.2018.02.043.

[160] Shin, S.; Kim, S. H.; Shin, S. W.; Grav, L. M.; Pedersen, L. E.; Lee, J. S.; Lee, G. M. **(2020)**, "Comprehensive Analysis of Genomic Safe Harbors as Target Sites for Stable Expression of the Heterologous Gene in HEK293 Cells", *ACS synthetic biology*, 9, pp. 1263–1269, DOI: 10.1021/acssynbio.0c00097.

[161] Luo, Y.; Rao, M.; Zou, J. **(2014)**, "Generation of GFP Reporter Human Induced Pluripotent Stem Cells Using AAVS1 Safe Harbor Transcription Activator-Like Effector Nuclease", *Current protocols in stem cell biology*, 29, 5A.7.1-18, DOI: 10.1002/9780470151808.sc05a07s29.

[162] Lino, C. A.; Harper, J. C.; Carney, J. P.; Timlin, J. A. **(2018)**, "Delivering CRISPR: a review of the challenges and approaches", *Drug delivery*, 25, pp. 1234–1257, DOI: 10.1080/10717544.2018.1474964.

[163] Li, L. H.; Biagi, E.; Allen, C.; Shivakumar, R.; Weiss, J. M.; Feller, S.; Yvon, E.; Fratantoni, J. C.; Liu, L. N. **(2006)**, "Rapid and efficient nonviral gene delivery of CD154 to primary chronic lymphocytic leukemia cells", *Cancer gene therapy*, 13, pp. 215–224, DOI: 10.1038/sj.cgt.7700883.

[164] Bäckström, A.; Kugel, L.; Gnann, C.; Xu, H.; Aslan, J. E.; Lundberg, E.; Stadler, C., *A sample preparation protocol for high throughput immunofluorescence of suspension cells* **2020**.

[165] McMahon, S. B.; Norvell, A.; Levine, K. J.; Monroe, J. G. **(1995)**, "Transient transfection of murine B lymphocyte blasts as a method for examining gene regulation in primary B cells", *Journal of immunological methods*, 179, pp. 251–259, DOI: 10.1016/0022-1759(94)00292-5.

[166] Richter, M.; Piwocka, O.; Musielak, M.; Piotrowski, I.; Suchorska, W. M.; Trzeciak, T. **(2021)**, "From Donor to the Lab: A Fascinating Journey of Primary Cell Lines", *Frontiers in cell and developmental biology*, 9, p. 711381, DOI: 10.3389/fcell.2021.711381.

[167] Mitra, A.; Mishra, L.; Li, S. **(2013)**, "Technologies for deriving primary tumor cells for use in personalized cancer therapy", *Trends in biotechnology*, 31, pp. 347–354, DOI: 10.1016/j.tibtech.2013.03.006.

[168] Remaut, K.; Symens, N.; Lucas, B.; Demeester, J.; Smedt, S. C. de **(2014)**, "Cell division responsive peptides for optimized plasmid DNA delivery: the mitotic window of opportunity?", *Journal of controlled release : official journal of the Controlled Release Society*, 179, pp. 1–9, DOI: 10.1016/j.jconrel.2014.01.013.

[169] Zhang, P.; Wagner, E. **(2017)**, "History of Polymeric Gene Delivery Systems", *Topics in current chemistry (Cham)*, 375, p. 26, DOI: 10.1007/s41061-017-0112-0.

[170] Subramanian, S.; Srienc, F. **(1996)**, "Quantitative analysis of transient gene expression in mammalian cells using the green fluorescent protein", *Journal of biotechnology*, 49, pp. 137–151, DOI: 10.1016/0168-1656(96)01536-2.

[171] Seiffert, M.; Stilgenbauer, S.; Döhner, H.; Lichter, P. **(2007)**, "Efficient nucleofection of primary human B cells and B-CLL cells induces apoptosis, which depends on the microenvironment and on the structure of transfected nucleic acids", *Leukemia*, 21, pp. 1977–1983, DOI: 10.1038/sj.leu.2404863.

[172] Dias, C.; Nylandsted, J. **(2021)**, "Plasma membrane integrity in health and disease: significance and therapeutic potential", *Cell discovery*, 7, p. 4, DOI: 10.1038/s41421-020-00233-2.

[173] Chen, X.; Zhang, H.; Mou, W.; Qi, Z.; Ren, X.; Wang, G.; Jiao, H.; Kong, X.; Gui, J. **(2016**), "Flow cytometric analyses of the viability, surface marker expression and function of lymphocytes from children following cryopreservation", *Molecular medicine reports*, 14, pp. 4301–4308, DOI: 10.3892/mmr.2016.5780.

[174] Rasmussen, S. M.; Bilgrau, A. E.; Schmitz, A.; Falgreen, S.; Bergkvist, K. S.; Tramm, A. M.; Baech, J.; Jacobsen, C. L.; Gaihede, M.; Kjeldsen, M. K.; Bødker, J. S.; Dybkaer, K.; Bøgsted, M.; Johnsen, H. E. **(2015)**, "Stable phenotype of B-cell subsets following cryopreservation and thawing of normal human lymphocytes stored in a tissue biobank", *Cytometry. Part B, Clinical cytometry*, 88, pp. 40–49, DOI: 10.1002/cyto.b.21192.

[175] Marasco, E.; Farroni, C.; Cascioli, S.; Marcellini, V.; Scarsella, M.; Giorda, E.; Piano Mortari, E.; Leonardi, L.; Scarselli, A.; Valentini, D.; Cancrini, C.; Duse, M.; Grimsholm, O.; Carsetti, R. **(2017)**, "B-cell activation with CD40L or CpG measures the function of B-cell subsets and identifies specific defects in immunodeficient patients", *European journal of immunology*, 47, pp. 131–143, DOI: 10.1002/eji.201646574.

[176] Robinson, M. J.; Pitt, C.; Brodie, E. J.; Valk, A. M.; O'Donnell, K.; Nitschke, L.; Jones, S.; Tarlinton, D. M. **(2019)**, "BAFF, IL-4 and IL-21 separably program germinal center-like phenotype acquisition, BCL6 expression, proliferation and survival of CD40L-activated B cells in vitro", *Immunology and cell biology*, 97, pp. 826–839, DOI: 10.1111/imcb.12283.

[177] Brown, A. J.; Sweeney, B.; Mainwaring, D. O.; James, D. C. **(2015)**, "NF-κB, CRE and YY1 elements are key functional regulators of CMV promoter-driven transient gene expression in CHO cells", *Biotechnology journal*, 10, pp. 1019–1028, DOI: 10.1002/biot.201400744.

[178] Stinski, M. F.; Isomura, H. **(2008)**, "Role of the cytomegalovirus major immediate early enhancer in acute infection and reactivation from latency", *Medical microbiology and immunology*, 197, pp. 223–231, DOI: 10.1007/s00430-007-0069-7.

[179] Elgueta, R.; Benson, M. J.; Vries, V. C. de; Wasiuk, A.; Guo, Y.; Noelle, R. J. **(2009)**, "Molecular mechanism and function of CD40/CD40L engagement in the immune system", *Immunological reviews*, 229, pp. 152–172, DOI: 10.1111/j.1600-065X.2009.00782.x.

[180] Hostager, B. S.; Bishop, G. A. **(2013)**, "CD40-Mediated Activation of the NF-κB2 Pathway", *Frontiers in immunology*, 4, p. 376, DOI: 10.3389/fimmu.2013.00376.

[181] Huse, K.; Wogsland, C. E.; Polikowsky, H. G.; Diggins, K. E.; Smeland, E. B.; Myklebust, J. H.; Irish, J. M. **(2019)**, "Human Germinal Center B Cells Differ from Naïve and Memory B Cells in CD40 Expression and CD40L-Induced Signaling Response", *Cytometry. Part A : the journal of the International Society for Analytical Cytology*, 95, pp. 442–449, DOI: 10.1002/cyto.a.23737.

[182] Roy, K.; Mitchell, S.; Liu, Y.; Ohta, S.; Lin, Y.-S.; Metzig, M. O.; Nutt, S. L.; Hoffmann, A. **(2019)**, "A Regulatory Circuit Controlling the Dynamics of NFκB cRel Transitions B Cells from Proliferation to Plasma Cell Differentiation", *Immunity*, 50, 616-628.e6, DOI: 10.1016/j.immuni.2019.02.004.

[183] Canoy, R. J.; André, F.; Shmakova, A.; Wiels, J.; Lipinski, M.; Vassetzky, Y.; Germini, D. **(2023)**, "Easy and robust electrotransfection protocol for efficient ectopic gene expression and genome editing in human B cells", *Gene therapy*, 30, pp. 167–171, DOI: 10.1038/s41434-020-00194-x.

[184] Chopra, S.; Ruzgys, P.; Maciulevičius, M.; Šatkauskas, S. **(2020)**, "Effect of Cell Passage Time on the Electrotransfection Efficiency", *Biol Bull Russ Acad Sci*, 47, pp. 441–447, DOI: 10.1134/S1062359020550014.

[185] Mullins, C. S.; Wegner, T.; Klar, E.; Classen, C.-F.; Linnebacher, M. **(2015)**, "Optimizing the process of nucleofection for professional antigen presenting cells", *BMC research notes*, 8, p. 472, DOI: 10.1186/s13104-015-1446-8.

[186] Moghimi, B.; Zolotukhin, I.; Sack, B. K.; Herzog, R. W.; Cao, O. **(2011)**, "High Efficiency Ex Vivo Gene Transfer to Primary Murine B Cells Using Plasmid or Viral Vectors", *Journal of genetic syndromes & gene therapy*, 2, DOI: 10.4172/2157-7412.1000103.

[187] Nutt, S. L.; Hodgkin, P. D.; Tarlinton, D. M.; Corcoran, L. M. **(2015)**, "The generation of antibody-secreting plasma cells", *Nature reviews. Immunology*, 15, pp. 160–171, DOI: 10.1038/nri3795.

[188] McLendon, P. M.; Buckwalter, D. J.; Davis, E. M.; Reineke, T. M. **(2010)**, "Interaction of poly(glycoamidoamine) DNA delivery vehicles with cell-surface glycosaminoglycans leads to polyplex internalization in a manner not solely dependent on charge", *Molecular pharmaceutics*, 7, pp. 1757–1768, DOI: 10.1021/mp100135n.

[189] Mislick, K. A.; Baldeschwieler, J. D. **(1996)**, "Evidence for the role of proteoglycans in cation-mediated gene transfer", *Proceedings of the National Academy of Sciences of the United States of America*, 93, pp. 12349–12354, DOI: 10.1073/pnas.93.22.12349.

[190] Ruponen, M.; Rönkkö, S.; Honkakoski, P.; Pelkonen, J.; Tammi, M.; Urtti, A. **(2001)**, "Extracellular glycosaminoglycans modify cellular trafficking of lipoplexes and polyplexes", *The Journal of biological chemistry*, 276, pp. 33875–33880, DOI: 10.1074/jbc.M011553200.

[191] Monnery, B. D. **(2021)**, "Polycation-Mediated Transfection: Mechanisms of Internalization and Intracellular Trafficking", *Biomacromolecules*, 22, pp. 4060–4083, DOI: 10.1021/acs.biomac.1c00697.

[192] Oracki, S. A.; Walker, J. A.; Hibbs, M. L.; Corcoran, L. M.; Tarlinton, D. M. **(2010)**, "Plasma cell development and survival", *Immunological reviews*, 237, pp. 140–159, DOI: 10.1111/j.1600-065X.2010.00940.x.

[193] Dimova, R. **(2014)**, "Recent developments in the field of bending rigidity measurements on membranes", *Advances in colloid and interface science*, 208, pp. 225–234, DOI: 10.1016/j.cis.2014.03.003.

[194] Ganini, D.; Leinisch, F.; Kumar, A.; Jiang, J.; Tokar, E. J.; Malone, C. C.; Petrovich, R. M.; Mason, R. P. **(2017)**, "Fluorescent proteins such as eGFP lead to catalytic oxidative stress in cells", *Redox biology*, 12, pp. 462–468, DOI: 10.1016/j.redox.2017.03.002.

[195] Qin, J. Y.; Zhang, L.; Clift, K. L.; Hulur, I.; Xiang, A. P.; Ren, B.-Z.; Lahn, B. T. **(2010)**, "Systematic comparison of constitutive promoters and the doxycycline-inducible promoter", *PloS one*, 5, e10611, DOI: 10.1371/journal.pone.0010611.

[196] Helm, M. (**2023**), "*Ex Vivo* Expansion and Differentiation of Primary Human B Lymphocytes in Suspension and Encapsulated Cultures for Novel Culturing Approaches", University of Bayreuth, DOI: 10.15495/EPub_UBT_00007078.

Tabellarischer Lebenslauf

Daniel Keim

Anschrift:	Gottfried-Semper-Weg 14, 95444 Bayreuth
Geboren:	08.05.1994 in Fritzlar
Tel.:	+49 152 53156724
E-Mail:	Daniel.keim85@gmail.com

Bildungsweg

06/2020 – 01/2024	**Promotion im Bereich Biotechnologie**
	Universität Bayreuth, Lehrstuhl Bioprozesstechnik
	"Optimizing Polycationic Transfection for Improved Gene Delivery in Mammalian Cells"
04/2017 – 03/2020	**Natur- und Wirkstoffchemie M.Sc.**
	Universität Bayreuth
10/2013 – 03/2017	**Chemie B.Sc.**
	Universität Bayreuth
08/2005 – 06/2013	**Abitur**
	CJD Christophorusschule, 34596 Bad Zwesten

Sprachkenntnisse

Deutsch - Muttersprache

English – fließend in Wort und Schrift

Latinum